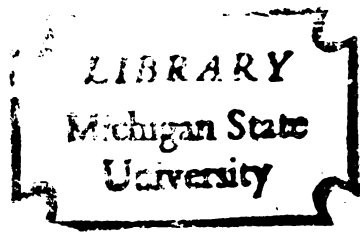




3 1293 10465 8632

THESIS



This is to certify that the
thesis entitled

A NUMERICAL HEAT TRANSFER ANALYSIS
OF A CRYOMICROSCOPE CONDUCTION STAGE

presented by

Vorapot Khompis

has been accepted towards fulfillment
of the requirements for

Master's degree in Mechanical Engineering

R. C. Rosenberg
Major professor

Date Aug. 4, 1980



OVERDUE FINES:
25¢ per day per item

RETURNING LIBRARY MATERIALS:
Place in book return to remove
charge from circulation records

C. 240

A NUMERICAL HEAT TRANSFER ANALYSIS
OF A CRYOMICROSCOPE CONDUCTION STAGE

By

Vorapot Khompis

A THESIS

Submitted to
Michigan State University
in partial fulfillment of the requirements
for the degree of

MASTER OF SCIENCE

Department of Mechanical Engineering

1980

6116597

ABSTRACT

A NUMERICAL HEAT TRANSFER ANALYSIS OF A CRYOMICROSCOPE CONDUCTION STAGE

By

Vorapot Khompis

Numerical heat transfer analyses of a Cryomicroscope Conduction Stage have been performed for the two-dimensional steady-state and transient cases. The Gauss-Seidel finite difference method has been applied for the steady-state solution and the explicit finite difference method has been applied for the transient solution. Both computer programs are written in general form to include variable boundary conditions, non-uniform grid size, and composite materials.

Experimental tests were performed on an existing Cryomicroscope Conduction Stage and compared with computer predictions. The computer models yielded results accurate to within 5% of the actual temperatures observed.

Potential modifications for improvement of the Cryomicroscope Conduction Stage design were considered by performing a parametric study using the computer model developed. Factors studied included: a) variable convection boundary condition; b) heater dissipation area; c) heater thickness; d) heater material (quartz versus glass).

The work has demonstrated that the Cryomicroscope Conduction Stage performance is mostly effected by a change in the natural convective heat transfer coefficient of the surrounding air. The heater dissipation

area plays a major role in the Cryomicroscope Conduction Stage performance.

In general, modifications yielding an isothermal temperature will yield a slower transient response for the Cryomicroscope Conduction Stage. Therefore an ideal design is impossible and a choice must be made between the desirable characteristics of uniform temperature and rapid response.

To - My Father, My Mother, Teachers
and the Royal Thai Air Force

ACKNOWLEDGEMENTS

To all the individuals who have helped and encourage me during the research and writing of this dissertation, I offer my sincere thanks. Foremost appreciation is extended to my thesis advisor, Dr. John J. McGrath, who supplied the original motivation and continued to give generously of his time and valuable consultations during the course of this work.

Other thesis guidance committee members, Drs. Ronald C. Rosenberg, James V. Beck, and John R. Thome, are also warmly thanked for their concern and interest in this work. A special note of thanks is due to my academic advisor, Dr. Ronald C. Rosenberg, for his guidance and numerous suggestions throughout my study.

Grateful thanks are extended to the Royal Thai Air Force for providing funds to finance my graduate program.

TABLE OF CONTENTS

LIST OF TABLES	iii
LIST OF FIGURES.	vi
NOMENCLATURE	ix
SUBSCRIPT NOMENCLATURE	x
GREEK NOMENCLATURE	xi
Chapter	
1. INTRODUCTION.	1
The Cryomicroscope Conduction Stage	1
2. CONDUCTION STAGE DESIGN CONSIDERATIONS.	7
3. THE THEORY OF FINITE DIFFERENCE	10
3.1 Introduction to the Finite Difference Technique. . .	10
3.2 Mathematical Model and Governing Equations	11
3.3 Two-Dimensional Steady-State Conduction.	14
3.4 Two-Dimensional Transient Conduction	23
3.5 Finite Difference Formulation in Explicit Method . .	26
4. APPLICATION OF THE FINITE DIFFERENCE TECHNIQUE TO HEAT TRANSFER OF THE CRYOMICROSCOPE CONDUCTION STAGE	34
4.1 Assumptions.	34
4.2 Numerical Analysis for Two-Dimensional Steady State Conduction	37
4.3 Numerical Analysis for Two-Dimensional Transient Conduction	42
5. EXPERIMENTAL RESULTS FOR THE CRYOMICROSCOPE CONDUCTION STAGE	52
5.1 Description of the Experimental Equipment.	52
5.2 Experimental Technique for Steady State Conduction .	55
5.3 Experimental Technique from Transient Conduction . .	56
6. COMPARISON OF THE COMPUTER MODEL RESULTS WITH EXPERIMENTAL RESULTS	61

7. CONCLUSIONS AND SUGGESTIONS FOR FUTURE WORK	69
7.1 Conclusions.	69
7.2 Suggestions for Future Work.	82
APPENDICES	
A: Nodal Equations for Two-Dimensional Steady-State Conduction .	84
B: Nodal Equations for Two-Dimensional Transient Conduction. . .	88
C: Assumptions of the Cryomicroscope Conduction Stage.	91
D: The Convective Heat Transfer Coefficient for the Refrigerant and Surrounding Air	93
REFERENCES	96

LIST OF FIGURES

1.1	Top and Cross-sectional View of the Copper Stage	2
1.2	Half Sectional View of the Cryomicroscope Conduction Stage . .	4
1.3	The Conduction Stage	5
3.1	Differential Element	12
3.2	Interior Node and Grid Network	15
3.3	The Example of Different Locations of Nodes to be Used in Node Equations for the Cryomicroscope Conduction Stage . . .	18
3.4	Interior Node for Composite Materials.	20
3.5	Surface Node	20
3.6	Corner Node.	22
3.7	Interior Corner Node for Composite Materials	22
3.8	Space-Time Grid Network.	28
4.1	Three-Dimensional Conduction Stage Temperature Profile	35
4.2	Approximation Grid Network of the Cryomicroscope Conduction Stage.	36
4.3	Flow Diagram for the Steady-State Computer Program	39
4.4	Two-Dimensional Steady-State Conduction of the Cryomicroscope Conduction Stage	43
4.5	Flow Diagram for the Transient Conduction Program.	48
4.6	Computer Modeling Results for the Transient Conduction	50
5.1	Experimental Schematic of the Cryomicroscope Conduction Stage.	53
5.2	Temperature Measurement with the Thermocouples at Various Radial Positions	54
5.3	The Change of Temperature with Time Plotted from the Strip Chart Recorder	58

6.1	Comparison of Non-Dimensional Temperature Between the Computer Modeling Results and the Experimental Results for the Steady-State Conduction of the Cryomicroscope Conduction Stage	62
6.2	Comparison of the Change of Temperature with Time at the Centerline	63
6.3	Comparison of the Change of Temperature with Time at $r = 0.047$ in. from the Centerline; $T = T_2$	64
6.4	Comparison of the Change of Temperature with Time at $r = 0.08$ in. from the Centerline; $T = T_3$	65
6.5	Comparison of the Change of Temperature with Time at $r = 0.18$ in. from the Centerline; $T = T_4$	66
6.6	Comparison of the Change of Temperature with Time at $r = 0.24$ in. from the Centerline; $T = T_5$	67
7.1	Typical Heater Dimensions.	71
7.2	The Temperature Difference Between Nodes ($T_C - T_D$) by Fixing the Diameters, Materials and Thickness and Varying the Width W	72
7.3	Effects of the Potential Cryomicroscope Conduction Stage Modification on Transient Response	74
7.4	The Temperature Difference Between Nodes ($T_C - T_D$) by Fixing the Diameters, Materials, the Width W and Varying the Thickness.	76
7.5	The Temperature Difference Between Nodes ($T_C - T_D$) by Changing Materials from Quartz to Glass	78
7.6	Comparison of the Change of Temperature with Time by Changing Materials from Quartz to Glass	79
7.7	Comparison of Non-dimensional Temperature Distribution on the Top Surface of the Cryomicroscope Conduction Stage . . .	80
7.8	Comparison of Non-dimensional Temperature Distribution on the Top Surface of the Cryomicroscope Conduction Stage . . .	81

LIST OF TABLES

4.1	Variables for the Steady-State Conduction Program	41
4.2	Variables for the Transient Conduction Program.	47
5.1	Numerical Experimental Results for Steady-State Conduction of the Cryomicroscope Conduction Stage.	57
5.2	Numerical Experimental Results for Transient Conduction (at the Top Surface) of the Cryomicroscope Conduction Stage	59
7.1	The Temperature Differences Expected Between Nodes ($T_C - T_D$) by Varying Width W	71
7.2	The Temperature Difference Expected Between Nodes ($T_C - T_D$) by Varying the Quartz Thickness	75
7.3	The Temperature Differences Expected by Changing the Materials from Quartz to Glass.	76

NOMENCLATURE

A	Area
Bi	Biot number
C_p	Specific heat at constant pressure
D_H	Hydraulic diameter
F	Convergence criterion
Fo	Fourier number
\bar{h}	Average convective heat transfer coefficient
k	Thermal conductivity
ℓ	Length
m	Proportional of ΔX and ΔY
\bar{m}	Mass
$N1, N2, N'$	Non-dimensional heat generation
Nu	Nusselt number
P	Power
Pr	Prandtl number
Q	Uniform heat generation
R	Thermal resistance
\bar{R}	Electrical resistance
Re	Reynolds number
T	Temperature
T_i	Initial temperature
t	Time
t'	Thickness
\bar{U}	Internal energy
V	Velocity
\bar{V}	Voltage
\bar{X}	Non-dimensional length in X-direction
\bar{Y}	Non-dimensional length in Y-direction
ΔP	Pressure difference
ΔX	Grid size in X-direction
ΔY	Grid size in Y-direction

SUBSCRIPT NOMENCLATURE

B	Boundary or refrigerant
C	Centerline
D	Viewing hole
E	End surface
i	Increment in a spatial variable in Y-direction
j	Increment in a spatial variable in X-direction
L	Left surface
R	Right surface
T	Top surface
X	X-direction of rectangular coordinate
Y	Y-direction of rectangular coordinate
Z	Z-direction of rectangular coordinate

SUPERSCRIPIT NOMENCLATURE

n	Time interval
---	---------------

GREEK NOMENCLATURE

α	Thermal diffusivity
θ	Non-dimensional temperature
ρ	Density
μ	Dynamic viscosity
ψ	Angular distance
μ	10^{-6} meter

CHAPTER I

INTRODUCTION

Cryomicroscope is a tool designed to yield visual evidence of the changes that occur in and around cells (or small samples of living material) as they are frozen and thawed.

The Cryomicroscope Conduction Stage

The conduction stage under consideration was designed by John J. McGrath as a modification of the Diller-Cravalho conduction stage. (M.S.M.E. Thesis, MIT. Feb, 1974) The purpose of this modification was to allow fluorescence optics to be employed as a means of detecting of cell viability on the microscope.

The top and side view of the copper conduction stage are shown in Figure 1.1. The design is essentially a sheet of copper with a tiny viewing hole in the center. The top surface of the stage is completely flat for a convenient working area and allows room for auxiliary parts such as clamping or measuring devices that might be added at a later time. The circular heater is attached to the top surface with its center coincident with the center of the viewing hole. The large center hole is cut out of the stage to allow the oil immersion condenser to be positioned close enough to the specimen to be properly focused.

Channels are also cut in the bottom of the copper plate for

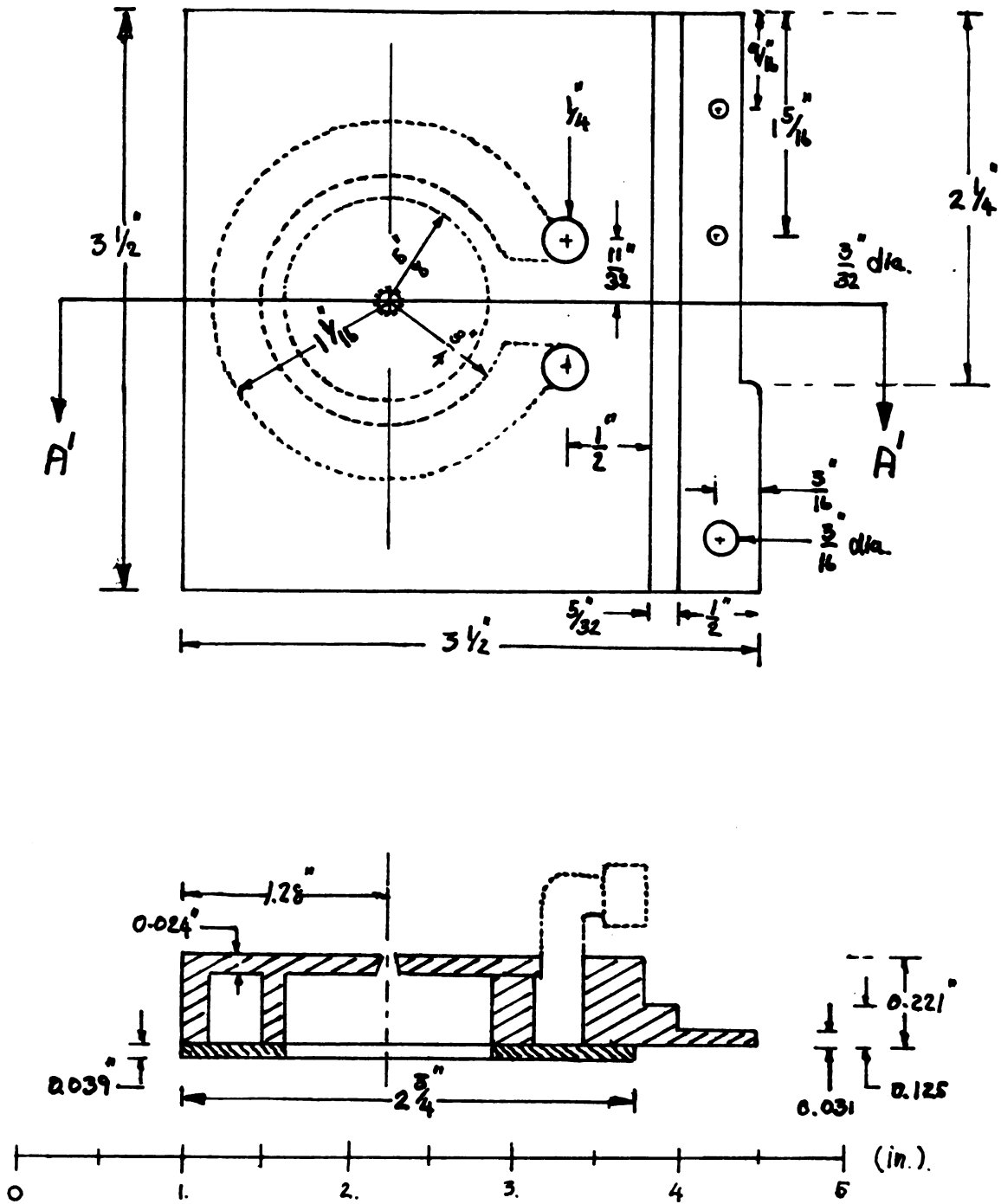


Figure 1.1. Top and Cross-sectional View of the Copper Stage.

refrigerant to flow circumferentially around the heater. The refrigerant enters and exits the stage through the elbows soldered through the top.

A plug is inserted in the channel between the entrance and exit elbows to prevent short-circuit flows.

A bottom plate with a center condenser hole cut out is soldered on the bottom of the stage to seal the bottom of the flow passage.

The top surface of the copper is covered with a thin (0.0025 in.) layer of mylar tape to electrically insulate the resistance heater from the stage.

Dynaloy silver paint is used as both an adhesive and as an electrical conductor. A layer of this paint between the heater and the tape bonds the heater to the top of the stage. Each side of the heater is attached to the stage in this manner with no paint in the center part of the heater so that the current passes through the resistive coating and dissipates joule heating. The paint layer on each side of the heater is extended laterally beyond the edges of the heater so that electrical leads can be attached.

The silver paint attachment is not as permanent as epoxy which was used previously but this is advantageous. New heater configurations can be applied and be ready for use within two hours after deciding the previous unit undesirable. Acetone dissolves the paint bond without damaging the old heater which can be saved for future applications. There are also indications that the use of epoxy restrains the heater too rigidly such that thermally induced stresses will crack the heaters. Further details of the Cryomicroscope conduction are discussed in Ref. 1.

The work that follows presents a numerical heat transfer analysis

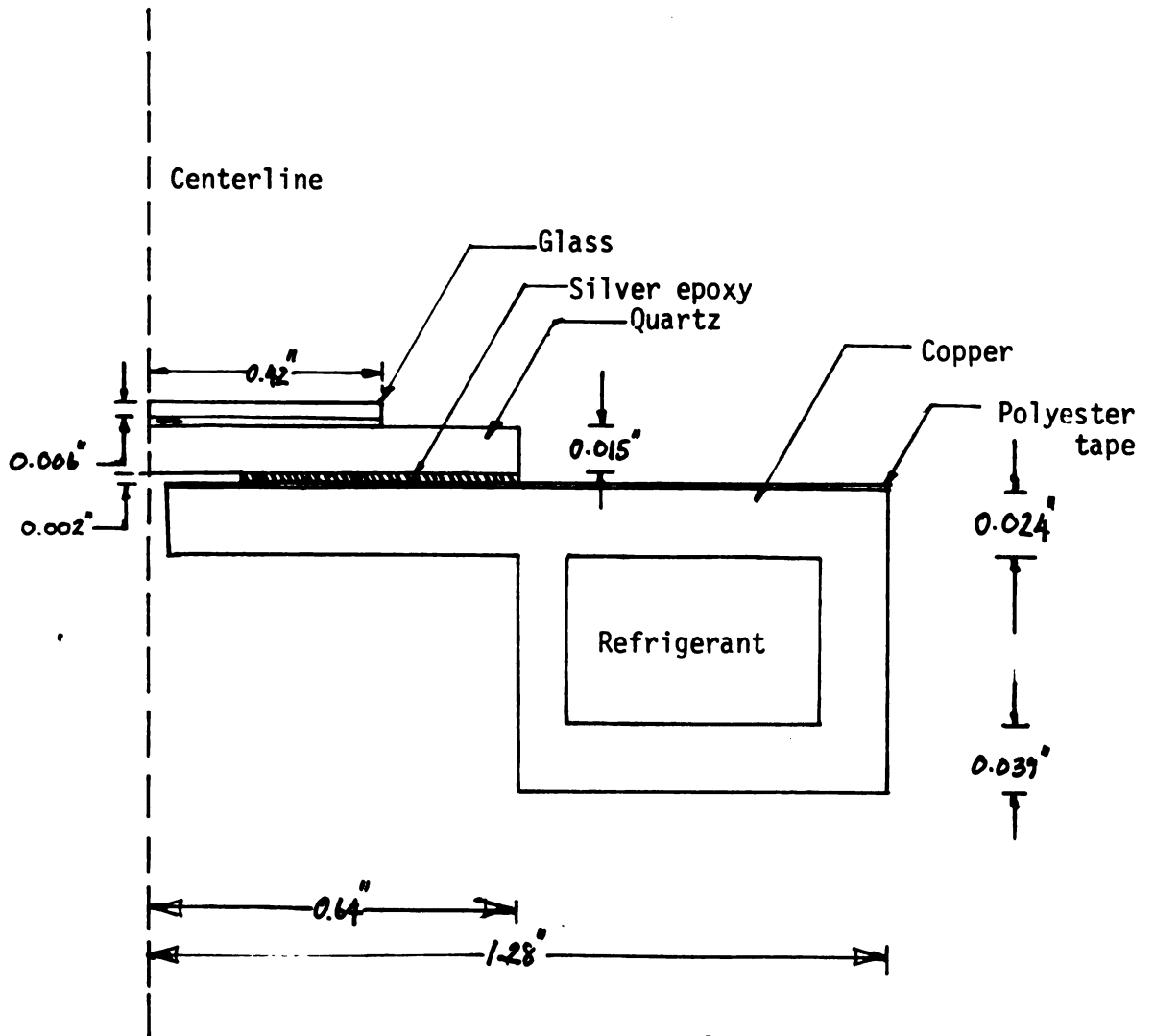


Figure 1.2 Half Sectional View of the Cryomicroscope Conduction Stage.

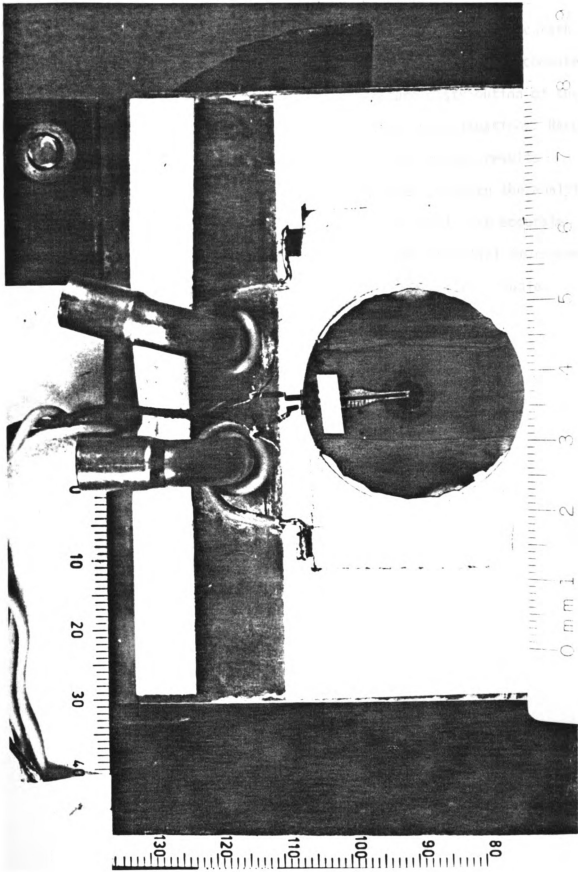


Figure 1.3 The Conduction Stage.

of the Cryomicroscope Conduction Stage designed by Dr. J. J. McGrath. The technique of finite difference is chosen to apply and the computer model is generated to investigate the temperature distribution of the conduction stage for both steady-state and transient situations. Results of the computer simulations are compared to experimental results performed as part of this thesis. Close agreement between the analytical and experimental results indicates that the models are accurate to within 5%. The models have been used to study potential improvements of the cryomicroscope design. Preliminary parametric studies are presented.

CHAPTER 2

CONDUCTION STAGE DESIGN CONSIDERATIONS

The two most important measurements for the Cryomicroscope Conduction Stage are temperature and its time rate of change. It is important to be able to determine these two variables accurately and in a reproducible fashion.

The ideal Cryomicroscope Conduction Stage should be an easily operated tool for the cryobiologist, which allows him to visually observe small samples of living material and to control precisely the temperature and its time rate of change during observation. On the basis of experience with the present system, the ideal stage should possess the following list of features:

- 1) The temperature and the rate of change of temperature should be measurable and controllable
- 2) The operational temperature range should be specified
- 3) The stage should be capable of being used with the highest possible magnification and the maximum mechanical flexibility
- 4) It should be of sturdy construction and easily mounted on a standard light microscope
- 5) It should be designed for convenient experimental procedures

One factor that should not be overlooked is that generally, even subminiature thermocouples yield bulk temperature measurements on the cellular scale. This is obvious when one compares the average human red blood cell diameter of 8μ with the thermocouple junction

width of 125 μ presently used in the system. However, this is not a critical shortcoming since thermodynamic models which use information generated from the cryomicroscope data will often assume isothermal conditions immediately surrounding the cell. Hence an acceptable temperature is the bulk measurement if the thermocouple junction is not placed in a severe thermal gradient.

If it is assumed that the bulk measurement is valid for the moment, the question becomes one of locating the thermocouple to eliminate handling of the miniature thermocouple. One of the designs considered involves embedding the thermocouple in either the glass heater or in the top coverslip covering the sample, such that it is displaced from the sample by some vertical distances.

The designer must be extremely careful in selecting the path over which the thermocouple leads are routed from the point of temperature measurement at the junction to the point where ambient temperature exists on the lead wires. The thermocouple leads act as fins, conducting along their length when placed in a thermal gradient. Many times during the course of the experiments the thermocouple was observed to be in error depending on the routing of the leads from the site of temperature measurement. This error was noted by microscopically observing the phase change during ice formation in a sample around the thermocouple junction.

The solution to this problem is to remove the leads as much as possible from the areas of steepest gradients and to reduce the cross-sectional area of the leads so that longitudinal conduction is minimized.

For the conduction stage a foil copper-constantan thermocouple

junction is placed at the center of the viewing hole in the copper plate. This places the junction at the very center of the stage. This center temperature is the temperature being controlled since this thermocouple is interfaced with the analog control unit.

CHAPTER 3

THE THEORY OF FINITE-DIFFERENCES

3.1 Introduction to the Finite Difference Technique

The finite difference method is used to approximate differential increments in temperature and space coordinates. The smaller we choose these finite increments, the more closely the true temperature distribution will be approximated.

The problem of steady-state two-dimensional conduction, which is the first type of problem considered in this thesis, is a special case of the general three-dimensional, transient conduction problem. The conservation of energy principle is applied to a properly chosen differential element, and Fourier's Law of conduction is used to derive the governing equation for the temperature distribution.

Since the dependent variable, temperature, is a function of more than one independent variable, we expect the temperature distribution to be specified by a partial differential equation. The resulting partial differential equation, along with associated boundary conditions, forms the mathematical model which predicts the temperature field and heat transfer rates. The solution to this partial differential equation can be obtained by analytical or numerical means. For the present work an analytical solution technique was chosen.

3.2 Mathematical Model and Governing Equations

Consider the governing partial differential equation for three-dimensional transient heat conduction in rectangular coordinates. A differential element describing this case is shown in Figure 3.1. This element, which is a closed thermodynamic system is located entirely within a solid material for the present work. Thus, the energy crossing the boundaries of this system is a result of conduction due to temperature gradients and internal heat generation.

Assuming a stationary, homogeneous, isotropic material, the conduction of energy across the differential element can be accounted for by applying the First Law of Thermodynamics. For the net heat conduction across each of the orthogonal surfaces normal to the X, Y, Z directions shown in Figure 3.1, we will obtain:

$$\begin{aligned} q_x + dx/2 - q_x - dx/2 &= \left(q_x + \frac{\partial q_x}{\partial x} \frac{dx}{2} \right) - \left(q_x + \frac{\partial q_x}{\partial x} \left(-\frac{dx}{2} \right) \right) \\ &= \frac{\partial q_x}{\partial x} dx \end{aligned}$$

In a similar manner:

$$\begin{aligned} q_y + dy/2 - q_y - dy/2 &= \frac{\partial q_y}{\partial y} dy \\ q_z + dz/2 - q_z - dz/2 &= \frac{\partial q_z}{\partial z} dz \end{aligned}$$

For the heat generation rate within the differential system, the internal heat generation per unit volume Q is multiplied by the differential volume $dx dy dz$. The internal heat generation is treated as a uniform source from which energy enters the system.

The conservation of energy principle requires that the internal heat generation rate equal the net heat transfer rate crossing the surfaces

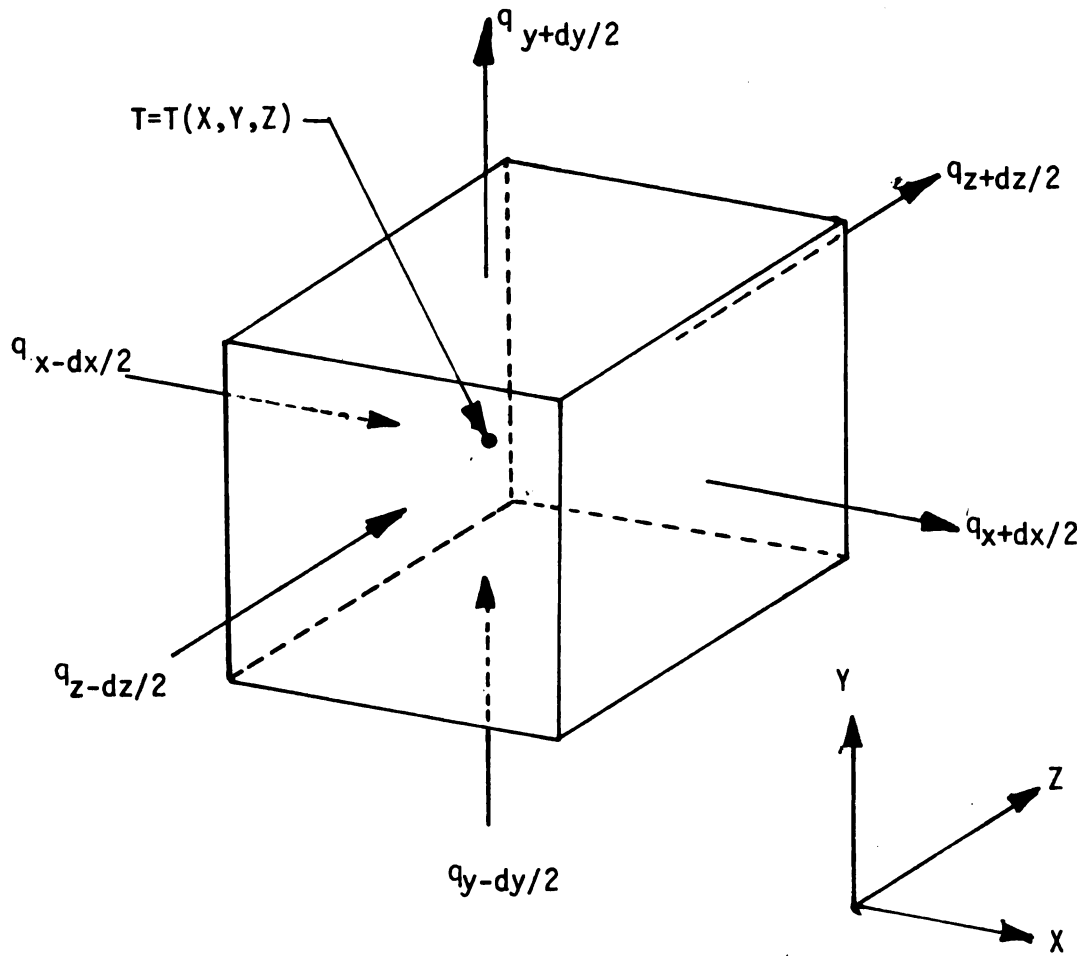


Figure 3.1 Differential Element.

by conduction plus the rate of change of internal energy within the system.

The rate of change of internal energy can be expressed as $d\bar{U}/dt = \bar{m}c_p(dT/dt) = \rho dx dy dz c_p (\partial T / \partial t)$.

Thus we can write

$$Q dx dy dz = \frac{\partial q_x}{\partial x} dx + \frac{\partial q_y}{\partial y} dy + \frac{\partial q_z}{\partial z} dz + \rho dx dy dz c_p \frac{\partial T}{\partial t}$$

Using Fourier's Law of Conduction to relate heat flux and temperatures:

$$q_x = -kA_x (\partial T / \partial X)$$

where $A_x = dy dz$

Also, $q_y = -k dz dx (\partial T / \partial Y)$

$$q_z = -k dx dy (\partial T / \partial Z)$$

Then we can obtain the Energy Equation for Conduction which applies to the present case:

$$\frac{\partial}{\partial x} (k \frac{\partial T}{\partial X}) + \frac{\partial}{\partial y} (k \frac{\partial T}{\partial Y}) + \frac{\partial}{\partial z} (k \frac{\partial T}{\partial Z}) + Q = \rho c_p \frac{\partial T}{\partial t} \quad (3-1)$$

If we assume constant thermal conductivity and two-dimensional conduction in the X and Y directions, the energy equation reduces to

$$\alpha \left(\frac{\partial^2 T}{\partial x^2} + \frac{\partial^2 T}{\partial y^2} \right) + \frac{Q}{\rho c_p} = \frac{\partial T}{\partial t} \quad (3-2)$$

where α is the thermal diffusivity: $\alpha = k / \rho c_p$.

For steady-state, two-dimensional conduction the temperature distribution is not a function of time, and the governing equation can be written as:

$$\frac{\partial^2 T}{\partial X^2} + \frac{\partial^2 T}{\partial Y^2} + \frac{Q}{k} = 0. \quad (3-3)$$

3.3 Two-Dimensional Steady-State Conduction

For a finite difference analysis of two-dimensional conduction, an element of unit depth and dimensions ΔX and ΔY on the sides is chosen as the system to which the conservation of energy principle is applied.

A node is defined at the center of each finite volume. A temperature is assigned to each node, and it is assumed that this one value gives the temperature of the entire element.

The sum of finite elements forms a grid network as shown in Figure 3.2(a).

An interior, finite element of unit depth with width ΔX and height ΔY is shown shaded in Figure 3.2(a). The curved line represents the temperature variation through the solid material. In a finite difference formulation the temperature gradient is calculated as though a linear profile exists between nodes as shown in Figure 3.2(b). At the same time, the nodal representation of the temperature field implies a linear change in temperature across the interface between two adjacent elements. This formulation is obviously more accurate as the distance between nodes decreases.

The principle of conservation of energy for steady state heat transfer is now applied to an interior node. The temperature gradient between nodes is assumed constant. For the heat transfer crossing the boundaries of the system using Fourier's Law

$$q_x = -kA_x \frac{\partial T}{\partial X}$$

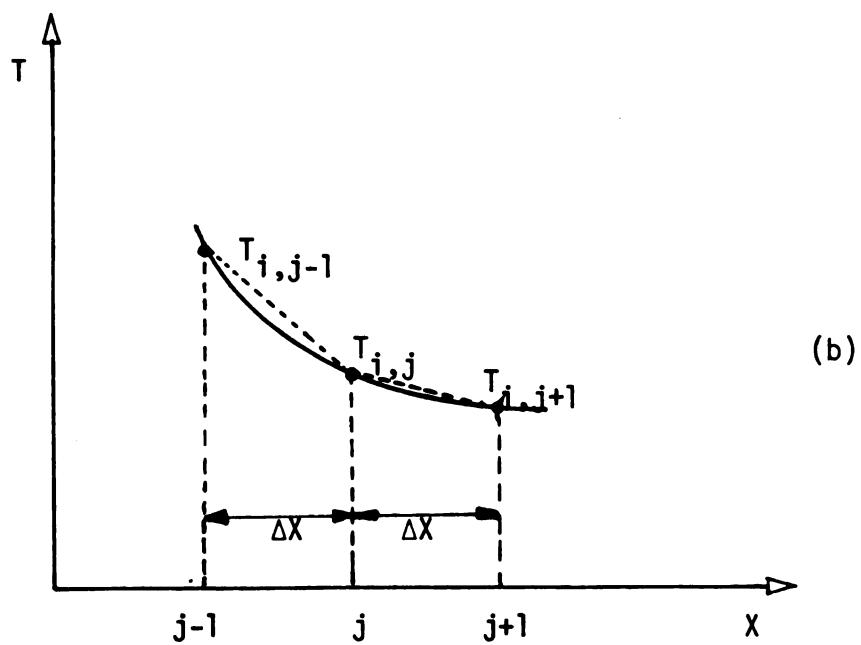
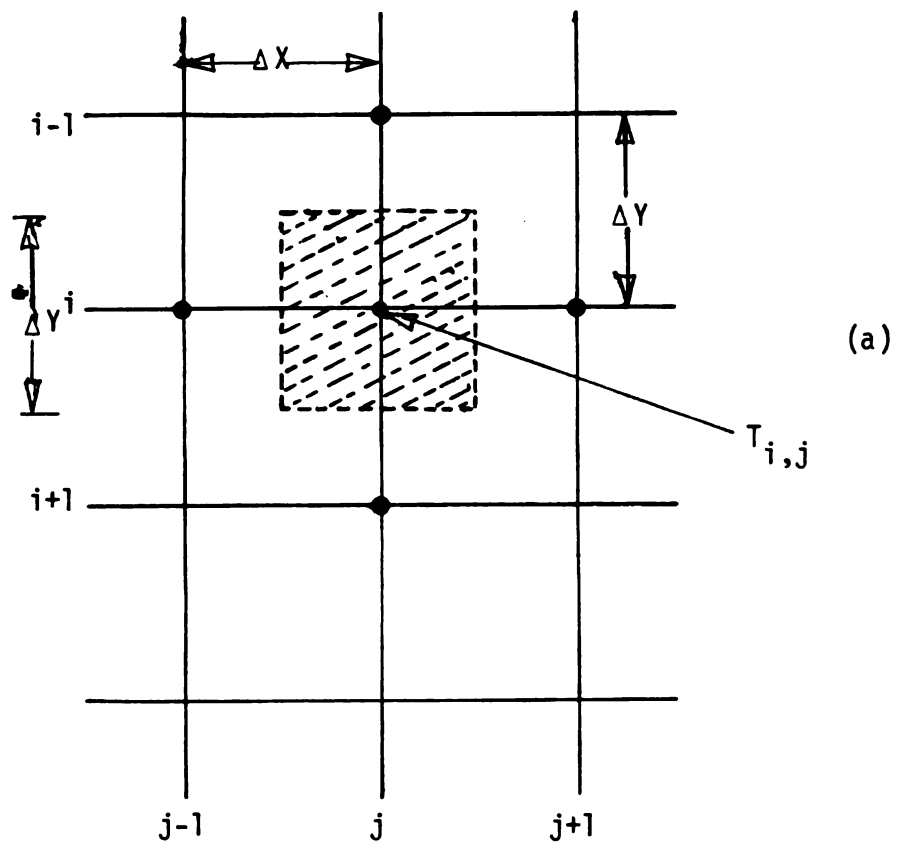


Figure 3.2 Interior Node and Grid Network.

If the temperature of the central node $T_{i,j}$ is larger than $T_{i,j-1}$, the heat transfer between nodes i, j and $i, j-1$ is approximated as follows:

$$q_x = k\Delta Y(1) \frac{T_{i,j-1} - T_{i,j}}{\Delta X}$$

If one uses similar equations for the other three surrounding nodes and accounts for internal heat generation, application of the conservation of energy principle will lead to the following equation:

$$\begin{aligned} k\Delta Y(1) \frac{T_{i,j-1} - T_{i,j}}{\Delta X} + k\Delta X(1) \frac{T_{i-1,j} - T_{i,j}}{\Delta Y} + k\Delta Y(1) \frac{T_{i,j+1} - T_{i,j}}{\Delta X} \\ + k\Delta X(1) \frac{T_{i+1,j} - T_{i,j}}{\Delta Y} + Q\Delta X\Delta Y(1) = 0 \end{aligned}$$

The application considered in this thesis required cases where ΔX and ΔY were unequal. Hence a general formulation is developed where $\Delta Y = m\Delta X$.

$$\begin{aligned} mk(T_{i,j-1} - T_{i,j}) + \frac{k}{m}(T_{i-1,j} - T_{i,j}) + mk(T_{i,j+1} - T_{i,j}) \\ + \frac{k}{m}(T_{i+1,j} - T_{i,j}) + mQ(\Delta X)^2 = 0 \end{aligned}$$

$$\begin{aligned} m^2(T_{i,j-1} - T_{i,j}) + (T_{i-1,j} - T_{i,j}) + m^2(T_{i,j+1} - T_{i,j}) \\ + (T_{i+1,j} - T_{i,j}) + \frac{m^2}{k}Q(\Delta X)^2 = 0 \end{aligned}$$

$$(2m^2 + 2)T_{i,j} = m^2T_{i,j-1} + m^2T_{i,j+1} + T_{i-1,j} + T_{i+1,j} + \frac{m^2}{k}Q(\Delta X)^2$$

The following variables are defined in order to non-dimensionalize the governing equations:

$$\theta = \frac{T - T_B}{T_C - T_B}$$

$$\bar{Y} = \frac{Y}{\ell}$$

$$\bar{X} = \frac{X}{\ell}$$

where T_C , T_B , and ℓ are chosen reference temperatures and a reference length, respectively.

Then the above equation can be written as

$$(2m^2 + 2)\theta_{i,j} = m^2\theta_{i,j-1} + m^2\theta_{i,j+1} + \theta_{i-1,j} + \theta_{i+1,j} + m^2(\Delta X)^2 \frac{Q\ell^2}{k(T_C - T_B)}$$

Define:

$$N1 = \frac{Q\ell^2}{k(T_C - T_B)} = \frac{Q\ell^3}{k\ell^2(T_C - T_B)/\ell}$$

where $N1$ is a non-dimensional heat generation term.

The numerator is a heat transfer rate resulting from internal generation in a reference volume ℓ^3 . The dominator is a reference heat conduction term across a reference area ℓ^2 and along a reference temperature gradient $(T_C - T_B)/\ell$. Thus $N1$ can be thought of as a ratio of energy internally generated to energy conducted.

Thus, the final form of the finite difference equation for all interior nodes for steady-state, two dimensional conduction becomes

$$\theta_{i,j} = \frac{m^2\theta_{i,j-1} + m^2\theta_{i,j+1} + \theta_{i-1,j} + \theta_{i+1,j} + m^2(\Delta X)^2 N1}{(2m^2 + 2)} \quad (3-4)$$

It is necessary to use the different node equations for the different locations of node in the Cryomicroscope Conduction Stage as shown in Figure 3.3 (details in Figure 3.1 through Figure 3.7).

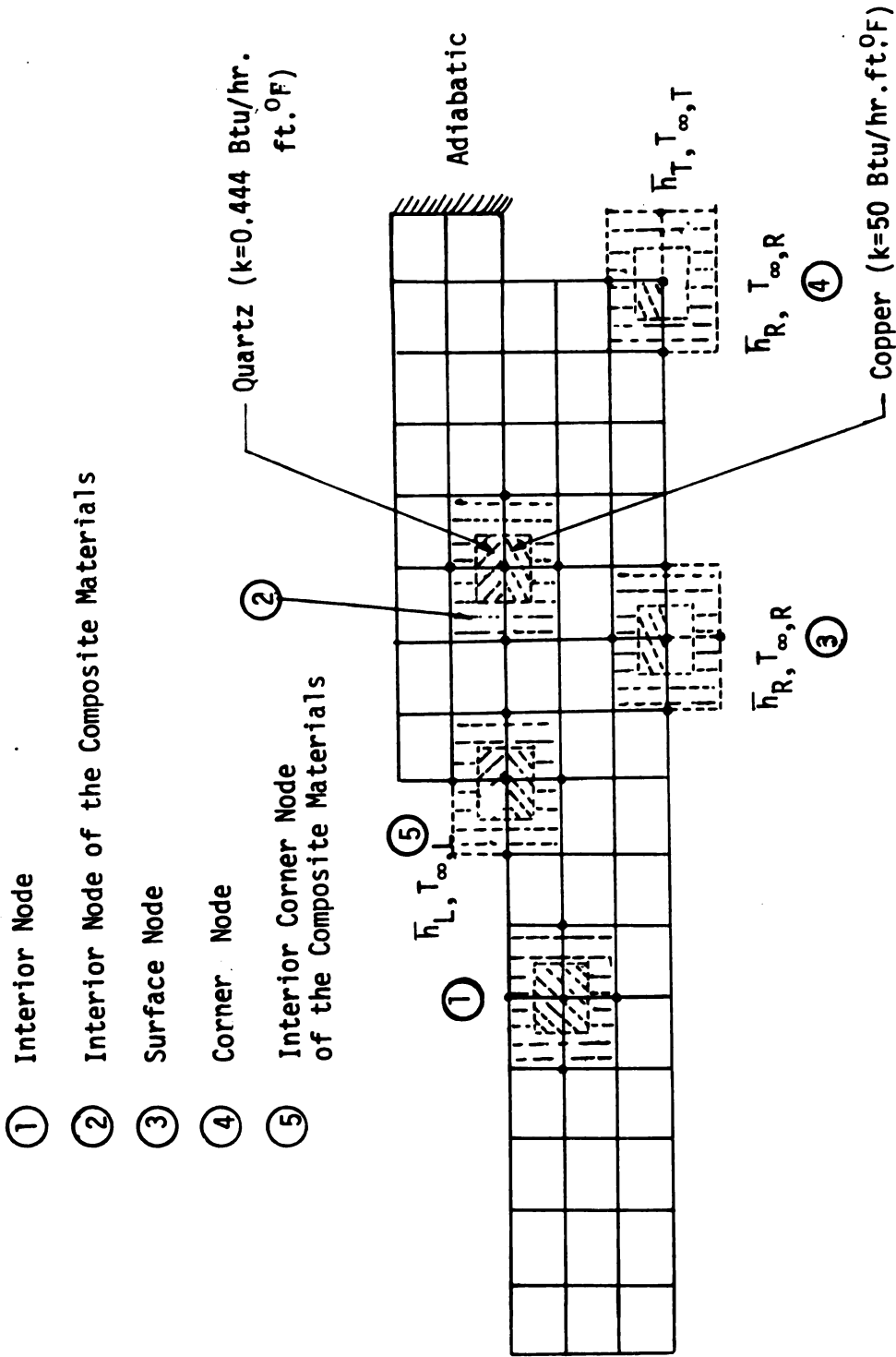


Figure 3.3 The Example of Different Locations of Nodes to be used in Node Equations for the Cryomicroscope Conduction Stage.

In the same manner (details in Appendix A), the interior node equation for composite materials is given as:

$$\theta_{i,j} = \frac{\theta_{i+1,j} + \theta_{i-1,j} + 2m^2(k_1\theta_{i,j-1} + k_2\theta_{i,j+1})/k_3 + m^2(\overline{\Delta X})^2 N_2/k_3}{(2m^2+2)} \quad (3-5)$$

where k_1 = The thermal conductivity of material 1.

k_2 = The thermal conductivity of material 2.

$k_3 = k_1 + k_2$.

In convection boundary conditions, for the general situation, we consider the environment temperatures at the different sides of the Cryomicroscope Conduction Stage are not equal to the refrigerant temperature T_B ($T_{\infty,L} \neq T_{\infty,R} \neq T_{\infty,E} \neq T_{\infty,T} \neq T_B$). We also consider the Biot number $Bi_B \neq Bi_L \neq Bi_R \neq Bi_E \neq Bi_T$.

The node equation for convection at the right vertical surface:

$$\theta_{i,j} = \frac{\theta_{i+1,j} + 2m^2\theta_{i,j-1} + \theta_{i-1,j} + 2m^2\overline{\Delta X}Bi_R\theta_R + m^2(\overline{\Delta X})^2 N_1}{(2m^2 + 2 + 2m^2\overline{\Delta X}Bi_R)} \quad (3-6)$$

The node equation for convection at the left vertical surface:

$$\theta_{i,j} = \frac{\theta_{i+1,j} + 2m^2\theta_{i,j+1} + \theta_{i-1,j} + 2m^2\overline{\Delta X}Bi_L\theta_L + m^2(\overline{\Delta X})^2 N_1}{(2m^2 + 2 + 2m^2\overline{\Delta X}Bi_L)} \quad (3-7)$$

where: Bi = Biot Number = $\bar{h}l/k$.

The node equation for convection at the top surface:

For the left corner node

$$\theta_{i,j} = \frac{\theta_{i+1,j} + m^2\theta_{i,j+1} + mBi_T\overline{\Delta X}\theta_T + m^2Bi_L\overline{\Delta X}\theta_L + \frac{m^2}{2}(\overline{\Delta X})^2 N_1}{(m^2+1 + mBi_T\overline{\Delta X} + m^2Bi_L\overline{\Delta X})} \quad (3-8)$$

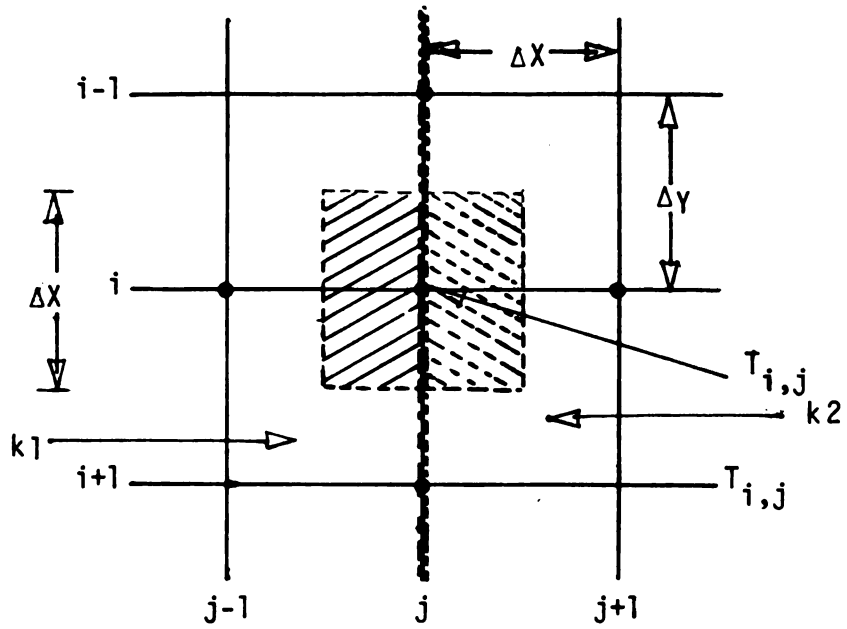


Figure 3.4 Interior Node for Composite Materials

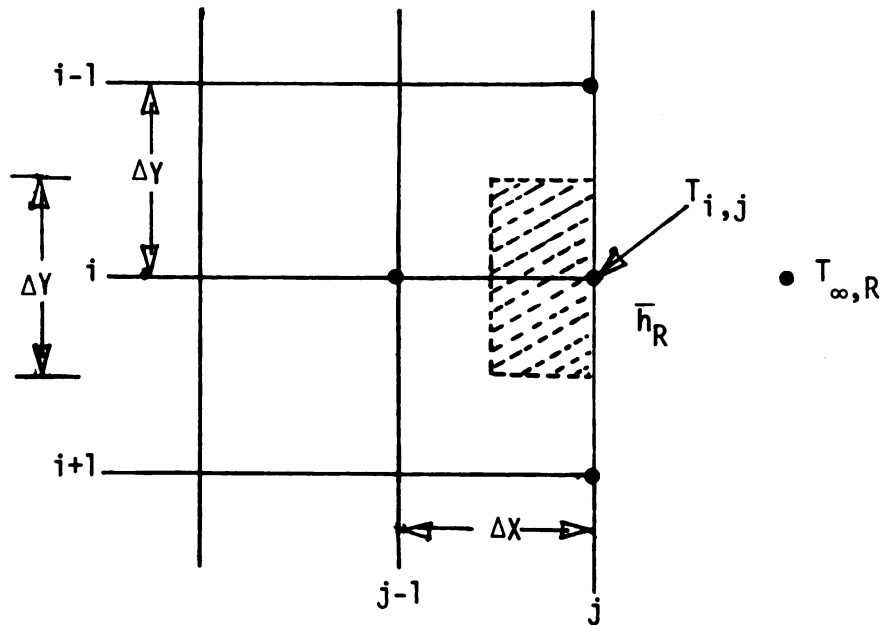


Figure 3.5 Surface Node

For the right corner node

$$\theta_{i,j} = \frac{\theta_{i+1,j} + m^2\theta_{i,j-1} + mBi_T\overline{\Delta X}\theta_T + m^2Bi_L\overline{\Delta X}\theta_L + \frac{m^2}{2}(\overline{\Delta X})^2N_1}{(m^2+1 + mBi_T\overline{\Delta X} + m^2Bi_L\overline{\Delta X})} \quad (3-9)$$

For the remaining top surface nodes

$$\theta_{i,j} = \frac{\theta_{i+1,j} + \frac{m^2}{2}(\theta_{i,j-1} + \theta_{i,j+1}) + mBi_T\overline{\Delta X}\theta_T + \frac{m^2}{2}(\overline{\Delta X})^2N_1}{(m^2+1 + mBi_T\overline{\Delta X})} \quad (3-10)$$

The node equation for convection at the end surface:

For the left corner node

$$\theta_{i,j} = \frac{\theta_{i-1,j} + m^2\theta_{i,j+1} + mBi_E\overline{\Delta X}\theta_E + m^2Bi_L\overline{\Delta X}\theta_L + \frac{m^2}{2}(\overline{\Delta X})^2N_1}{(m^2+1 + mBi_E\overline{\Delta X} + m^2Bi_L\overline{\Delta X})} \quad (3-11)$$

For the right corner

$$\theta_{i,j} = \frac{\theta_{i-1,j} + m^2\theta_{i,j-1} + mBi_E\overline{\Delta X}\theta_E + m^2Bi_R\overline{\Delta X}\theta_R + \frac{m^2}{2}(\overline{\Delta X})^2N_1}{(m^2+1 + mBi_E\overline{\Delta X} + m^2Bi_R\overline{\Delta X})} \quad (3-12)$$

For the remaining end surface nodes

$$\theta_{i,j} = \frac{\theta_{i-1,j} + \frac{m^2}{2}(\theta_{i,j+1} + \theta_{i,j-1}) + mBi_E\overline{\Delta X}\theta_E + \frac{m^2}{2}(\overline{\Delta X})^2N_1}{(m^2 + 1 + mBi_E\overline{\Delta X})} \quad (3-13)$$

where $\theta_L = (T_{\infty,L} - T_B)/(T_C - T_B)$, $\theta_R = (T_{\infty,R} - T_B)/(T_C - T_B)$

$\theta_T = (T_{\infty,T} - T_B)/(T_C - T_B)$, $\theta_E = (T_{\infty,E} - T_B)/(T_C - T_B)$.

The node equations for convection at an interior corner node with composite materials are given as:

For the top right interior corner node

$$\theta_{i,j} = \frac{2m^2k_4\theta_{i,j-1} + k_4\theta_{i-1,j} + (m^2+m)Bi'\overline{\Delta X}\theta_R + m^2k_5\theta_{i,j+1} + \theta_{i+1,j} + \frac{3}{2}m^2(\overline{\Delta X})^2N_1}{((2m^2+1)k_4 + m^2k_5 + (m^2+m)Bi'\overline{\Delta X} + 1)} \quad (3-14)$$

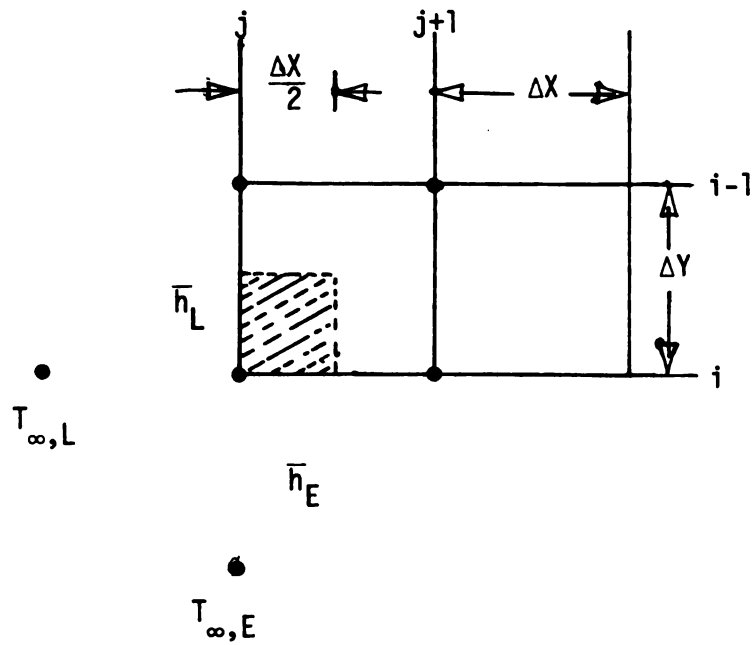


Figure 3.6 Corner Node

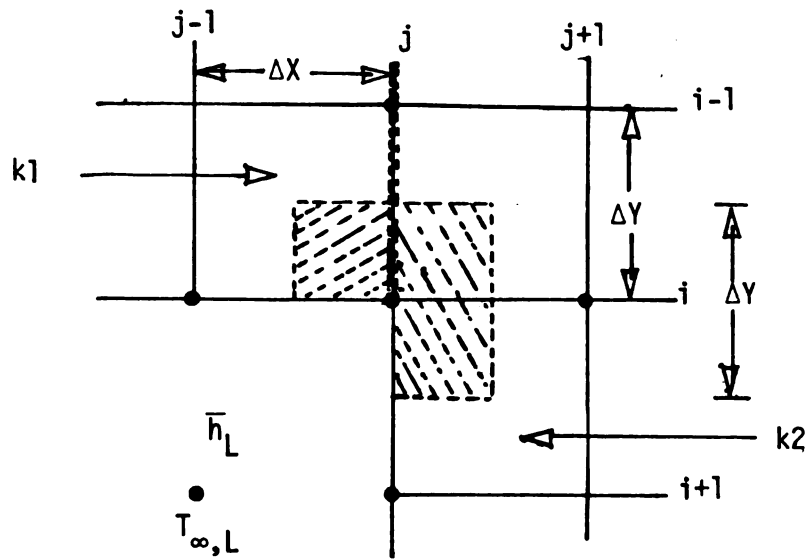


Figure 3.7 Interior Corner node for Composite Materials.

For the end left interior corner node

$$\theta_{i,j} = \frac{2m^2 k_5 \theta_{i,j+1} + k_5 \theta_{i+1,j} + (m^2+m) Bi' \overline{\Delta X} \theta_L + m^2 k_4 \theta_{i,j-1} + \theta_{i-1,j} + \frac{3}{2} m^2 (\overline{\Delta X})^2 N'}{(2m^2+1)k_5 + m^2 k_4 + (m^2+m) Bi' \overline{\Delta X} + 1} \quad (3-15)$$

where $k_3 = k_1 + k_2$

$$k_4 = k_1/k_3$$

$$k_5 = k_2/k_3$$

$$Bi' = \overline{h}_L \ell / k_3$$

$$Bi'' = \overline{h}_R \ell / k_3 \quad \text{and} \quad N' = Q \ell^2 / k_3 (T_C - T_B)$$

For adiabatic surfaces the node equations are identical except the Biot Number Bi is zero.

3.4 Two-Dimensional Transient Conduction

When a solid body is suddenly subjected to a change in environment, some time must elapse before an equilibrium temperature will prevail in the body. We refer to the equilibrium condition as the steady state condition and calculate the temperature distribution and heat transfer by the finite difference method described previously. In the transient heating or cooling process which takes place in the interim period before equilibrium is established, the analysis must be modified to take into account the change in internal energy of the body with time, and the boundary conditions must be adjusted to match the physical situation which is apparent in the transient heat-transfer problem. For the cryomicroscope system a transient heat transfer analysis is important because we can approximate the transient response, the temperature gradient and the steady-state situation from this analysis.

To analyze a transient heat-transfer problem, we will proceed by solving from the energy equation as obtained in Equation (3-1)

$$\frac{\partial}{\partial X}(k\frac{\partial T}{\partial X}) + \frac{\partial}{\partial Y}(k\frac{\partial T}{\partial Y}) + Q = \rho C_p \frac{\partial T}{\partial t}$$

In general $T = T(X, Y, T)$.

For constant properties, we can write

$$\frac{\partial^2 T}{\partial X^2} + \frac{\partial^2 T}{\partial Y^2} + \frac{Q}{k} = \frac{1}{\alpha} \frac{\partial T}{\partial t} \quad (3-16)$$

where $\alpha = k/\rho C_p$ (ft²/sec).

It is instructive to non-dimensionalize Equation (3-16) and its associated boundary conditions.

For a convective boundary condition the following non-dimensional variables are used:

$$\Theta = \frac{T - T_B}{T_i - T_B}$$

$$\bar{X} = \frac{X}{l} ; \bar{Y} = \frac{Y}{l}$$

$$\bar{t} = \frac{\alpha t}{l^2} = Fo.$$

where T_i = initial temperature

T_B = refrigerant temperature

Fo is the Fourier Number

$$Fo = \frac{\alpha t}{l^2} = \frac{k l^2 (\Delta T/l)}{\rho C_p l^3 (\Delta T/t)}$$

$$\sim \frac{kA(\partial T/\partial X)}{\rho C_p (\partial T/\partial t)} \sim \frac{\text{Heat Transfer by Conduction}}{\text{Rate of Energy Storage}}$$

Introducing the non-dimensional variables defined above:

$$\frac{\partial T}{\partial X} = \frac{\partial \theta}{\partial \bar{X}} \frac{\partial \bar{X}}{\partial X} \frac{\partial T}{\partial \theta} = \frac{T_i - T_B}{\ell} \frac{\partial \theta}{\partial \bar{X}}$$

$$\frac{\partial T}{\partial Y} = \frac{\partial \theta}{\partial \bar{Y}} \frac{\partial \bar{Y}}{\partial Y} \frac{\partial T}{\partial \theta} = \frac{T_i - T_B}{\ell} \frac{\partial \theta}{\partial \bar{Y}}$$

$$\begin{aligned} \frac{\partial^2 T}{\partial X^2} &= \frac{\partial}{\partial \bar{X}} \left(\frac{\partial T}{\partial X} \right) \frac{\partial \bar{X}}{\partial X} = \frac{\partial}{\partial \bar{X}} \left(\frac{T_i - T_B}{\ell} \frac{\partial \theta}{\partial \bar{X}} \right) \frac{\partial \bar{X}}{\partial X} \\ &= \frac{T_i - T_B}{\ell^2} \left(\frac{\partial^2 \theta}{\partial \bar{X}^2} \right) \end{aligned}$$

$$\frac{\partial^2 T}{\partial Y^2} = \frac{T_i - T_B}{\ell^2} \left(\frac{\partial^2 \theta}{\partial \bar{Y}^2} \right)$$

$$\frac{\partial T}{\partial t} = \frac{\partial \theta}{\partial Fo} \frac{\partial Fo}{\partial t} \frac{\partial T}{\partial \theta} = \alpha \frac{T_i - T_B}{\ell^2} \left(\frac{\partial \theta}{\partial Fo} \right)$$

Substituting these three above equations into Equation (3-16) gives

$$\frac{\partial^2 \theta}{\partial \bar{X}^2} + \frac{\partial^2 \theta}{\partial \bar{Y}^2} + \frac{Q\ell^2}{k(T_i - T_B)} = \frac{\partial \theta}{\partial Fo}$$

The non-dimensional internal heat generation term is employed here as it was for the steady state case:

$$N1 = \frac{Q\ell^2}{k(T_i - T_B)} = \frac{Q\ell^3}{k\ell^2(T_i - T_B)/\ell}$$

$$\sim \frac{\text{Energy Generation Rate}}{\text{Heat Transfer by Conduction}}$$

The non-dimensional governing equation for a two dimensional transient conduction problem with heat generation is written:

$$\frac{\partial^2 \theta}{\partial X^2} + \frac{\partial^2 \theta}{\partial Y^2} + N1 = \frac{\partial \theta}{\partial Fo} \quad (3-17)$$

3.5 Finite Difference Formulation by the Explicit Method

Although the finite difference form of an equation can be obtained directly from the governing equation, the grid network of Figure 3.2 is now reconsidered. In Figure 3.2(b), a forward finite difference approximation to the derivative $\partial T/\partial X$ at $X_{i,j}$ is based on an assumed constant linear temperature gradient between nodes and is given by

$$\left(\frac{\partial T}{\partial X}\right)_{i,j} \approx \frac{T_{i,j+1} - T_{i,j}}{\Delta X}$$

In a similar manner a backward finite difference approximation to the derivative at the node i,j will be

$$\left(\frac{\partial T}{\partial X}\right)_{i,j} \approx \frac{T_{i,j} - T_{i,j-1}}{\Delta X}$$

For a more accurate approximation to the temperature derivative at a node a central finite difference technique which is based on the temperature of both the forward and backward nodes is applied.

The approximation can be expressed as:

$$\left(\frac{\partial T}{\partial X}\right)_{i,j} \approx \frac{T_{i,j+1} - T_{i,j-1}}{2 \Delta X} \approx \frac{T_{i,j+\frac{1}{2}} - T_{i,j-\frac{1}{2}}}{\Delta X} \quad (1)$$

Then the second derivative based on a central difference approximation becomes

$$\left(\frac{\partial^2 T}{\partial X^2}\right)_{i,j} \approx \frac{1}{\Delta X} \left[\left(\frac{\partial T}{\partial X}\right)_{i,j+\frac{1}{2}} - \left(\frac{\partial T}{\partial X}\right)_{i,j-\frac{1}{2}} \right] \quad (2)$$

Now we will express each of the first derivatives in terms of a central difference approximation using an equation similar to Equation(1). The approximation to the derivative at the location $i, j+\frac{1}{2}$ is made using the forward node $T_{i, j+1}$ and the backward node $T_{i, j}$.

Then Equation 2 can be written as

$$\begin{aligned} \left(\frac{\partial^2 T}{\partial X^2}\right)_{i, j} &\approx \frac{1}{\Delta X} \left(\frac{T_{i, j+1} - T_{i, j}}{\Delta X} - \frac{T_{i, j} - T_{i, j-1}}{\Delta X} \right) \\ &\approx \frac{1}{(\Delta X)^2} (T_{i, j+1} - 2T_{i, j} + T_{i, j-1}). \end{aligned}$$

In the same way

$$\left(\frac{\partial^2 T}{\partial Y^2}\right)_{i, j} \approx \frac{1}{(\Delta Y)^2} (T_{i+1, j} - 2T_{i, j} + T_{i-1, j}).$$

Consider transient conduction with constant properties. Figure 3.8 is a space-time grid network where it has been assumed that the plane is fixed. Since we initially consider only one independent space variable, only the subscript j is needed to indicate an increment in the spatial variable. A time interval is denoted by a superscript n .

Then the finite difference approximation to the second derivative can be written

$$\frac{\partial^2 T}{\partial X^2} = \frac{T_{i, j+1}^n - 2T_{i, j}^n + T_{i, j-1}^n}{(\Delta X)^2} \quad (3)$$

The time derivative can be expressed as a forward difference approximation

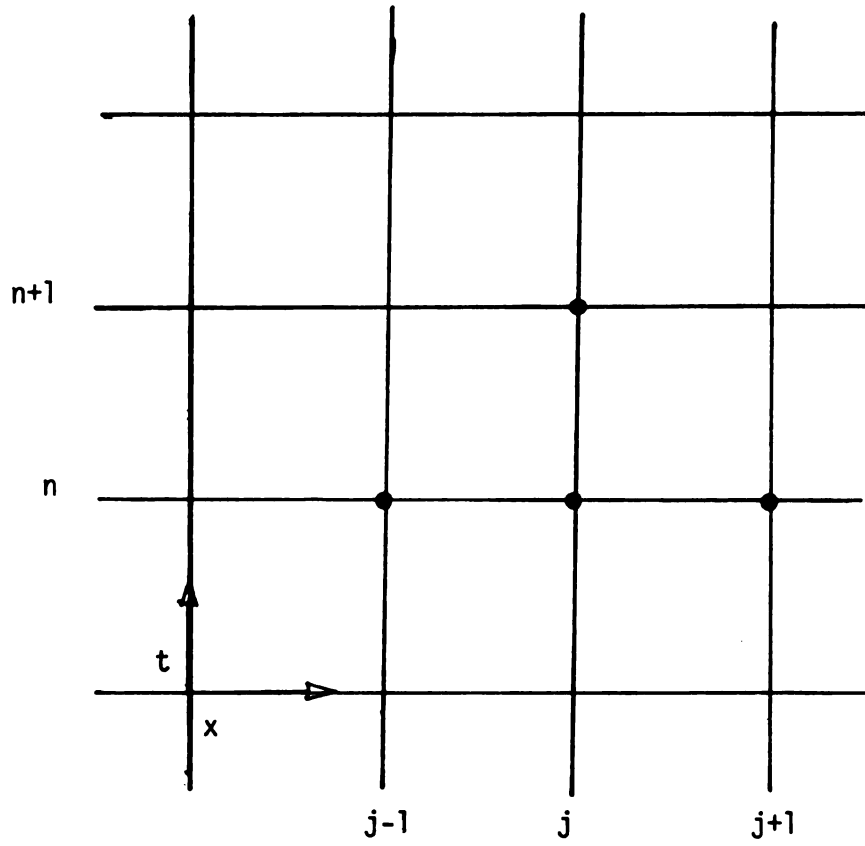


Figure 3.8 Space-Time Grid Network.

$$\frac{\partial T}{\partial t} = \frac{T_{i,j}^{n+1} - T_{i,j}^n}{\Delta t} \quad (4)$$

To clarify this notation, consider the space-time grid network shown in Figure 3.8. The increment $n+1$ refers to an increment in time and increment $j+1$ refers to an increment in space.

An approximation associated with this finite difference equation is that while the temperature at $T_{i,j}^n$ changes during a small time interval to a value $T_{i,j}^{n+1}$, the values of $T_{i,j+1}^n$ and $T_{i,j-1}^n$ are assumed to remain constant.

In a same manner, we can write

$$\frac{\partial^2 T}{\partial Y^2} = \frac{T_{i+1,j}^n - 2T_{i,j}^n + T_{i-1,j}^n}{(\Delta Y)^2} \quad (5)$$

The value of Δt is the time increment required for changing $T_{i,j}^n$ to $T_{i,j}^{n+1}$.

Equations (3), (4) and (5) can be nondimensionalized and substituted into Equation (3-17). The resulting equation is

$$\begin{aligned} \frac{1}{(\Delta X)^2} (\theta_{i,j+1}^n - 2\theta_{i,j}^n + \theta_{i,j-1}^n) + \frac{1}{(\Delta Y)^2} (\theta_{i+1,j}^n - 2\theta_{i,j}^n + \theta_{i-1,j}^n) + N1 \\ = \frac{\theta_{i,j}^{n+1} - \theta_{i,j}^n}{\Delta Fo} \end{aligned}$$

For the general case discussed before: $\Delta Y = m\Delta X$. Therefore:

$$\begin{aligned}
\Theta_{i,j}^{n+1} &= \frac{\Delta Fo}{(\Delta X)^2} (\Theta_{i,j+1}^n - 2\Theta_{i,j}^n + \Theta_{i,j-1}^n) + \frac{\Delta Fo}{m^2(\Delta X)^2} (\Theta_{i+1,j}^n - 2\Theta_{i,j}^n + \Theta_{i-1,j}^n) \\
&\quad + \Theta_{i,j}^n + N1\Delta Fo \\
&= \frac{1}{m^2} \Theta_{i,j}^n \left[m^2 - 2m^2 \frac{\Delta Fo}{(\Delta X)^2} - 2 \frac{\Delta Fo}{(\Delta X)^2} \right] + \frac{\Delta Fo}{(\Delta X)^2} \left[m^2 (\Theta_{i,j+1}^n + \Theta_{i,j-1}^n) \right. \\
&\quad \left. + \Theta_{i+1,j}^n + \Theta_{i-1,j}^n \right] + m^2 N1 \Delta Fo \}
\end{aligned}$$

Defining the Convergence Criterion F (Ref. 2)

$$\text{Let } F = \frac{\Delta Fo}{(\Delta X)^2} = \frac{\alpha \Delta t / l^2}{(\Delta X)^2 / l^2} = \frac{\alpha \Delta t}{(\Delta X)^2}$$

$$\begin{aligned}
\Theta_{i,j}^{n+1} &= \frac{1}{m^2} \left[\Theta_{i,j}^n (m^2 - (2m^2 + 2)F) + m^2 F (\Theta_{i,j+1}^n + \Theta_{i,j-1}^n) + F (\Theta_{i+1,j}^n + \Theta_{i-1,j}^n) \right. \\
&\quad \left. + m^2 N1 (\Delta X)^2 F \right] \tag{3-18}
\end{aligned}$$

This node equation is used to calculate the temperature of the interior node at time $n+1$.

In the same manner, we can solve the node equations for transient conduction with various boundary conditions (details show in Appendix B).

The equations involved are shown as follows:

The interior node equations for composite materials.

$$\begin{aligned}
\Theta_{i,j}^{n+1} &= 2F1 \frac{k1}{k3} (\Theta_{i,j-1}^n - \Theta_{i,j}^n) - 2F1 \frac{k2}{k3} (\Theta_{i,j}^n - \Theta_{i,j+1}^n) + \Theta_{i,j}^n \\
&\quad + \frac{F1}{m^2} (\Theta_{i-1,j}^n - 2\Theta_{i,j}^n + \Theta_{i+1,j}^n) + 2F1 N2 (\Delta X)^2 \tag{3-19}
\end{aligned}$$

where k_1 = The thermal conductivity of material 1.

k_2 = The thermal conductivity of material 2.

$K_3 = k_1 + k_2$.

$N_2 = Ql^2/k_3(T - T_B)$.

The node equation for convection at the left vertical surface.

$$\begin{aligned} \Theta_{i,j}^{n+1} = \frac{1}{m^2} \left[(m^2 - (2m^2+4)F) \Theta_{i,j}^n + 2m^2F\Theta_{i,j+1}^n + 2F(\Theta_{i+1,j}^n + \Theta_{i-1,j}^n) \right. \\ \left. + 2m^2N_1(\overline{\Delta X})^2F - 2m^2Bi_T \overline{\Delta X}F(\Theta_{i,j}^n - \Theta_T^n) \right] \end{aligned} \quad (3-20)$$

The node equation for convection at the right vertical surface

$$\begin{aligned} \Theta_{i,j}^{n+1} = \frac{1}{m^2} \left[(m^2 - (2m^2+4)F)\Theta_{i,j}^n + 2m^2F\Theta_{i,j-1}^n + 2F(\Theta_{i+1,j}^n + \Theta_{i-1,j}^n) \right. \\ \left. + 2m^2N_1(\overline{\Delta X})^2F - 2m^2Bi_R \overline{\Delta X}F(\Theta_{i,n}^n - \Theta_R^n) \right] \end{aligned} \quad (3-21)$$

The node equation for convection at the top surface:

For the left corner node

$$\begin{aligned} \Theta_{i,j}^{n+1} = \frac{1}{m^2} \left[(m^2 - (2m^2+2)F)\Theta_{i,j}^n + 2m^2F\Theta_{i,j+1}^n + 2F\Theta_{i+1,j}^n \right. \\ \left. + 2m^2N_1(\overline{\Delta X})^2F - 2m(m+1)Bi_T \overline{\Delta X}F(\Theta_{i,j}^n - \Theta_T^n) \right] \end{aligned} \quad (3-22)$$

For the right corner node

$$\begin{aligned} \Theta_{i,j}^{n+1} = \frac{1}{m^2} \left[(m^2 - (2m^2+2)F)\Theta_{i,j}^n + 2m^2F\Theta_{i,j-1}^n + 2F\Theta_{i+1,j}^n + 2m^2N_1(\overline{\Delta X})^2F \right. \\ \left. - 2m(m+1)Bi_T \overline{\Delta X}F(\Theta_{i,j}^n - \Theta_T^n) \right] \end{aligned} \quad (3-23)$$

For the remaining top surface nodes

$$\begin{aligned} \Theta_{i,j}^{n+1} = \frac{1}{m^2} & \left[(m^2 - (4m^2+2)F)\Theta_{i,j}^n + 2m^2F(\Theta_{i,j+1}^n + \Theta_{i,j-1}^n) + 2F\Theta_{i+1,j}^n \right. \\ & \left. + 2m^2N1(\overline{\Delta X})^2F - 2mB_{i_T}\overline{\Delta X}F(\Theta_{i,j}^n - \Theta_T^n) \right] \end{aligned} \quad (3-24)$$

The node equation for convection at the bottom (end) surface:

For the left corner node

$$\begin{aligned} \Theta_{i,j}^{n+1} = \frac{1}{m^2} & \left[(m^2 - (2m^2+2)F)\Theta_{i,j}^n + 2m^2F\Theta_{i,j+1}^n + 2F\Theta_{i-1,j}^n + 2m^2N1(\overline{\Delta X})^2F \right. \\ & \left. - 2m(m+1)\overline{\Delta X}B_{i_E}F(\Theta_{i,j}^n - \Theta_E^n) \right] \end{aligned} \quad (3-25)$$

For the right corner node

$$\begin{aligned} \Theta_{i,j}^{n+1} = \frac{1}{m^2} & \left[(m^2 - (2m^2+2)F)\Theta_{i,j}^n + 2m^2F\Theta_{i,j-1}^n + 2F\Theta_{i-1,j}^n + 2m^2N1(\overline{\Delta X})^2F \right. \\ & \left. - 2m(m+1)\overline{\Delta X}B_{i_E}F(\Theta_{i,j}^n - \Theta_E^n) \right] \end{aligned} \quad (3-26)$$

For the remaining end surface node

$$\begin{aligned} \Theta_{i,j}^{n+1} = \frac{1}{m^2} & \left[(m^2 - (4m^2-2)F)\Theta_{i,j}^n + 2m^2F(\Theta_{i,j+1}^n + \Theta_{i,j-1}^n) + 2F\Theta_{i-1,j}^n \right. \\ & \left. + 2m^2N1(\overline{\Delta X})^2F - 2m\overline{\Delta X}B_{i_E}F(\Theta_{i,j}^n - \Theta_E^n) \right] \end{aligned} \quad (3-27)$$

$$\text{where } \Theta_L^n = \frac{T_{\infty,L}^n - T_B^n}{T_i^n - T_B^n} = \Theta_E^n \text{ and } Bi_L = \frac{\bar{h}_L \ell}{k} = Bi_E$$

$$\Theta_T^n = \frac{T_{\infty,T}^n - T_B^n}{T_i^n - T_B^n} = \Theta_R^n \text{ and } Bi_T = \frac{\bar{h}_T \ell}{k} = Bi_R$$

For adiabatic surfaces the node equations are identical except the Biot number Bi is zero.

CHAPTER 4

APPLICATION OF THE FINITE DIFFERENCE TECHNIQUE TO HEAT TRANSFER OF THE CRYOMICROSCOPE CONDUCTION STAGE

Now that all of the necessary node equations of both steady-state and transient conduction have been developed, these node equations will be applied to the Cryomicroscope Conduction stage. The assumptions made to solve the problem are given below.

4.1 Assumptions

- 1) Neglect heat transfer in the glass, epoxy and the tape (see Appendix C).
- 2) Assume two-dimensional conduction (Unit depth) because earlier experimental data has shown that there is not much temperature difference in one dimension as shown in Figure 4.1.
- 3) Due to symmetry, we consider only one half of the Cryomicroscope Conduction Stage and therefore the centerline nodes are an adiabatic surface.
- 4) The equations are set up in rectangular coordinates because the heat dissipation area is a rectangular geometry. (This should be especially valid for the experimental results.)
- 5) The quartz and copper materials are assumed to be in perfect contact.
- 6) Each material is stationary and homogeneous with constant properties.

Figure 4.2 shows the grid network for the Cryomicroscope

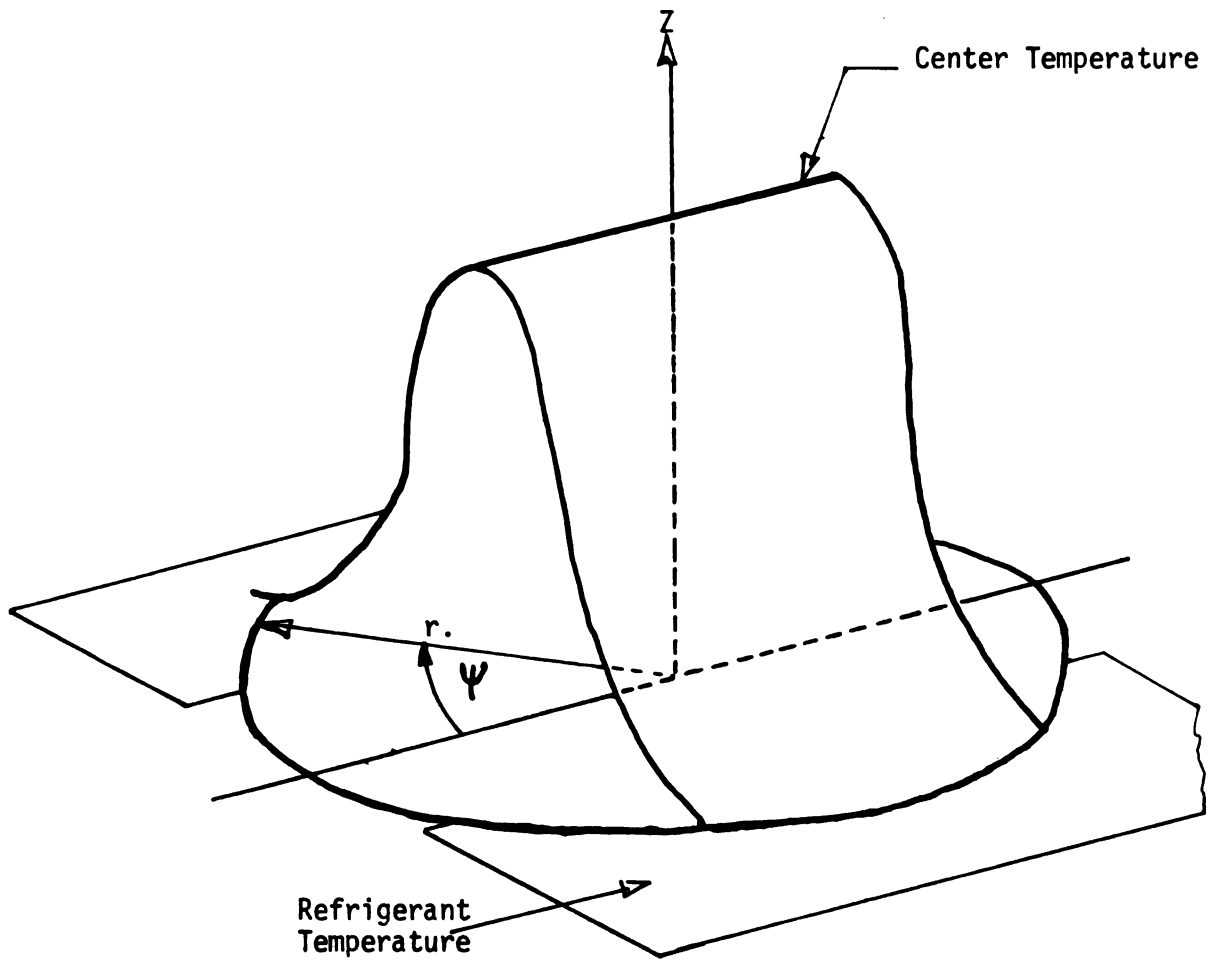


Figure 4.1 Three-Dimensional Conduction Stage Temperature Profile.

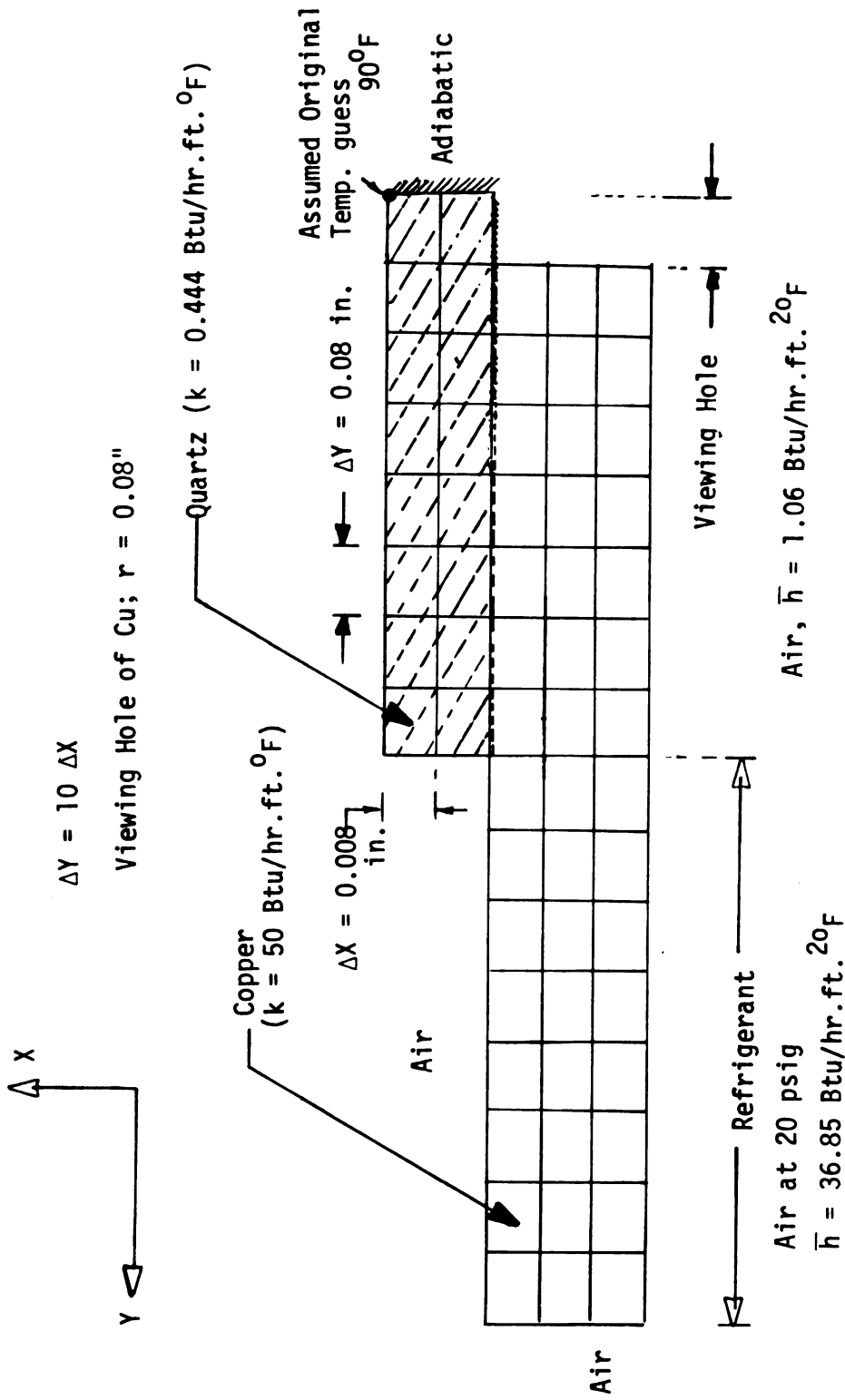


Figure 4.2 Approximation Grid Network of the Cryomicroscope Conduction Stage

Conduction Stage that will be used to approximate the temperature and heat transfer with the finite difference method.

The quartz on the top of the copper plate has a radius of 0.64 in. and is 0.016 in. thick.

The copper plate is 1.28 in. long and 0.024 in. thick with a viewing hole radius of 0.08 in. at the centerline.

All of the surfaces in Figure 4.2 are in contact with air where $\bar{h} = 1.06 \text{ Btu/hr ft}^2 \text{ } ^\circ\text{F}$ (see Appendix D-2). However, at a distance of 0.64 in. from the bottom end of the copper plate, the plate is cooled by the refrigerant (air) at 20 psig, 89°F with $\bar{h} = 36.85 \text{ Btu/hr ft}^2 \text{ } ^\circ\text{F}$ (see Appendix D-1) and the centerline grids are at an adiabatic surface.

The heat is assumed to be generated between the interface of quartz and copper within a distance of 0.24 in. from the centerline. It is assumed to dissipate a power of 5 watts, which corresponds to a heat generation of $8.5 \times 10^5 \text{ Btu/hr ft}^3$.

Assuming $\Delta X = 0.008 \text{ in.}$ and $\Delta Y = 0.08 \text{ in.}$, 82 nodes are created to approximate the temperature distribution for both steady-state and transient conduction cases.

4.2 Numerical Analysis for Two-Dimensional Steady State Conduction

The solution of two-dimensional steady-state conduction problems requires the determination of the nodal temperatures in the finite difference grid. The temperature of each node must satisfy the appropriate node equation. In order to calculate the temperature at each node in the grid, a scheme must be devised so that calculations at each node are made in a sequential manner by means of the proper

nodal equations until all nodal temperature are known. All nodes must be assigned an initial value to begin the calculations. These initial values should be based on known boundary conditions and estimated internal temperatures.

Consider a two-dimensional grid network of the conduction stage shown in Figure 4.2. The ambient temperature and the air refrigerant temperature are approximated as 89°F. Assume the initial temperature at the centerline to be $T_C \sim 90^\circ\text{F}$.

$$\text{Then } \theta_C = \frac{T_C - T_B}{T_C - T_B} = 1.0$$

$$\theta_B = \frac{T_B - T_B}{T_C - T_B} = 0$$

Thus the non-dimensional temperature distribution will vary from 0 to 1.

Now the computer model for steady-state conduction developed in Reference 2 will be applied. This computer program is written to solve the temperature distribution in the rectangular region of the Cryomicroscope Conduction Stage. The temperature of each node must satisfy the appropriate nodal equations from Equations (3-4) through (3-15). The variables and constants have been assigned in order to make the computer modeling simple and easy to use. A list of the variables used in this program is given in Table 4.1. The rows and columns in the computer program are noted by i's and j's, respectively.

The computer modeling program for the two-dimensional steady-state case for the Cryomicroscope Conduction Stage is shown in the form of a flow diagram (Figure 4.3). Throughout the calculations, $X(I,J)$ represents

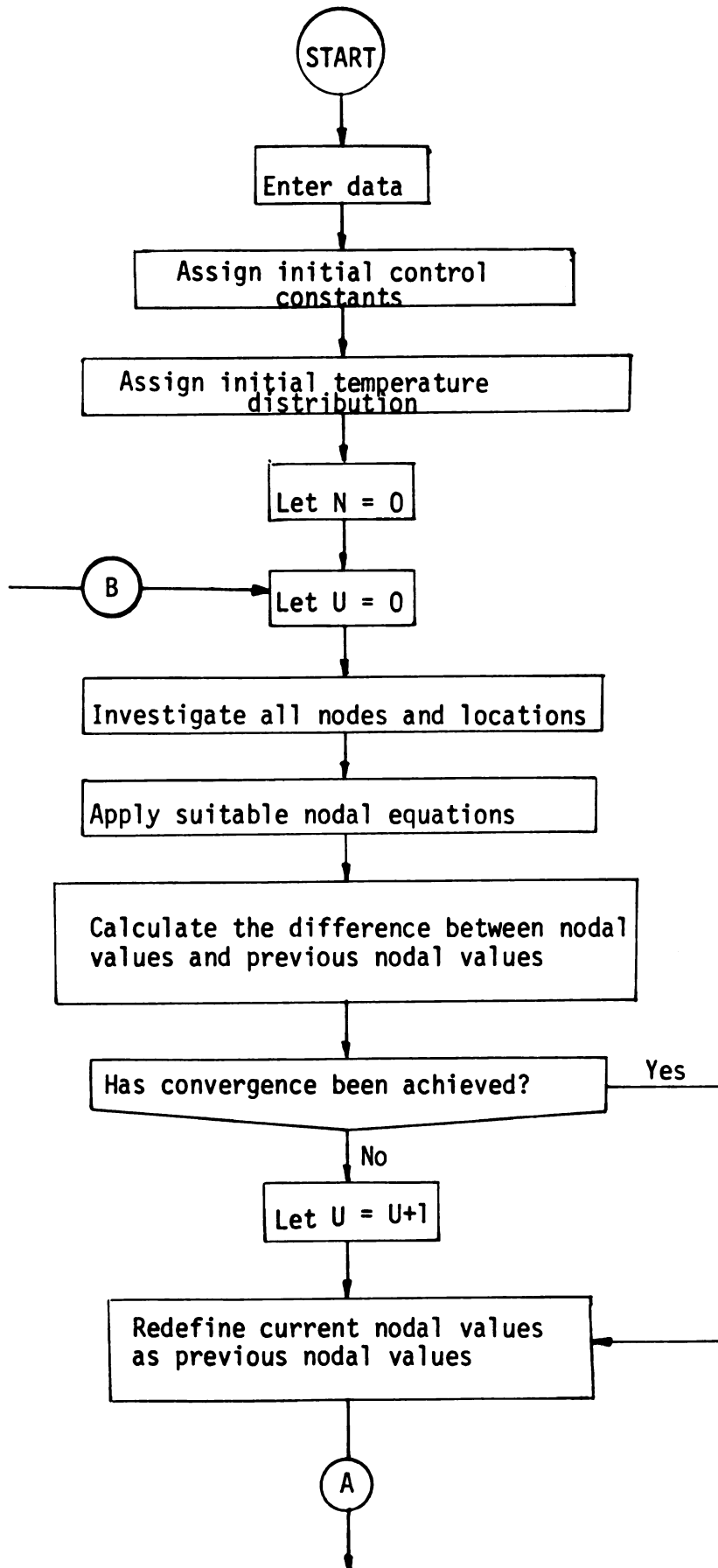


Figure 4.3 Flow Diagram for the Steady-State Computer Program.

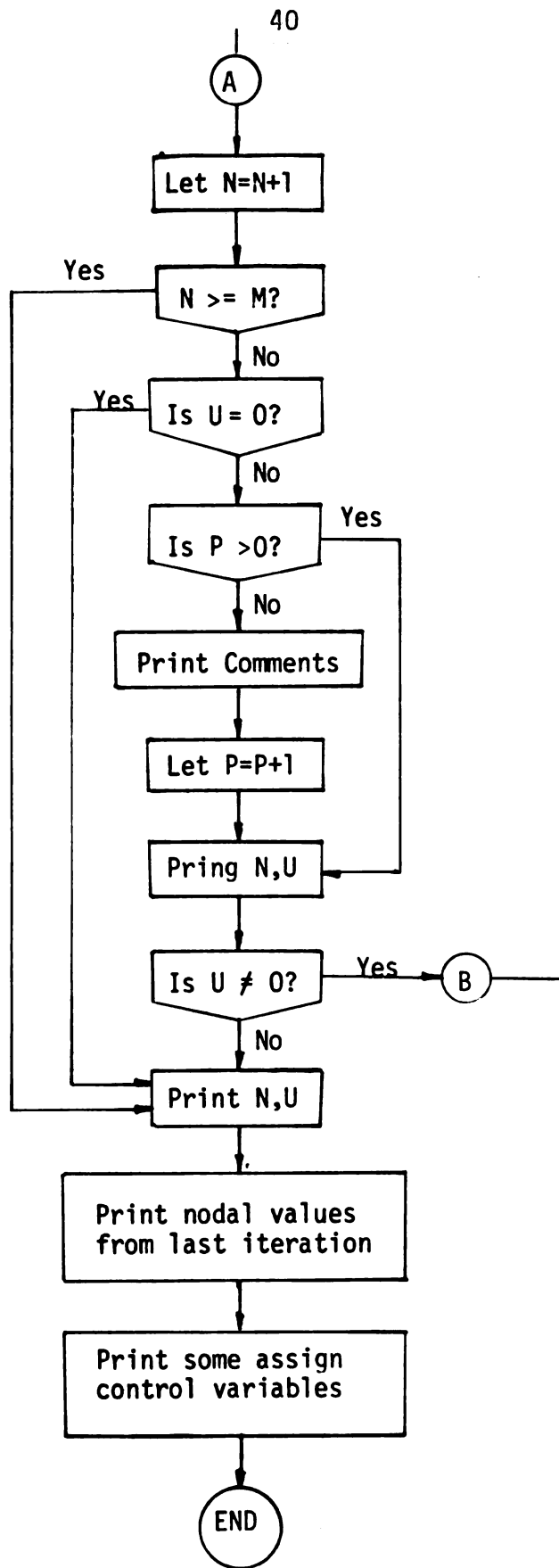


TABLE 4.1

Variables for the Steady-State
Conduction Program

<u>Variables</u>	<u>Definition</u>
T(I,J)	Current nodal temperature
X(I,J)	Newly calculated nodal temperature
Y(I,J)	Difference in nodal temperature
Z(I,J)	Truncated nodal temperature
B1	$Bi_L = \bar{h}_L \ell_1 / k_1 = 0.118$
B2	$Bi_E = \bar{h}_E \ell_1 / k_1 = 0.118$
B3	$Bi_R = \bar{h}_R \ell_2 / k_2 = 0.002$
B4	$Bi_T = \bar{h}_T \ell_2 / k_2 = 0.002$
B5	$Bi_{ref.} = \bar{h}_{ref.} \ell_2 / k_2 = 0.079$
B6	$Bi = \bar{h}_L \ell_1 / (k_1 + k_2) = 0.001$
D1	$\overline{\Delta X_1} = X / \ell_1$
D2	$\overline{\Delta X_2} = X / \ell_2$
E1	Convergence criterion = 0.001
I1, I2	Number of insulated nodes on the left and right surfaces
M,N,P	Counting variable
N1	$Q \ell_1^2 / k_1 (T_C - T_B) = 0$
N2	$Q \ell_1^2 / (k_1 + k_2) (T_C - T_B) = 24.2$
N3	$Q \ell_2^2 / k_2 (T_C - T_B) = 0$
U	Number of nodes not satisfying convergence criterion
X1	Number of grid points along $\bar{Y} = 0$
Y1	Number of grid points along $\bar{X} = 0$

the current calculated values in the nodal matrix, and $T(I,J)$ represents the previously calculated values in the nodal matrix. $Y(I,J)$ is the difference between the current nodal value and the previously calculated nodal value. The convergence of the calculation is indicated by the value of $Y(I,J)$. As the calculation proceeds, the difference between the newly calculated nodal values and the previously calculated values becomes smaller, and the correct temperature distribution is approached. The allowable difference is a function of the accuracy required in the calculations. This allowable difference is determined by the programmer and is read into the computer as the variable $E1$ (in this case $E1 = 0.001$).

After one complete iteration of all nodes, the value of N is increased by an increment $N = N+1$ to account for the number of iterations completed. If convergence has not been achieved after a maximum number of iterations ($M = 300$), provision is made to terminate the iteration procedure. The program concludes by printing out the final non-dimensional temperature along with parameters. Typical results are shown in graphical form in Figure 4.4 and these will be compared to the experimental data and the results discussed in the next chapter.

4.3 Numerical Analysis for Two-Dimensional Transient Conduction

Consider the analysis of transient, two-dimensional conduction of the Cryomicroscope Conduction Stage with constant properties and internal heat generation terms shown in Figure 4.2. In chapter 3 we obtained the node equations to use in the transient conduction case for various boundary conditions. Recall that in the finite difference

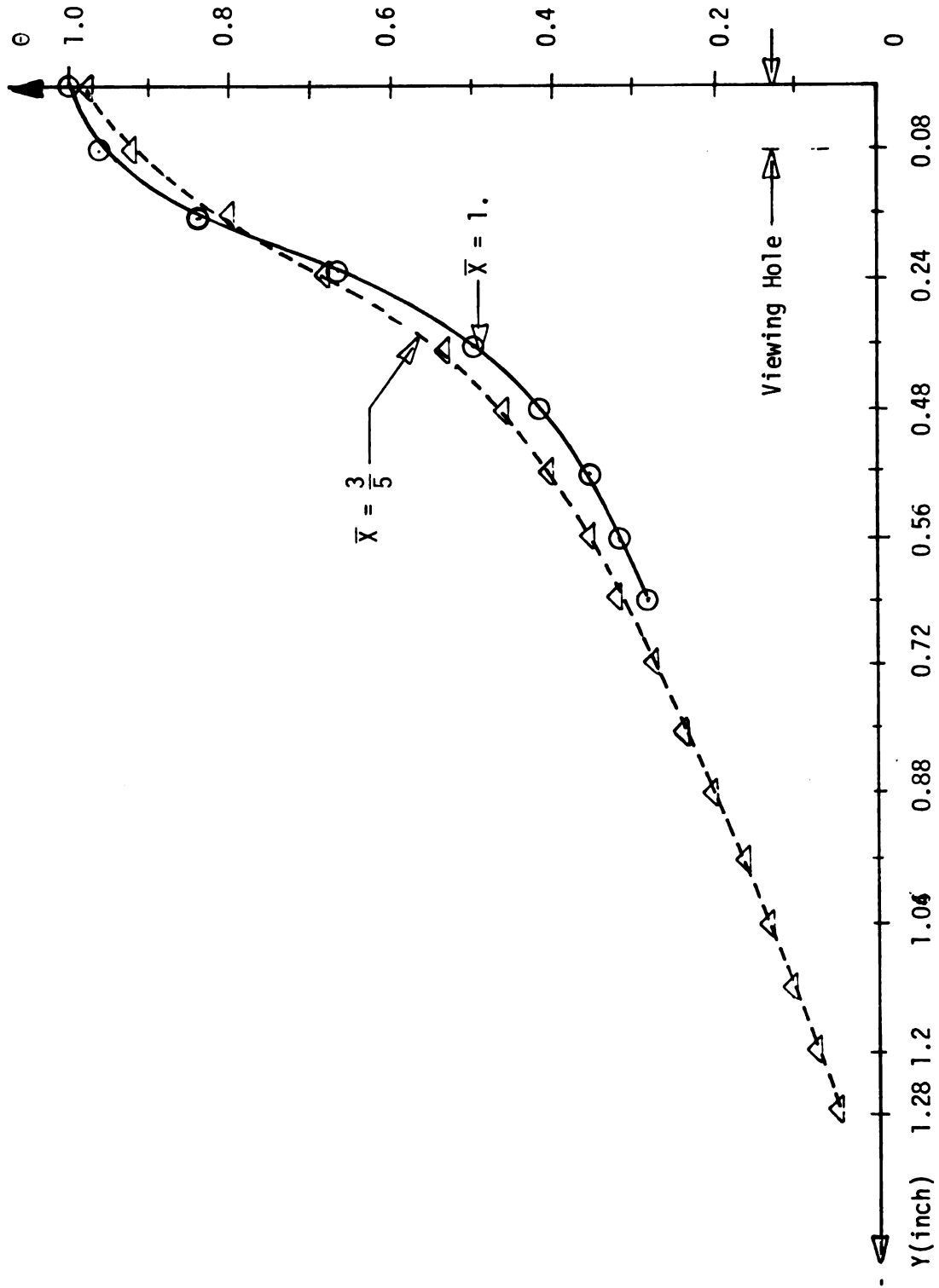


Figure 4.4 Two-Dimensional Steady-State Conduction of the Cryomicroscope Conduction Stage.

approximations to the governing equations, that it is necessary to initially assign arbitrary temperatures to all nodes within the grid under consideration.

In the analysis of transient conduction we must accurately specify the initial condition of each node within the grid. Therefore it is not necessary to continually recalculate the initially assigned temperature values to reach the solution. Once the proper step size ΔX , ΔY and a time increment Δt are chosen, we apply the finite difference equations to each nodal point for each successive time increment. A thermal disturbance propagates only at times greater than the initial disturbance which occurs at time $t = 0$.

In our case, we assumed that at time $t = 0$, the initial temperature of all nodes $T_{i,j}^0$ are equal to the ambient temperature (90°F) and the refrigerant temperature is 1°F lower than the initial nodal temperature with zero internal heat generation.

$$\text{For } \theta = \frac{T - T_B}{T_i - T_B}$$

$$\theta_{i,j}^0 = 1.0$$

$$\theta_B^0 = 0.$$

After increasing the time increment, and maintaining the refrigerant temperature at the boundaries, the heater is turned on which causes the temperature of all nodes to be increased by the heat generation term. In order to obtain the solution of the transient conduction problem, the temperature of each node at a given time must satisfy the appropriate nodal equation. The necessary nodal equations shown in Chapter 3 are applied to each node to calculate the new values of the nodal temperature

at the particular time increment.

For the explicit finite difference approximation method, it is necessary to insure convergence in order to calculate the temperature distribution with the node equations developed. According to Chapter 3 of Reference 4 and Chapter 4 of Reference 6, the limiting values of the convergence criterion $\alpha\Delta t/(\Delta X)^2$ when using the central difference approximation for convective boundary conditions cases is given by:

$$F = \frac{\overline{\Delta t}}{(\Delta X)^2} + \frac{\overline{\Delta t}}{(\Delta Y)^2} \leq \frac{1}{2+\overline{h}\Delta X/k}$$

In our case $\Delta Y = 10 \Delta X$, therefore:

$$F = \frac{101}{100} \frac{\alpha\Delta t}{(\Delta X)^2} \leq \frac{1}{2+\overline{h}\Delta X/k}$$

$$F = \frac{\alpha\Delta t}{(\Delta X)^2} \leq \frac{100}{101(2+Bi_0 \overline{\Delta X})} \quad (4-1)$$

where $Bi_0 = \frac{\overline{h}l}{k}$

Applying this criterion to the cryomicroscope conduction stage where the average $\overline{h} = 9.93 \text{ Btu/hr.ft}^{20}\text{F}$ (see Appendix D-3)

$$(\Delta X)^2 = 4.44 \times 10^{-5} \text{ ft}^2.$$

$$\Delta t = 0.25 \text{ sec.}$$

$$Bi_0 \leq 0.028$$

Substituting into Equation (4-1)

$$F = \frac{(7.8 \times 10^{-5} \text{ ft}^2/\text{sec})(0.25 \text{ sec})}{(4.44 \times 10^{-5} \text{ ft}^2)} \leq \frac{100}{101(2 + (0.025)(0.028))}$$

$$F = 0.437 \leq 0.495$$

This value gives acceptable accuracy for the finite difference approximation (Reference 4 and Reference 6).

The program discussed here has been written to obtain the solution to the transient temperature response for the boundary conditions and dimensions indicated in Figure 4.1. The variables, assigned constants and their physical meaning are given in Table 4.2 with the same Biot number and heat generation term as was used in the steady-state case.

The discussion above relates to the transient conduction program of the Cryomicroscope Conduction Stage given in the form of a flow diagram (Figure 4.4) and variables for the program in Table 4.2. The rows and columns in this computer program are denoted by i's and j's, respectively. The increment nondimensional time ($F_0^{n+1} - F_0^n = (\overline{\Delta X})^2 F_0^n$) where a time interval is denoted by a superscript n (Reference 2),

As the final steady-state temperature distribution is reached, the change in the nodal temperatures during each successive time interval approaches zero. For the boundary conditions being considered the values of $\theta_{i,j}^{n+1} - \theta_{i,j}^n$ approach zero, the steady-state value. The computation is terminated when the nondimensional temperature of a node is close to zero, $(\theta_{i,j}^{n+1} \leq \theta_{i,j}^n) \leq E$, where E is a small value (0.001).

An alternate way to terminate the calculations is to specify a maximum Fourier number. During the integration, the nondimensional temperatures for all nodes are changed to the actual temperatures ($^{\circ}F$) and printed at the specific time intervals expressed as both dimensional and nondimensional time. At the end of the program the values of k1, k2, B1, B2, B3, B4 and B5 are printed out after reaching the steady-state. The

TABLE 4.2

Variables for the Transient
Conduction Program

<u>Variables</u>	<u>Definition</u>
T(I,J)	Nondimensional temperature at time n
U(I,J)	Nondimensional temperature at time n+1
D(I,J)	Difference $U(I,J) - T(I,J)$
Z(I,J)	Nondimensional truncated temperatures
X(I,J)	Temperatures in Degree Fahrenheit used in the printout = $Z(I,J)(T_i - T_B) = T_B$
BO	$Bi_0 = 0.028$
C	Counting variable
E	Minimum value of D(I,J) used to terminate the computation
F	Convergence criterion = $\alpha \Delta t / (\Delta X)^2 = 0.437$
F0	Fourier number = $\alpha t / \ell^2$
F1	Convergence criterion of double material = $\alpha * \Delta t / (\Delta X)^2 = 0.371$
G	Time to be print out = $\ell^2 F0 / \alpha$
M	Number of grid points along $\bar{Y} = 0$
N	Number of grid points along $\bar{X} = 0$
P	Print interval
X1	$\overline{\Delta X1} = X / \ell 1$
X2	$\overline{\Delta X2} = X / \ell 2$

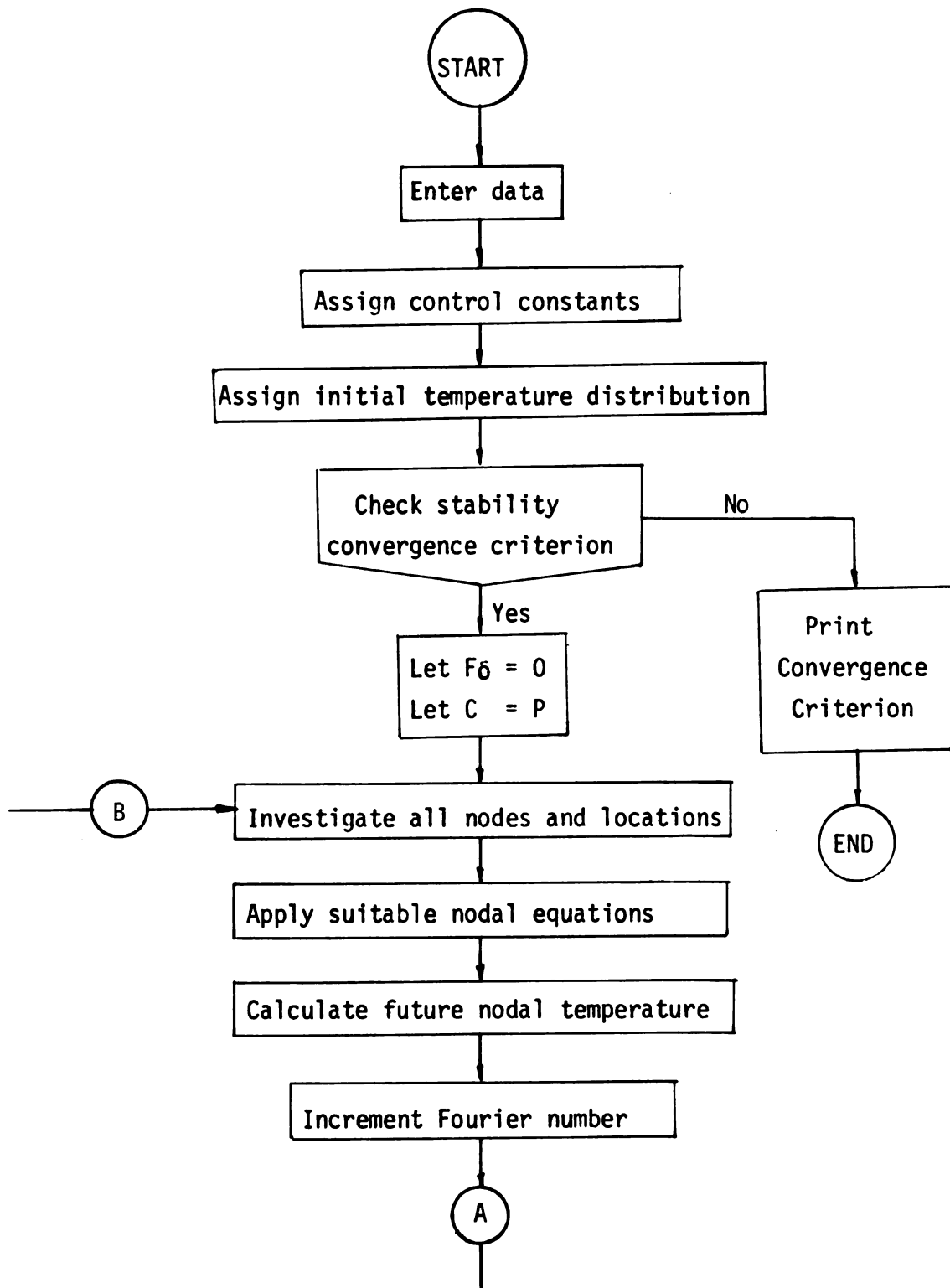
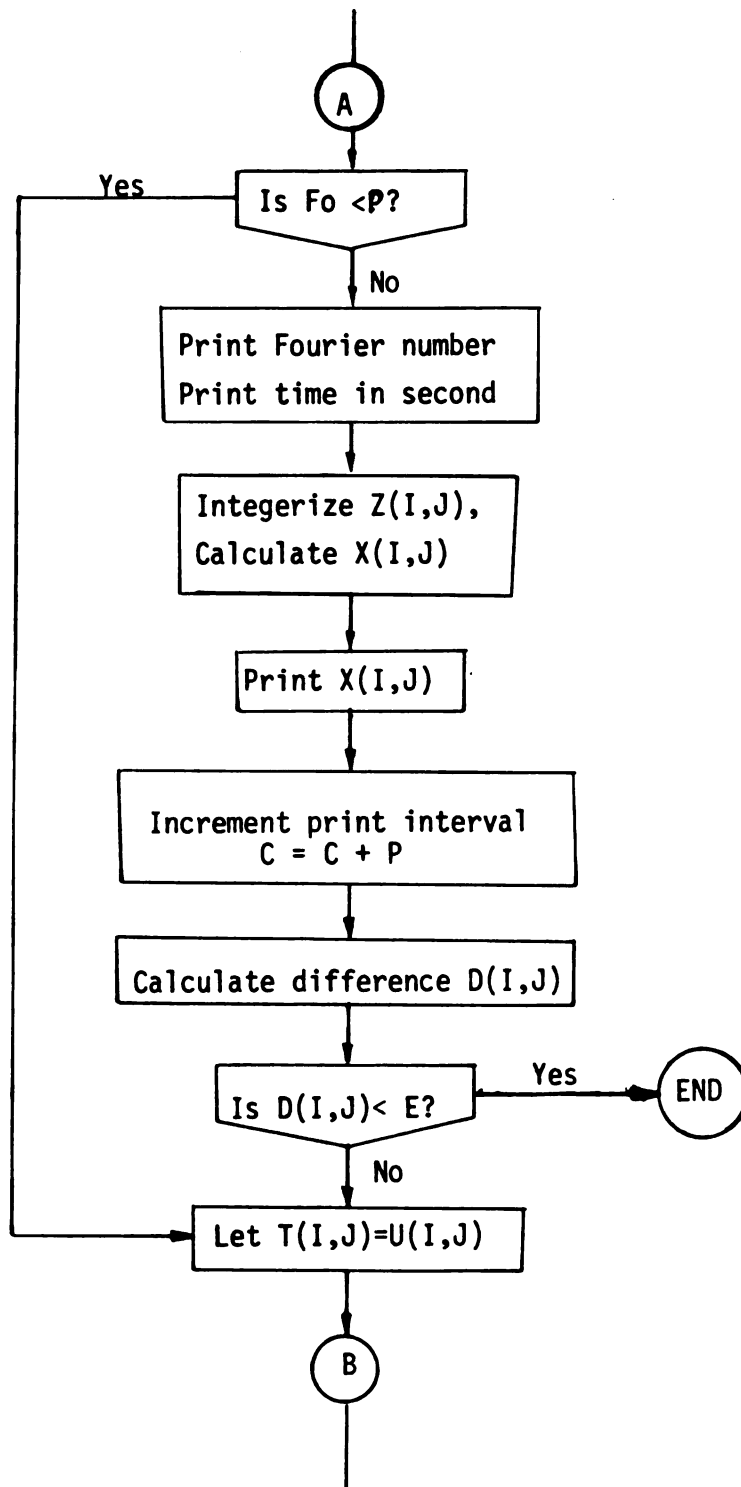


Figure 4.5 Flow Diagram for the Transient Conduction Program.



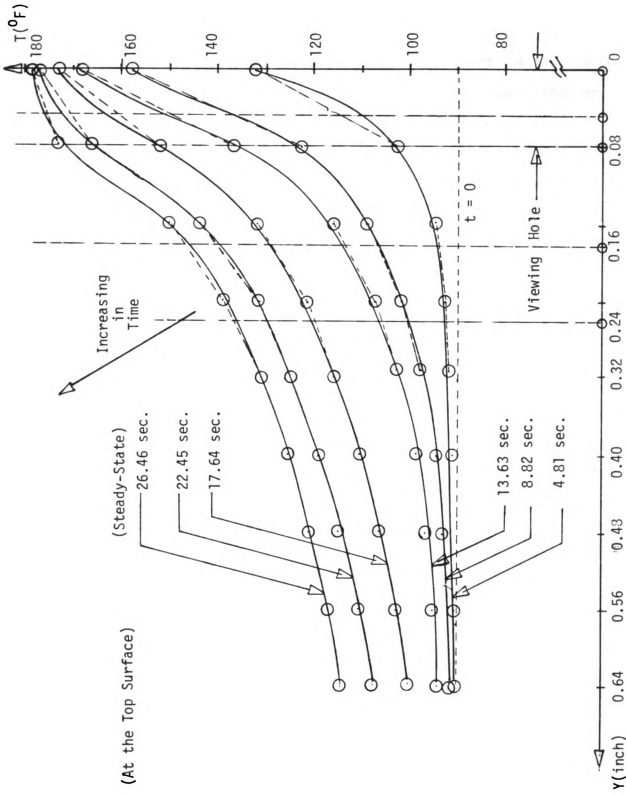


Figure 4.6 Computer Modeling Results for the Transient Conduction.

numerical results for transient conduction of the Cryomicroscope
Conduction stage shown in graphical form in Figure 4.6 will be compared
to the experimental data and discussed in the following chapter.

CHAPTER 5

EXPERIMENTAL RESULTS FOR THE CRYOMICROSCOPE CONDUCTION STAGE

5.1 Description of the Experimental Equipment

To test the validity of the numerical computer results, experiments were performed to find the temperature distribution on the Cryomicroscope Conduction Stage for the steady-state and transient conduction case. The experimental equipment shown schematically in Figure 5.1 was used to obtain these results.

Figure 5.1 shows the following set of equipment:

- 1) Cryomicroscope Conduction Stage
- 2) Precision Fine Wire Thermocouples (Copper-Constantan)
0.001 in. diameter
- 3) Regulated DC Power Supply
- 4) Selected Switch for Thermocouples
- 5) Digital Temperature Meter (DTM)
- 6) Strip Chart Recorder
- 7) Air Pressure Regulator

Six precision fine wire thermocouples (0.001" dia) were placed on the top surface of the Cryomicroscope Conduction Stage in various locations with tiny drops of epoxy as shown in Figure 5.2. The thermocouples were attached to the input of the Selected Switch. The output of this switch was plugged into the input of the DTM.

The Strip Chart Recorder was connected to the output of DTM to

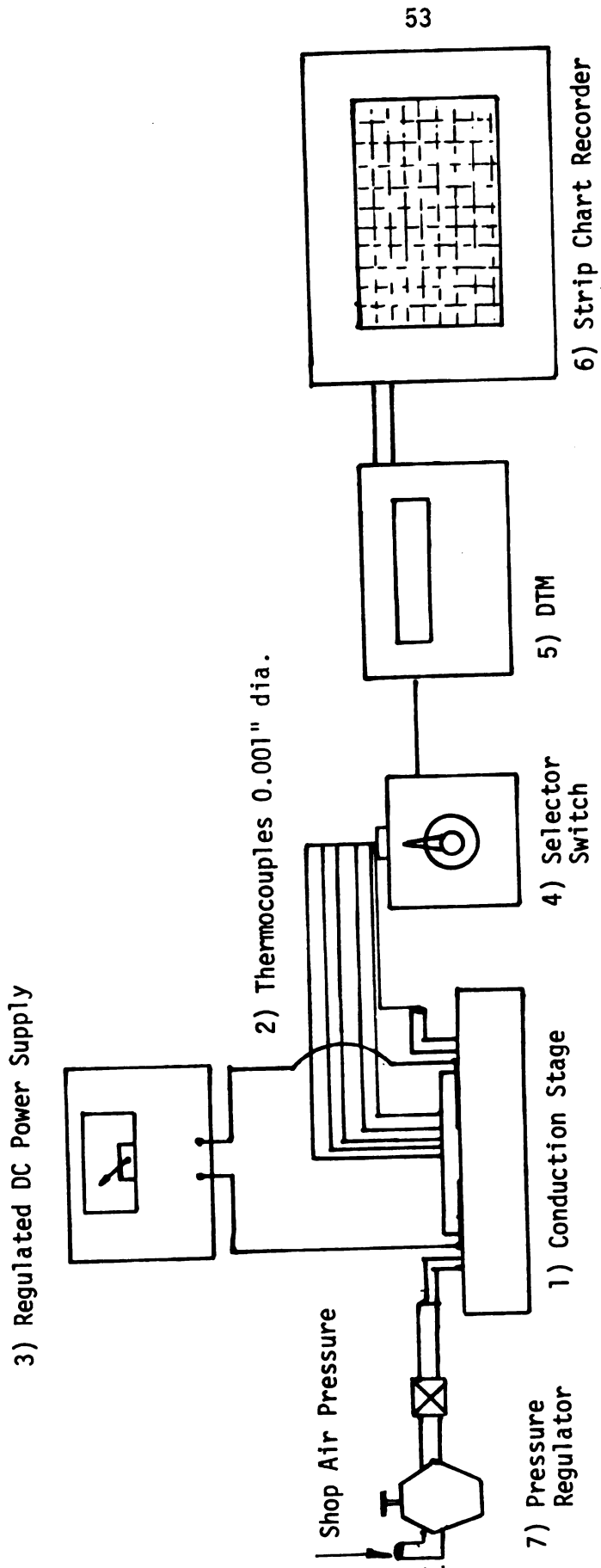
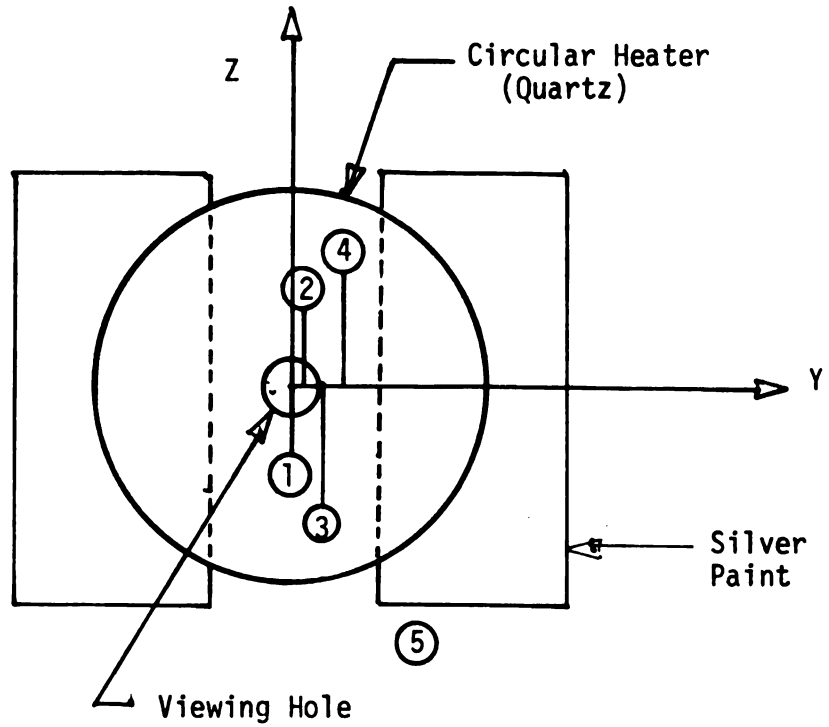


Figure 5.1 Experimental Schematic of the Cryomicroscope Conduction Stage.



- T_1 at ① Centerline
 T_2 at ② 0.047 in.
 T_3 at ③ 0.08 in.
 T_4 at ④ 0.18 in.
 T_5 at ⑤ 0.26 in.
 T_6 measured at Refrigerant exhaust

Figure 5.2 Temperature Measurement with the Thermocouples at Various Radial Positions.

record the change of temperature with time. The output of a Regulated DC Power Supply was connected to the copper power connections of the Cryomicroscope Conduction Stage to allow heat generation when desired.

The Air Pressure-Regulator was used to control the intake pressure of the refrigerant of the Cryomicroscope Conduction Stage. The other exit port exhausted to ambient pressure.

5.2 Experimental Technique for Steady-State Conduction

When the experimental equipment had been set up, the pressure from the Air Pressure Regulator was adjusted to 20 psig. The power supply was set at 5 Watts for this experiment with a total resistance of 17.0 ohms.

$$\text{From } P = \bar{V}^2 / \bar{R}$$

$$\bar{V} = \sqrt{P \times R}$$

$$= \sqrt{5 \times 17} = 9.22 \text{ volts}$$

Thus the Regulated DC Power Supply was set at 9.22 volts.

The Digital Temperature Meter (DTM) provides a linearized analog output (1mV/°C) with 0mV equal to 0°C. This output was used to drive the Strip Chart Recorder where the range was adjusted from 0 to 100 MV corresponding to the temperature range from 0 to 100°C. The chart speed used was 93.75 mm/min.

With no power dissipated in the heater, measurements showed that the Cryomicroscope Conduction Stage was isothermal, with a temperature reading at all six positions of 32°C.

Transient tests were initiated by a step input of power supplied to the heater by the Regulated Power Supply. This experimental method

also yielded steady-state data after "long" experimental times when all values at a given position converged to a final reading. Data from the Strip Chart Recorder indicated a rapid temperature increase in a short time (about 20-30 seconds) before remaining constant at about 82°C . Each experiment was repeated three times and the temperatures were recorded. The same procedure was repeated for each of the other positions of thermocouples three times and the temperatures were recorded from the DTM on the Strip Chart Recorder.

5.3 Experimental Technique for Transient Conduction

For the steady-state conduction situation we could read the temperature directly from the DTM as shown in Table 5.1 after long periods of time. For the transient conduction situation the approximate temperature and time were read from the graph plotted from the Strip Chart Recorder as shown in Figure 5.3. Figure 5.3 shows a typical change of temperature for the centerline position. The other thermocouple positions were similar to Figure 5.3.

Figure 5.3 is for the chart speed of 93.75 mm/min. , in the vertical direction of 10 mm. is equal to 6.4 seconds. We see that at time equal to zero the temperature shows about 32°C . After turning on the power supply from the Regulated DC Power Supply, the curve starts to rise at time zero until the temperature remains constant. We approximate the change of temperature with time at every point along the curve and the conclusions of the experimental results are shown in Table 5.2.

Table 5.1 and Table 5.2 are experimental results with:

Table 5.1

Numerical Experimental Results for the
Steady-State Conduction of the
Cryomicroscope Conduction Stage

Temperature	Degree Celsius ($^{\circ}\text{C}$)				$^{\circ}\text{F}$	θ
	1st	2nd	3rd	Average		
T_1	82.5	82	82	82.17	179.9	1.0
T_2	80.5	80.5	81	80.76	177.4	0.972
T_3	79	78	80	79	174.1	0.936
T_4	64.5	64	65	64.5	148.1	0.649
T_5	59.5	59.5	60	59.7	139.4	0.553
T_6	31.5	32	32	31.8	89.2	0

The above results (in $^{\circ}\text{C}$) were read from the DTM three times and the average temperatures are given for the steady-state case

$$\theta = \frac{T - T_B}{T_C - T_B} = \frac{T - T_6}{T_C - T_6}$$

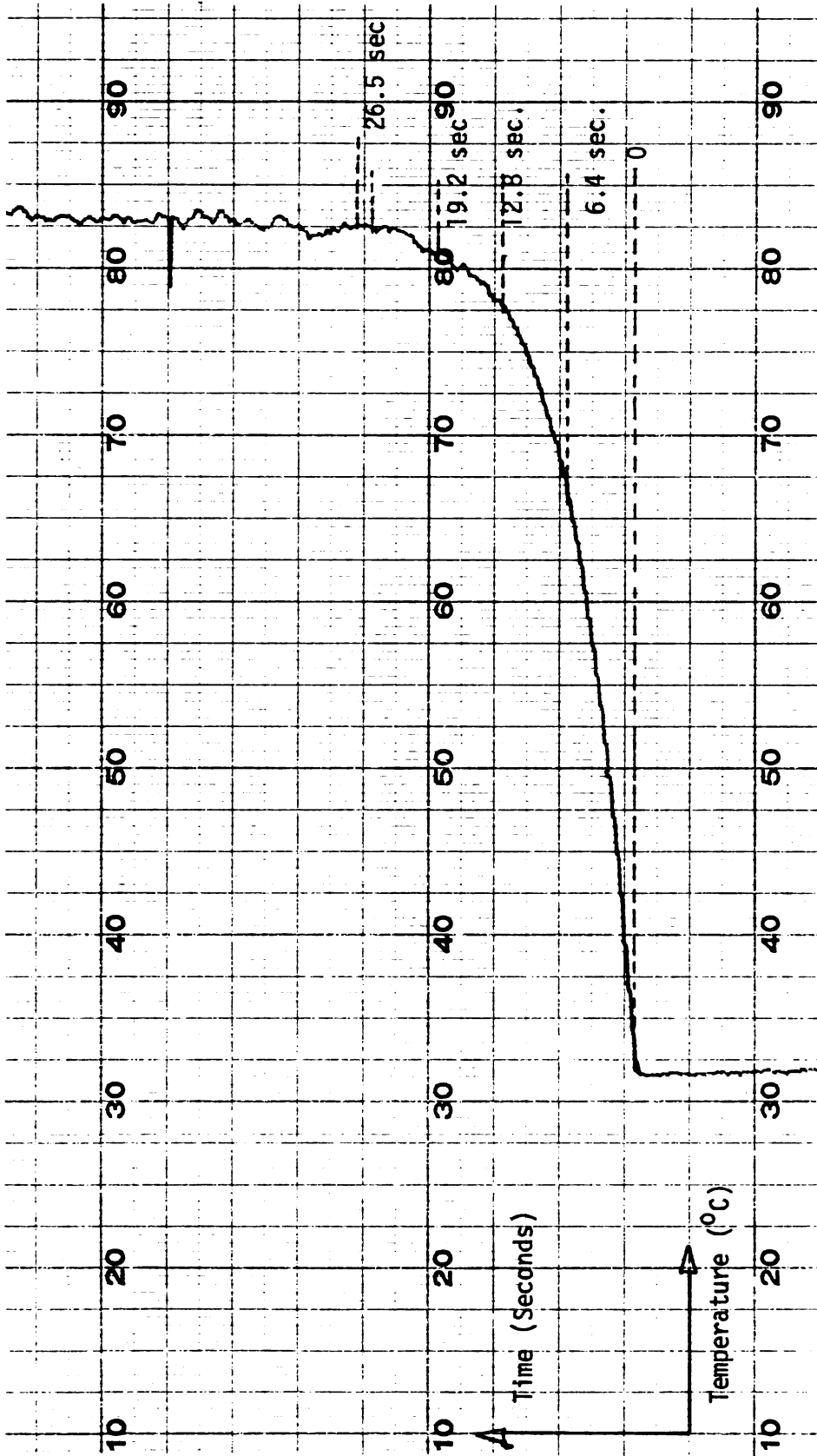


Figure 5.3 The Change of Temperature with Time Plotted from the Strip Chart Recorder (At the Centerline of the Cryomicroscope Conduction Stage).

Time	0 sec.		3.2 sec.		6.4 sec.		12.8 sec.		19.2 sec.		26.4 sec.	
	°C	°F	°C	°F	°C	°F	°C	°F	°C	°F	°C	°F
T ₁	32.2	90	54.5	130.1	64.5	147.1	77	177.5	81	177.8	82.2	179.9
T ₂	32.2	90	54.2	129.7	55.7	132.3	65.8	150.5	76.2	169.2	80.7	177.3
T ₃	32.2	90	37.2	99	55.5	131.9	60.6	141	70.2	158.4	79	174.3
T ₄	32.2	90	34.6	94.3	38.8	101.8	50	118.4	57.4	135.3	64.5	148.1
T ₅	32.2	90	33.4	92.1	36.4	97.5	42.3	108.2	51.3	124.3	59.7	139.4
T ₆	31.8	89.2	31.8	89.2	31.8	89.2	31.8	89.2	31.8	89.2	31.8	89.2

Table 5.2 Numerical Experimental Results for Transient Conduction (at the Top Surface) of the Cryomicroscope Conduction Stage.

Resistance 17 ohms

DC Power Supply 9.22 volts

Power 5 Watts

Ambient Temperature 90°F

Pressure of Air in the Refrigerant Chamber, 20 psig.

$T_1 = T_C$ at $r = 0$

T_2 at $r = 0.047$ inch

T_3 at $r = 0.08$ inch

T_4 at $r = 0.18$ inch

T_5 at $r = 0.26$ inch

$T_6 = T_B$ = The Refrigerant Temperature

CHAPTER 6

COMPARISON OF THE COMPUTER MODEL RESULTS WITH EXPERIMENTAL RESULTS

The purpose of this chapter is to compare the Computer Modeling Results with the Experimental Results of the Cryomicroscope Conduction Stage for both the steady-state and the transient conduction cases as shown in Figures 6.1 through Figure 6.7 in order to verify the accuracy of the model.

For the case of steady-state conduction, Figure 6.1 shows the comparison of the temperature distribution at the top surface of the Cryomicroscope Conduction Stage obtained from the Computer Modeling Results (curve 1) and from the Experimental Results (curve 2). We see that the temperature distributions of both curves are very similar but the temperature distribution from the Experimental Results (curve 2) is higher than the temperature distribution from the Computer Modeling Results. Overall, the temperature differences are less than 5% and can be considered satisfactory for an approximation to the actual temperature distribution for the steady-state performance of the Cryomicroscope Conduction Stage.

Recalling Figure 4.6 for the transient change of the temperature plotted from the Computer Modeling Results in the conduction case, if we use linear interpolation for each of the curves, we can approximate the temperatures at the same positions as those at the thermocouple position used in the experiment.

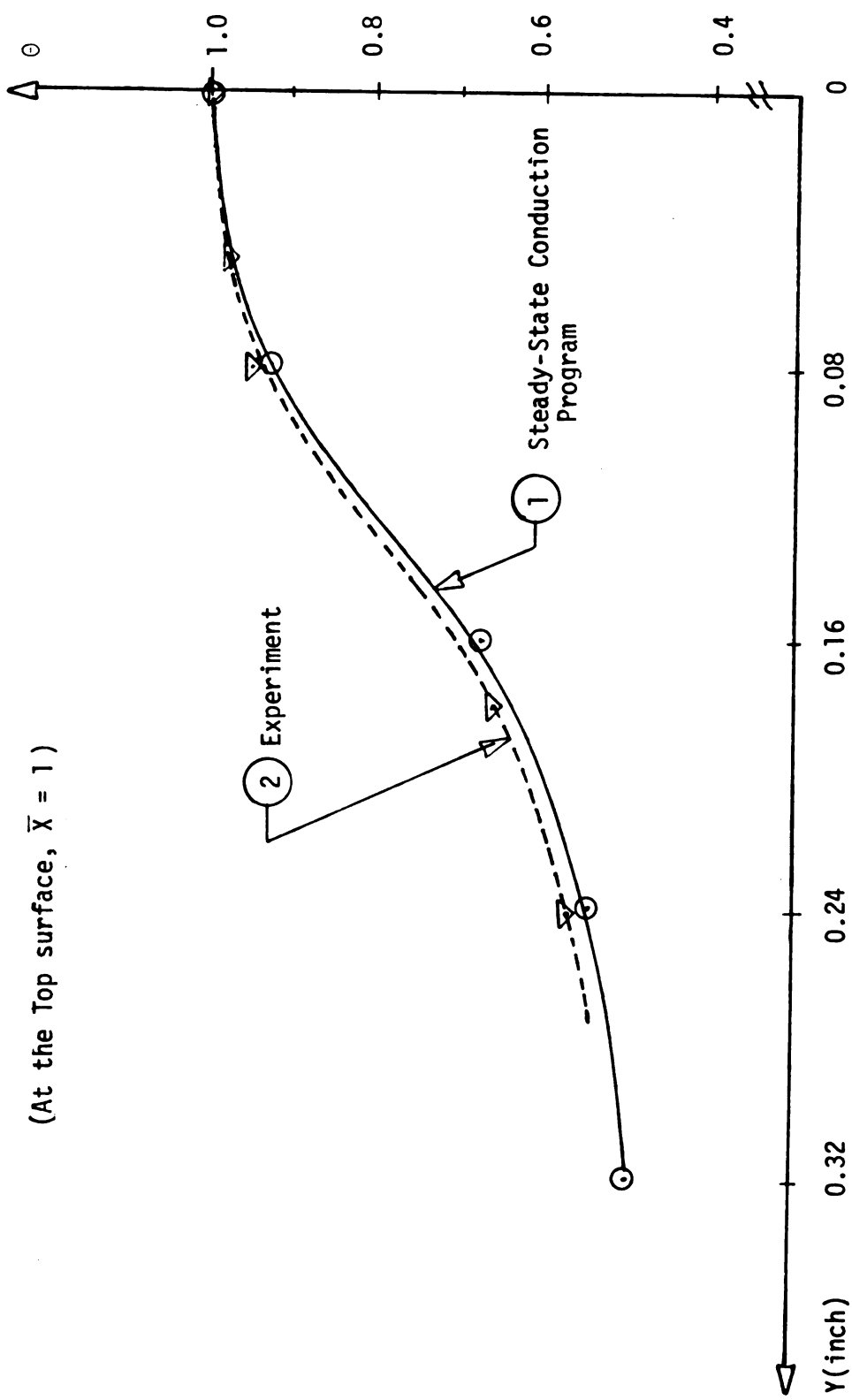


Figure 6.1 Comparison of Non-Dimensional Temperature Between the Computer Modeling Results and the Experimental Results for the Steady-State Conduction of the Cryomicroscope Conduction Stage.

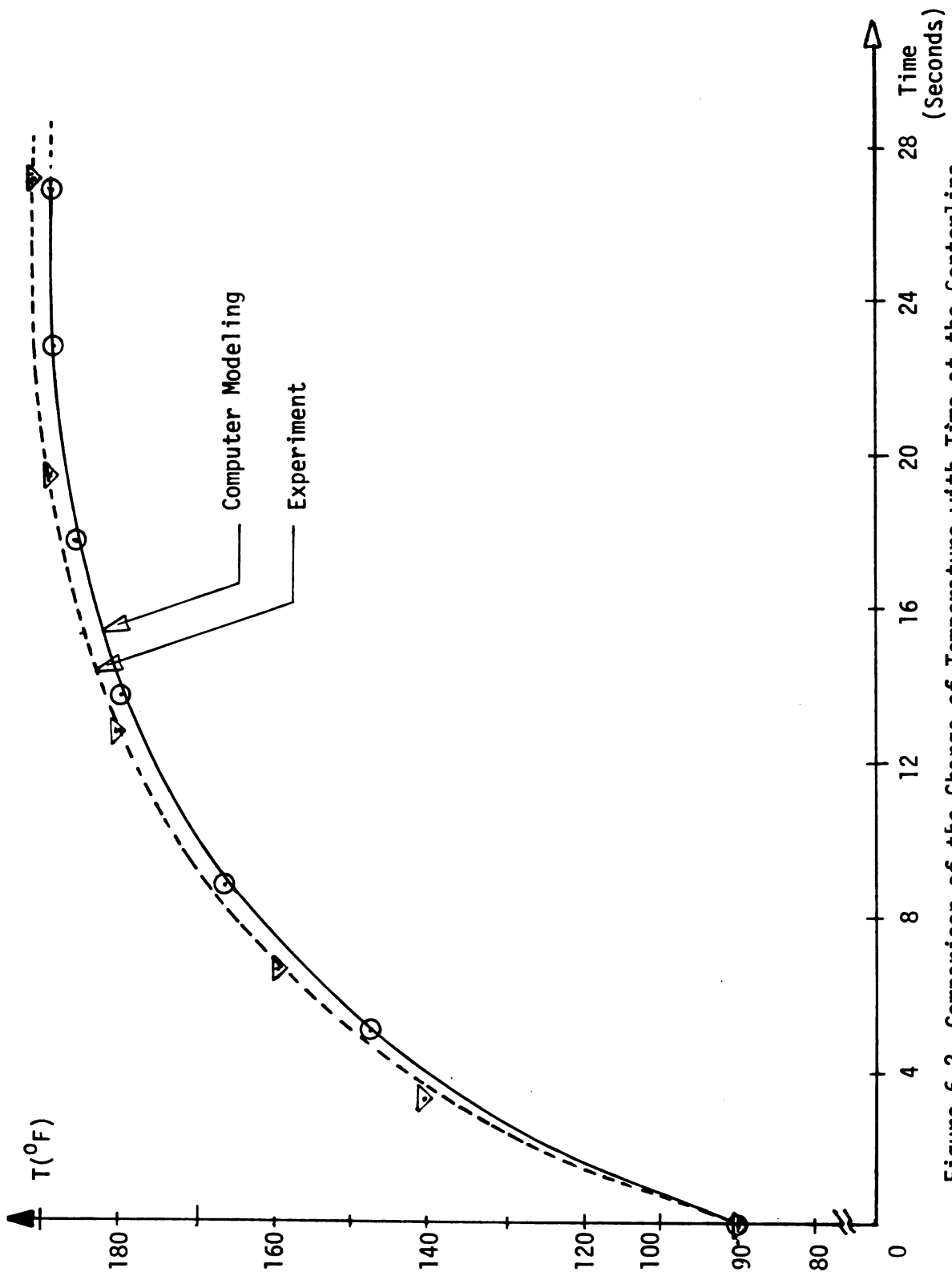


Figure 6.2 Comparison of the Change of Temperature with Time at the Centerline ($r = 0$); $T = T_1$.

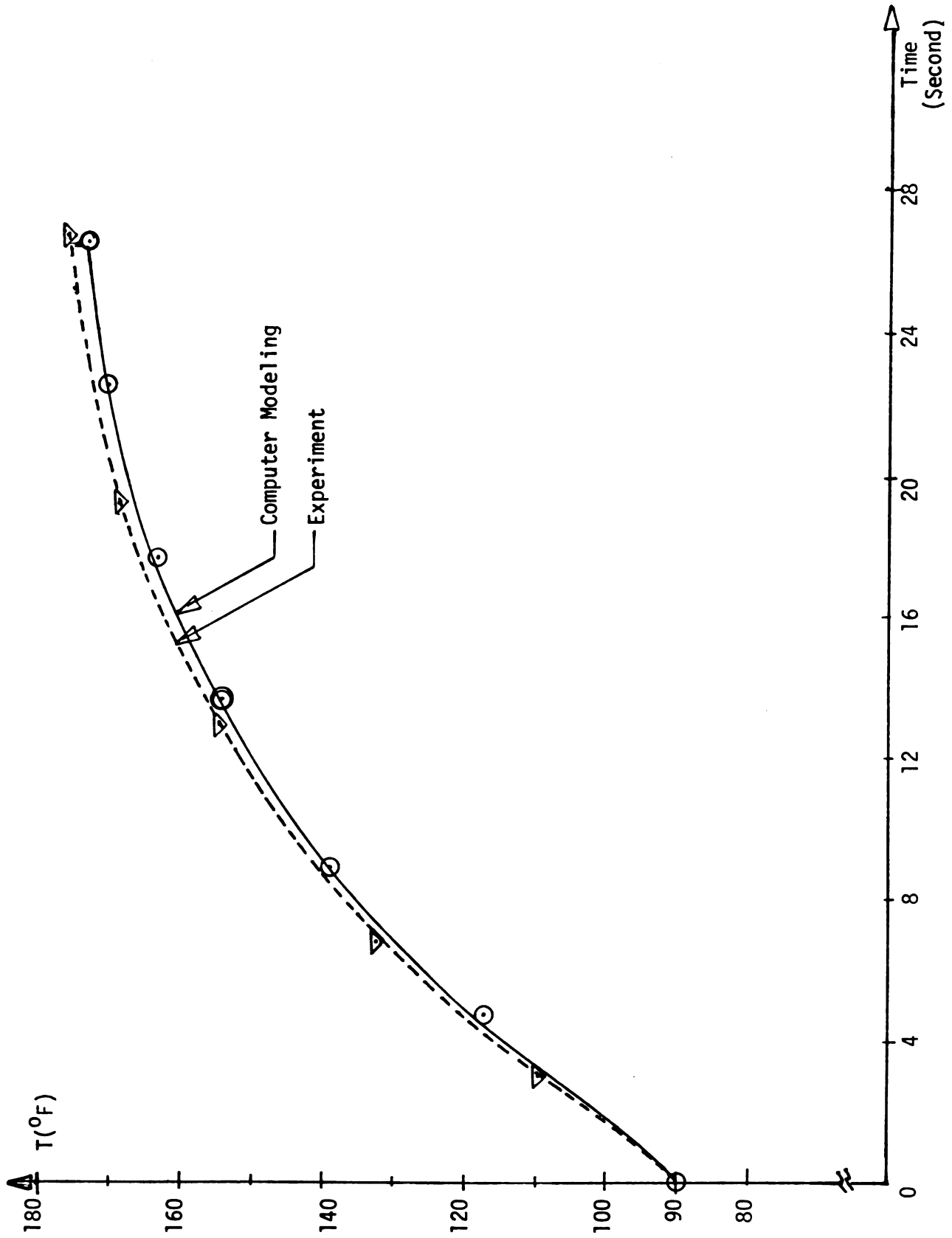


Figure 6.3 Comparison of the Change of Temperature with Time at $r = 0.047$ in. from the Centerline; $T = T_2$.

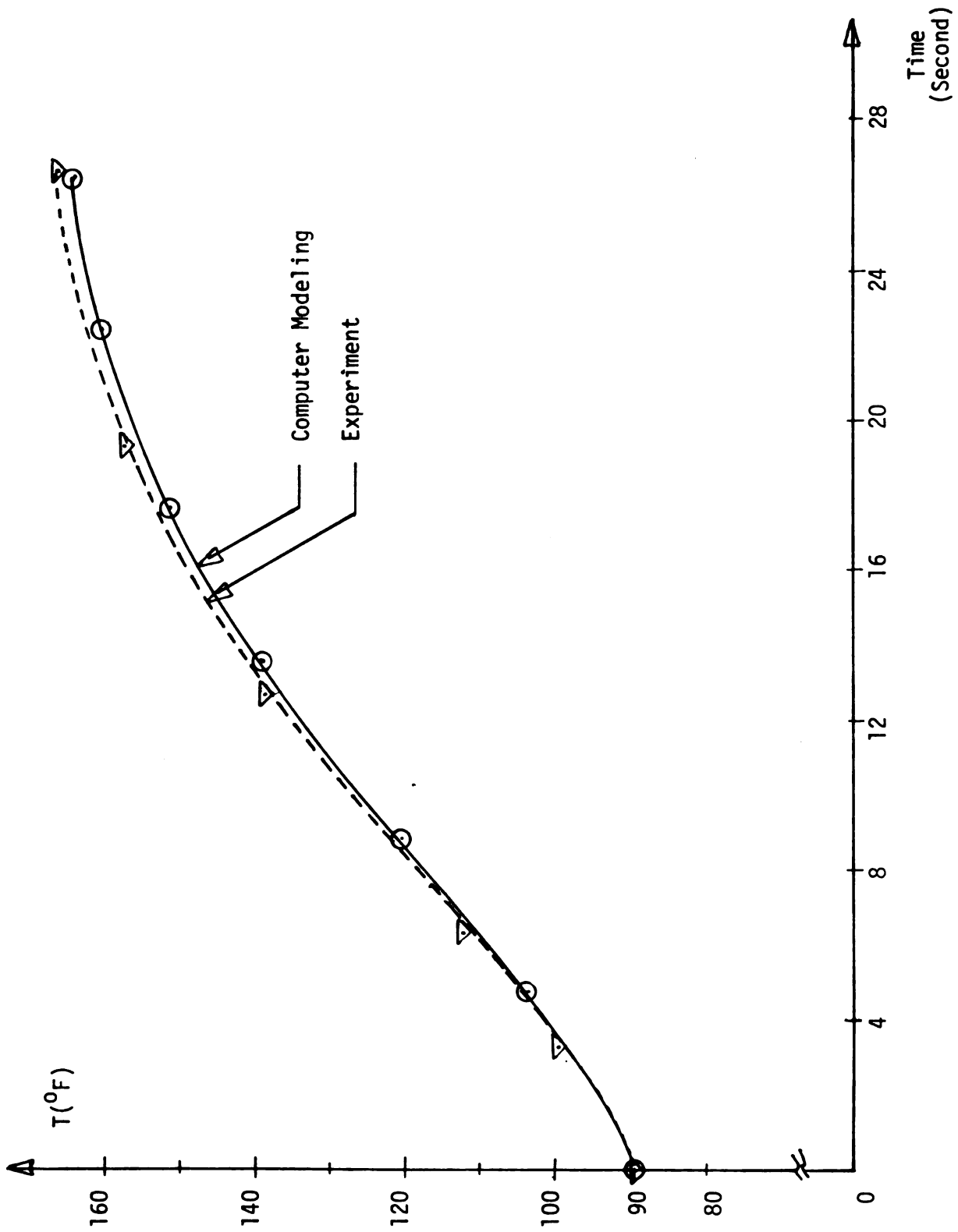


Figure 6.4 Comparison of the Change of Temperature with Time at $r = 0.08$ in. from the Centerline, $T = T_3$.

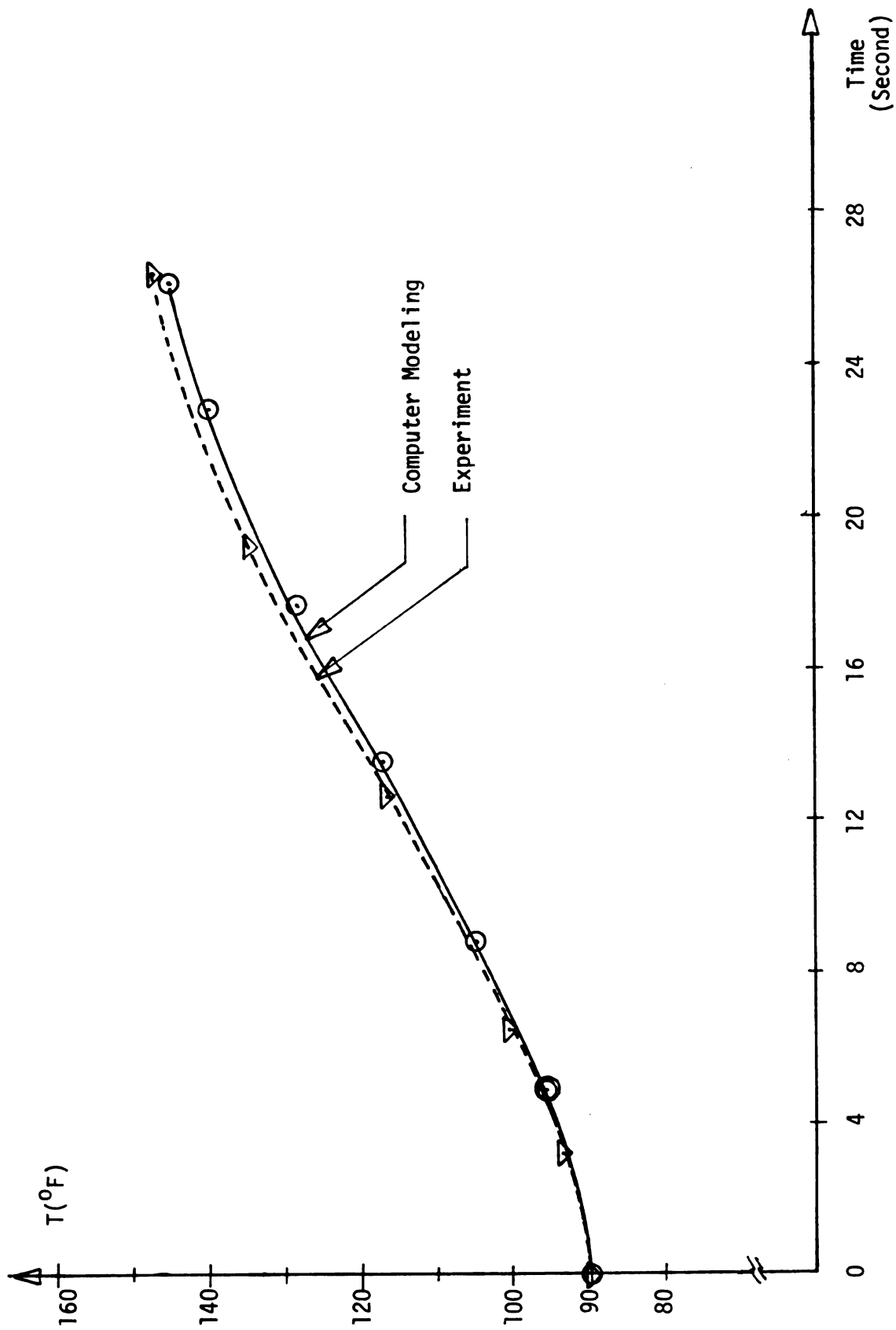


Figure 6.5 Comparison of the Change of Temperature with Time at $r = 0.18$ in. from the Centerline; $T = T_4$.

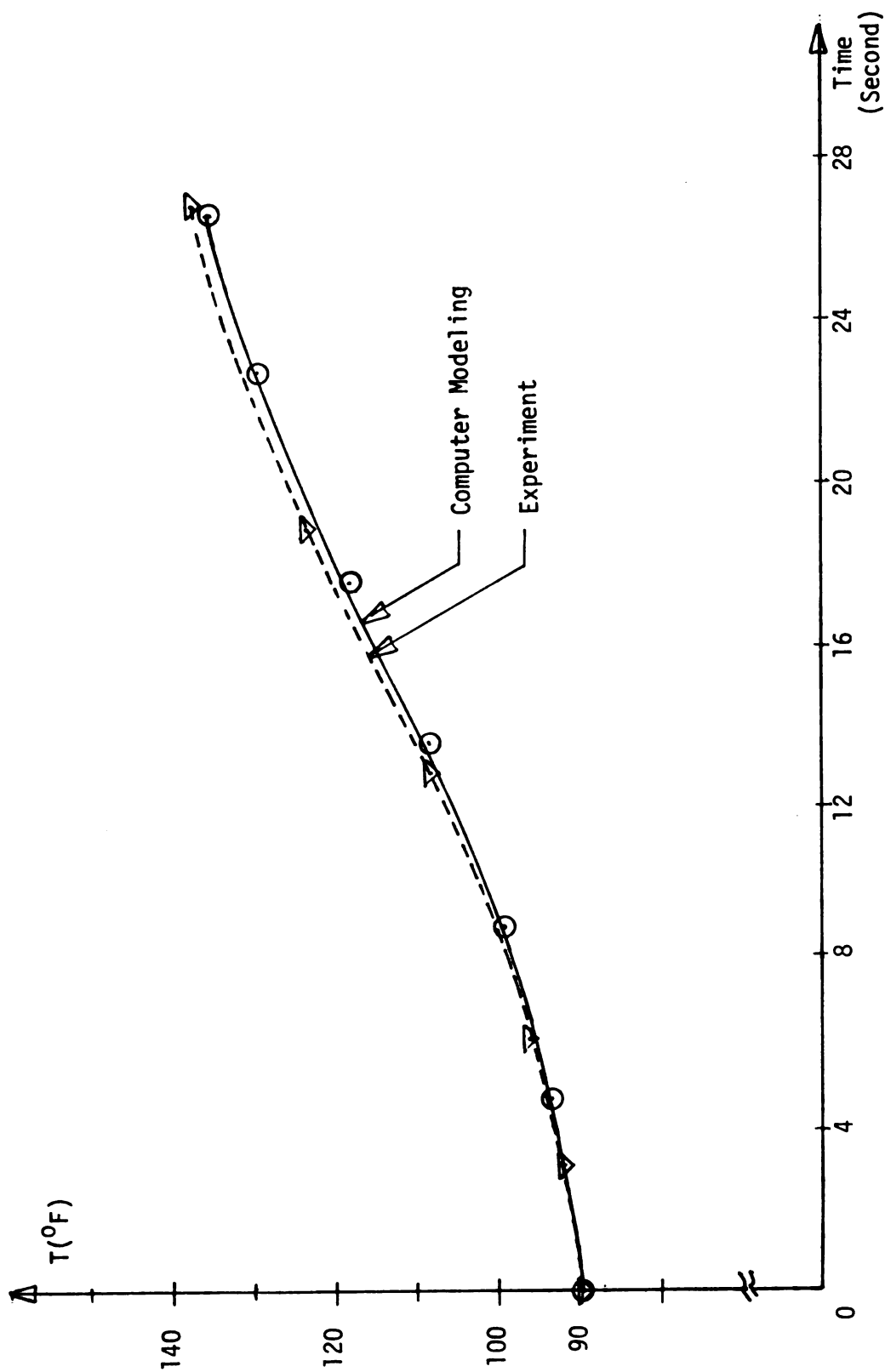


Figure 6.6 Comparison of the Change of Temperature with Time at $r = 0.24$ in. from the Centerline; $T = T_5$.

This procedure yields the temperature ($^{\circ}\text{F}$) VS. time (seconds) at various positions which can be plotted from the computer modeling results and compared with the experimental results as shown in Figure 6.2 through Figure 6.6 for various positions along the top surface of the Cryomicroscope Conduction Stage. In general the maximum error observed between experimental and numerical results was not more than 5%.

CHAPTER 7

CONCLUSIONS AND SUGGESTIONS FOR FUTURE WORK

7.1 Conclusions

1) The Gauss-Seidel Numerical Technique has been applied to obtain a steady-state solution to heat transfer on the Cryomicroscope Conduction Stage. This method is an appropriate technique yielding results in 6.3 seconds of computational time at a cost of \$0.30 per run. The total number of nodes is 102 and the program handles variable boundary conditions, non-uniform grid size, and composite materials.

2) The actual Cryomicroscope Conduction Stage was simplified by eliminating the mylar tape and silver epoxy component of its construction. These simplifications are justified in view of the fact that the difference of the computer modeling results and the experimental results are not more than 5%.

3) The explicit method for the finite difference approximation has been applied to solve the transient heat conduction in the Cryomicroscope Conduction Stage. This method is acceptable in obtaining the accurate results and yielding results in 7.5 seconds of computational time at a cost of \$0.55 per run. The total number of nodes is 102 and the program handles variable boundary conditions, non-uniform grid sizes, variable print interval of time and composite materials.

4) Since the transient model yields accurate results for the response of the present Cryomicroscope Conduction Stage as judged by comparison with experimental results, the transient model has been used to predict the response of proposed alternative Cryomicroscope Conduction Stages.

Two parameters are of primary interest in redesigning the existing Cryomicroscope Conduction Stage. An improved design would minimize the temperature gradient observed over the entire viewing hole. It is also desirable for the Cryomicroscope Conduction Stage to have a rapid thermal response so that a wider range of cooling and warming rate can be effected by the Cryomicroscope Conduction Stage.

The effects of some simple modifications of the Cryomicroscope based on the two criteria above were considered.

Width of Heater Dissipation

The width (W , see Figure 7.1) of the energy dissipation region is easily altered when the quartz heaters are attached to the Cryomicroscope Conduction Stage. The effect of increasing this width is shown in Table 7.1 and Figure 7.2 where:

$$\overline{\Delta T} = T_C - T_D$$

T_C = The Centerline temperature

T_D = The temperature at $r=0.08$ inch from the centerline
(viewing hole radius)

and Θ error = $(T_C - T_D)/(T_C - T_B)$

T_B = The Refrigerant temperature

These expressions for $\overline{\Delta T}$ and Θ error will be used throughout this thesis.

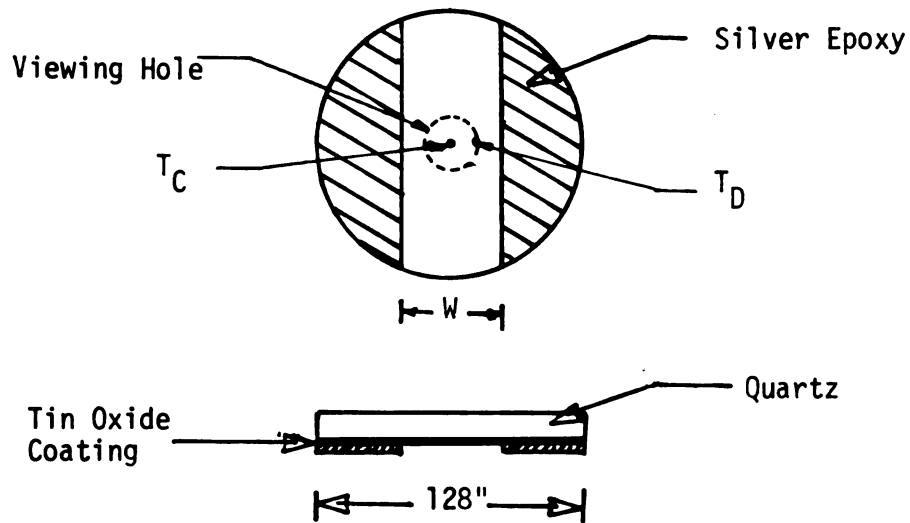


Figure 7.1 Typical Heater Dimensions

TABLE 7.1

The Temperature Differences Expected
Between Nodes ($T_C - T_D$)
by Varying Width W

Width	\bar{W}	$\bar{\Delta T}$	Θ Error
0.32 in	0.67	6.83 ⁰ F	0.0764
0.48 in.	1.0	5.36 ⁰ F	0.0589
0.64 in.	1.33	4.37 ⁰ F	0.0481
0.80 in.	1.67	3.34 ⁰ F	0.0367

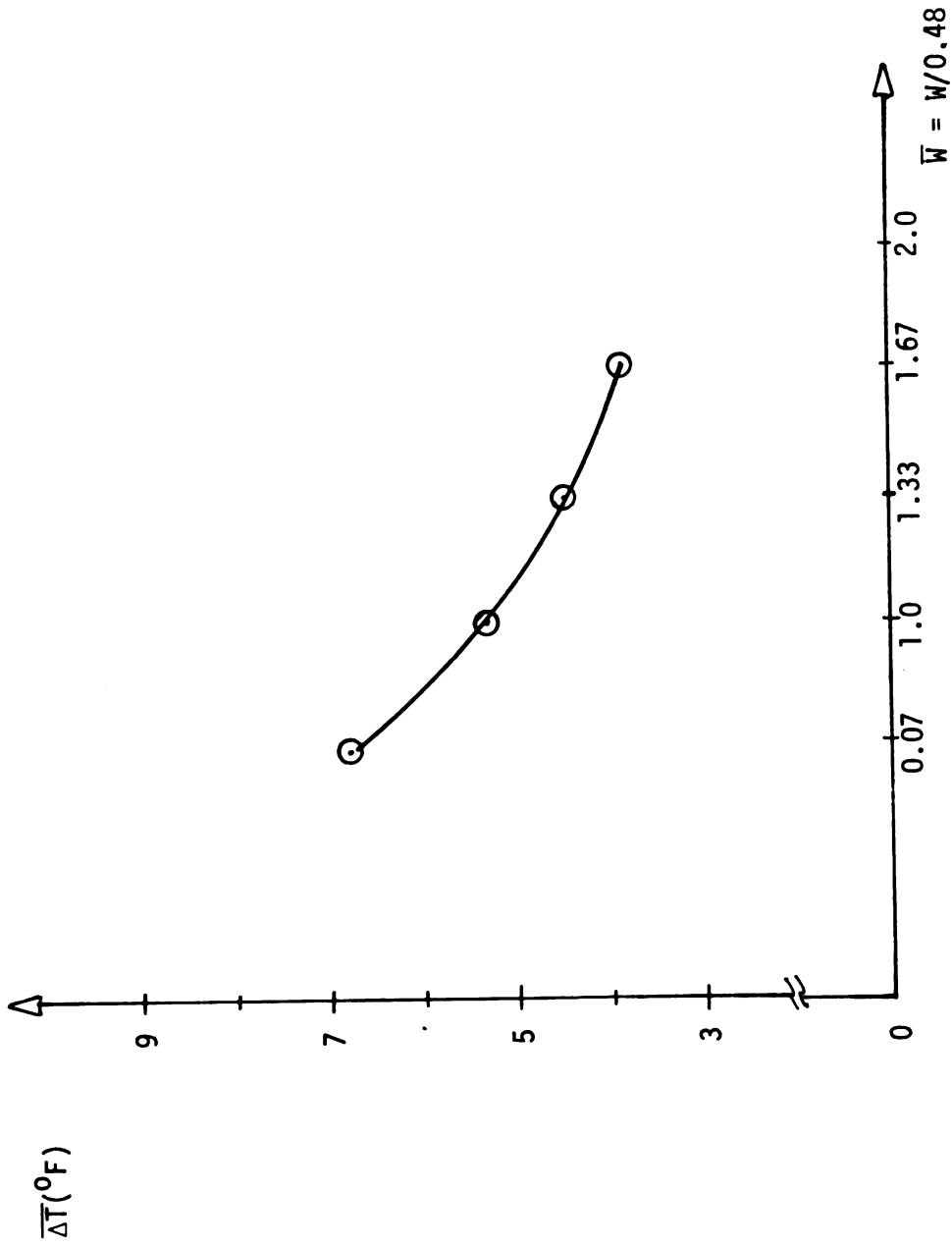


Figure 7.2 The Temperature Difference Between Nodes ($T_C - T_D$) by Fixing the Diameters, Materials and Thickness and Varying the Width W .

For Table 7.1 and Figure 7.2 the original configuration was $W = 0.48$ inch. Let $\bar{W} = W/0.48$

Increasing the width is a beneficial effect in that it makes the temperature at the top of the quartz more isothermal. Increasing the width of this dissipation region effects the transient response of the Cryomicroscope Conduction Stage by making the Cryomicroscope Conduction Stage respond more slowly. This effect is not desirable. The results are shown in Table 7.1, Figure 7.2, and Figure 7.3.

Thickness of the Quartz Heater

Quartz discs used as heaters are available in various thicknesses from the manufacturer. The effect of changing the existing heater from a thickness of 0.016 inch was examined.

In Table 7.2 and Figure 7.4, for the original configuration, the thickness of quartz was $t' = 0.016$ inch. Let $\bar{t} = t'/0.016$.

Table 7.2, Figure 7.3 and Figure 7.4 shows that an increased heater thickness is expected to decrease the temperature gradient at the top surface of the quartz (where the sample would be). This is a desired result. But the effect on the transient response of the Cryomicroscope Conduction Stage would be slower for increasing the heater thickness. This is an undesired result.

Using of Glass Heaters

Glass heaters were considered as a possibility since glass coverslips are readily available and economical.

The conclusions of the results are shown in Table 7.3, Figure 7.5 and Figure 7.6.

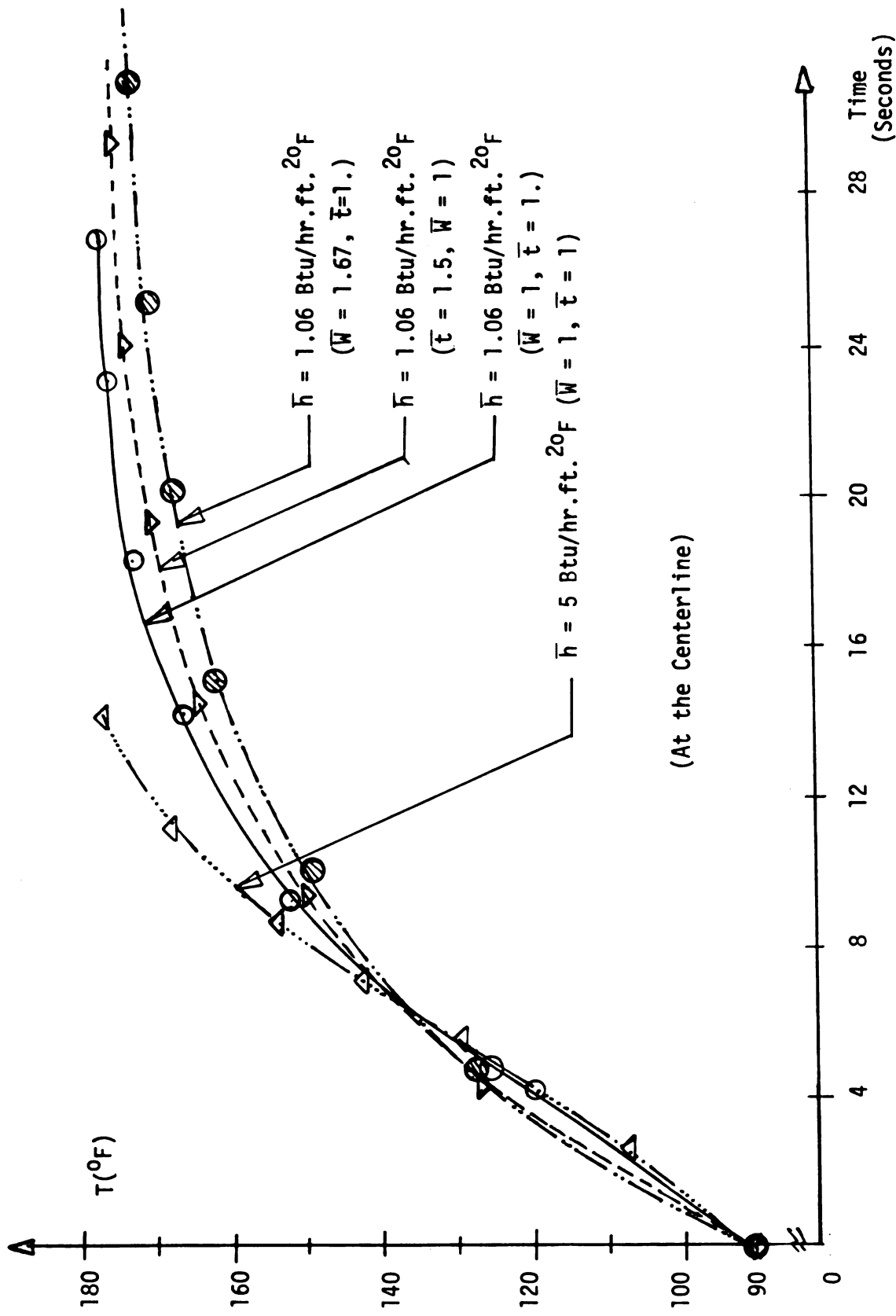


Figure 7.3 Effects of the Potential Cryomicroscope Conduction Stage Modification on Transient Response.

Table 7.2

The Temperature Difference Expected
Between Nodes ($T_C - T_D$) by
Varying the Quartz Thickness

Thickness	\bar{t}	\bar{T}	θ error
0.008 in.	0.5	6.74 °F	0.074
0.016 in.	1.0	5.36 °F	0.0589
0.024 in.	1.5	4.40 °F	0.0484
0.032 in.	2.0	3.61 °F	0.0397

Table 7.3

The Temperature Difference Expected
Between Nodes ($T_C - T_D$) by
Changing the Materials
from Quartz to Glass

Materials	Thermal Conductivity	\bar{k}	$\bar{\Delta T}$	θ error
Glass	0.07 Btu/hr ft ⁰ F	0.16	3.91 ⁰ F	0.0429
Glass	0.10 Btu/hr ft ⁰ F	0.225	4.32 ⁰ F	0.0475
Glass	0.15 Btu/hr ft ⁰ F	0.34	4.38 ⁰ F	0.0481
Quartz	0.444 Btu/hr ft ⁰ F	1.0	5.36 ⁰ F	0.0589

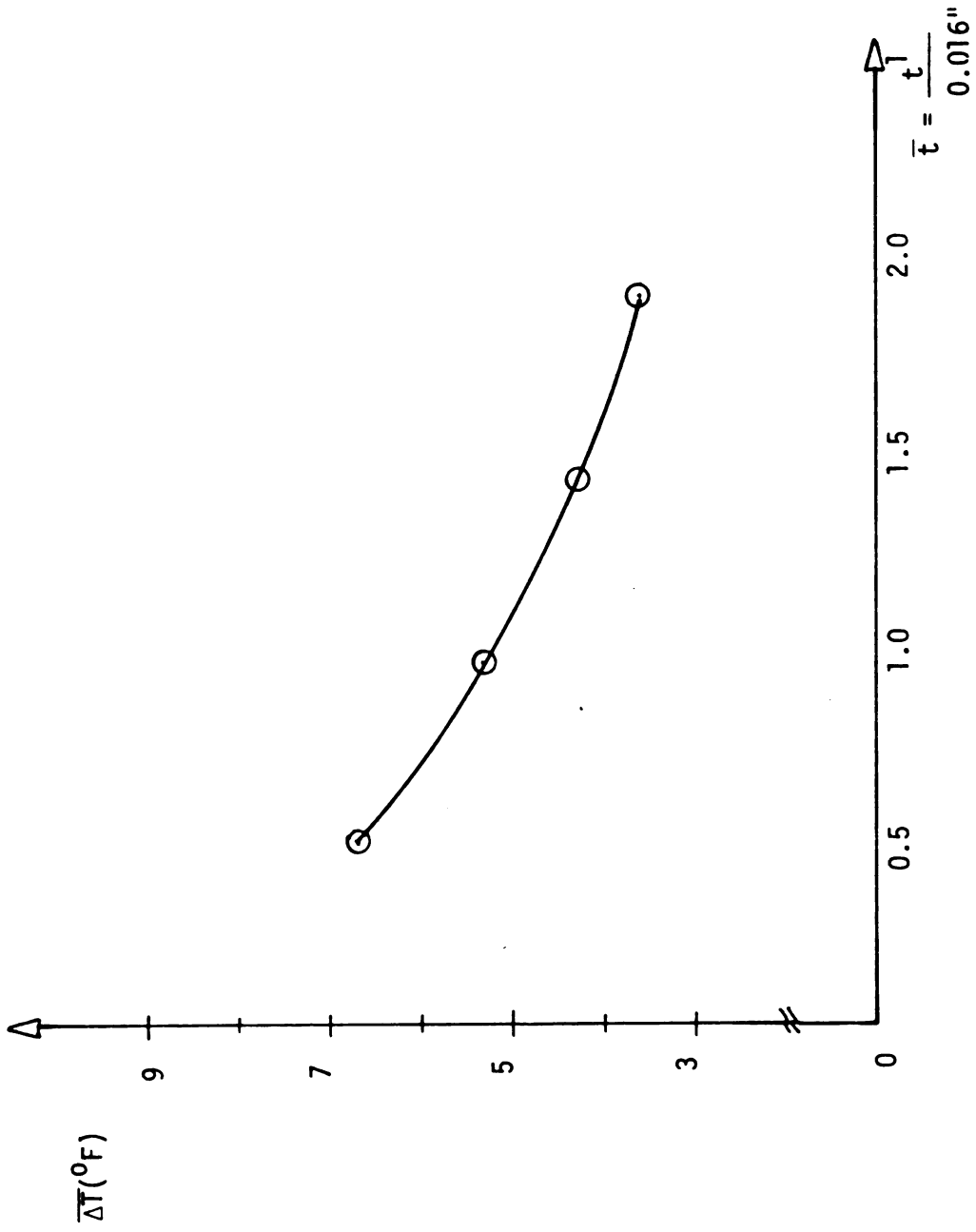


Figure 7.4 The Temperature Difference Between Nodes ($T_C - T_D$) by Fixing the Diameters, Materials, the Width W and Varying the Thickness.

For the thermal conductivity of quartz, $k = 0.44 \text{ Btu/hr ft } ^\circ\text{F}$,
let $\bar{k} = k/0.444$.

From Table 7.3 and Figure 7.5 show that there is not much difference in the temperature gradient (ΔT and θ error) in replacing the quartz heater with a glass heater. Figure 7.6 shows the comparison of the transient response at the centerline of the Cryomicroscope Conduction Stage. From this modification, we can see that it is possible to use glass, instead of quartz, as a heater for the Cryomicroscope Conduction Stage. This conclusion is based on the fact that there was not much difference in the temperature gradient and transient response by using glass instead of quartz as the heater. The time difference before reaching steady-state was about 6.6 seconds or approximately 25% slower for glass ($k = 0.1 \text{ Btu/hr ft } ^\circ\text{F}$).

The last part of this thesis is to show the comparison of the non-dimensional temperature distribution at the top surface of the Cryomicroscope Conduction Stage as shown in Figure 7.7. For curve (3) in Figure 7.7, we applied the Transient Conduction Program with all the same data used in curve (2) except we use glass ($k = 0.1 \text{ Btu/hr ft } ^\circ\text{F}$, diameter = 0.84 inch and thickness = 0.012 inch) as the heater of the Cryomicroscope Conduction Stage. The results show that it reached the steady-state rapidly (about 22 seconds) but that its temperature gradient was high.

In the case when we change the convective heat transfer coefficient for the surrounding air, Figure 7.8 shows that the temperature difference (at the same location of nodes) using $\bar{h} = 5 \text{ Btu/hr ft}^{20}\text{F}$ and $\bar{h} = 1.06 \text{ Btu/hr ft}^{20}\text{F}$ is about 10%.

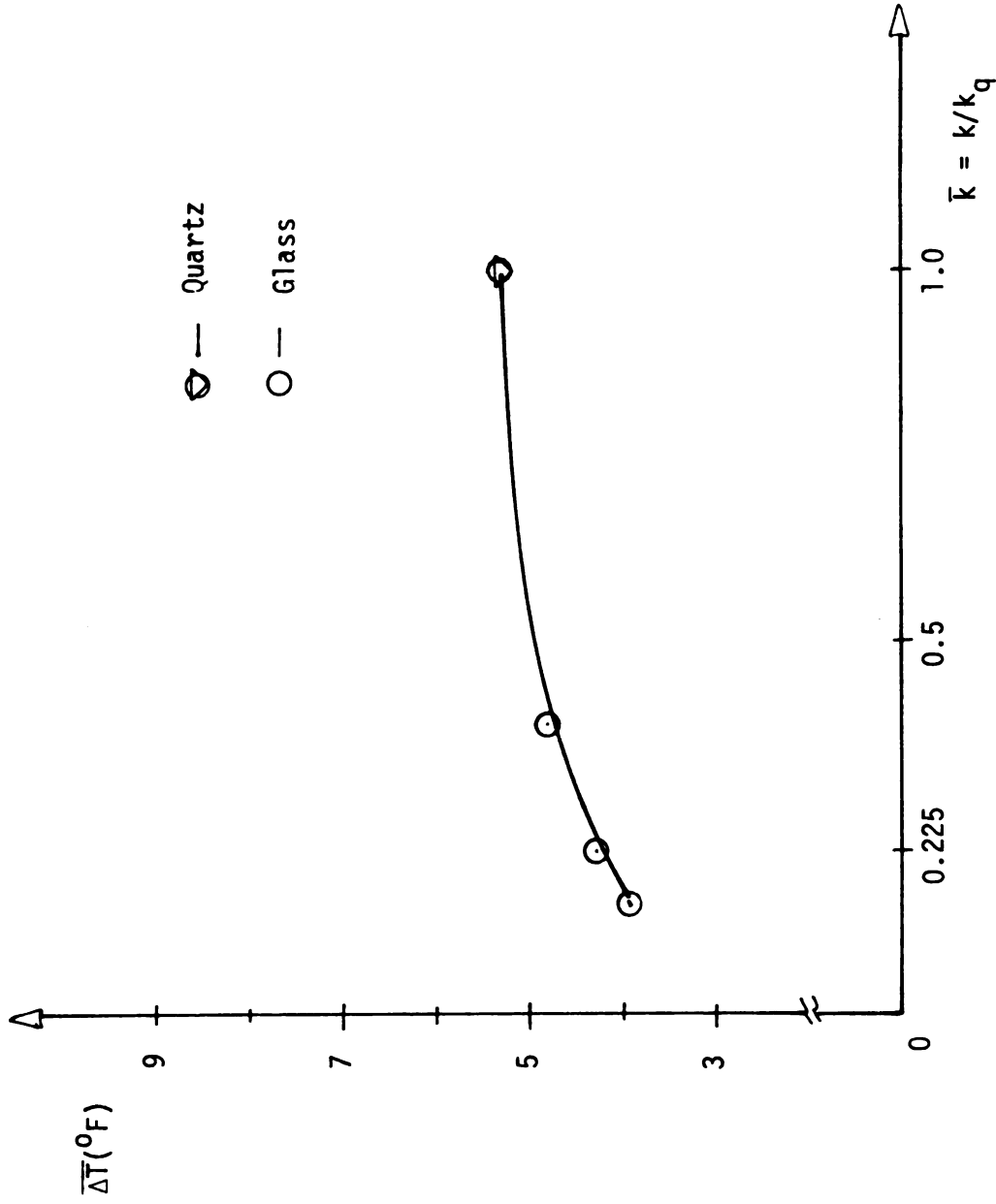


Figure 7.5 The Temperature Difference Between Nodes ($T_C - T_D$) by Changing Materials from Quartz to Glass (The Thermal Conductivity of Glass about 0.07 to 0.15 Btu/hr.ft.².F.)

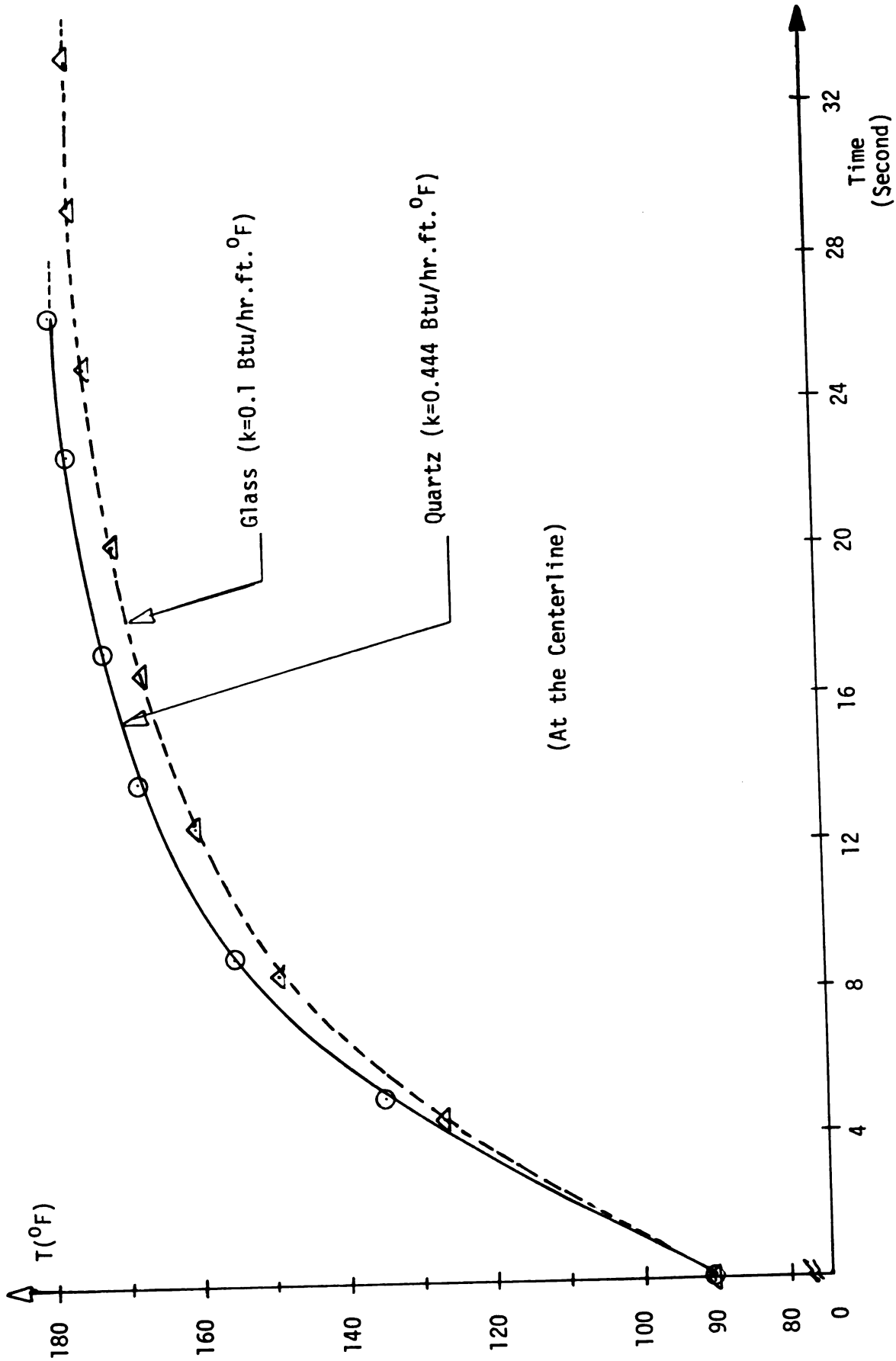


Figure 7.6 Comparison of the Change of Temperature with Time by Changing the Materials from Quartz to Glass.

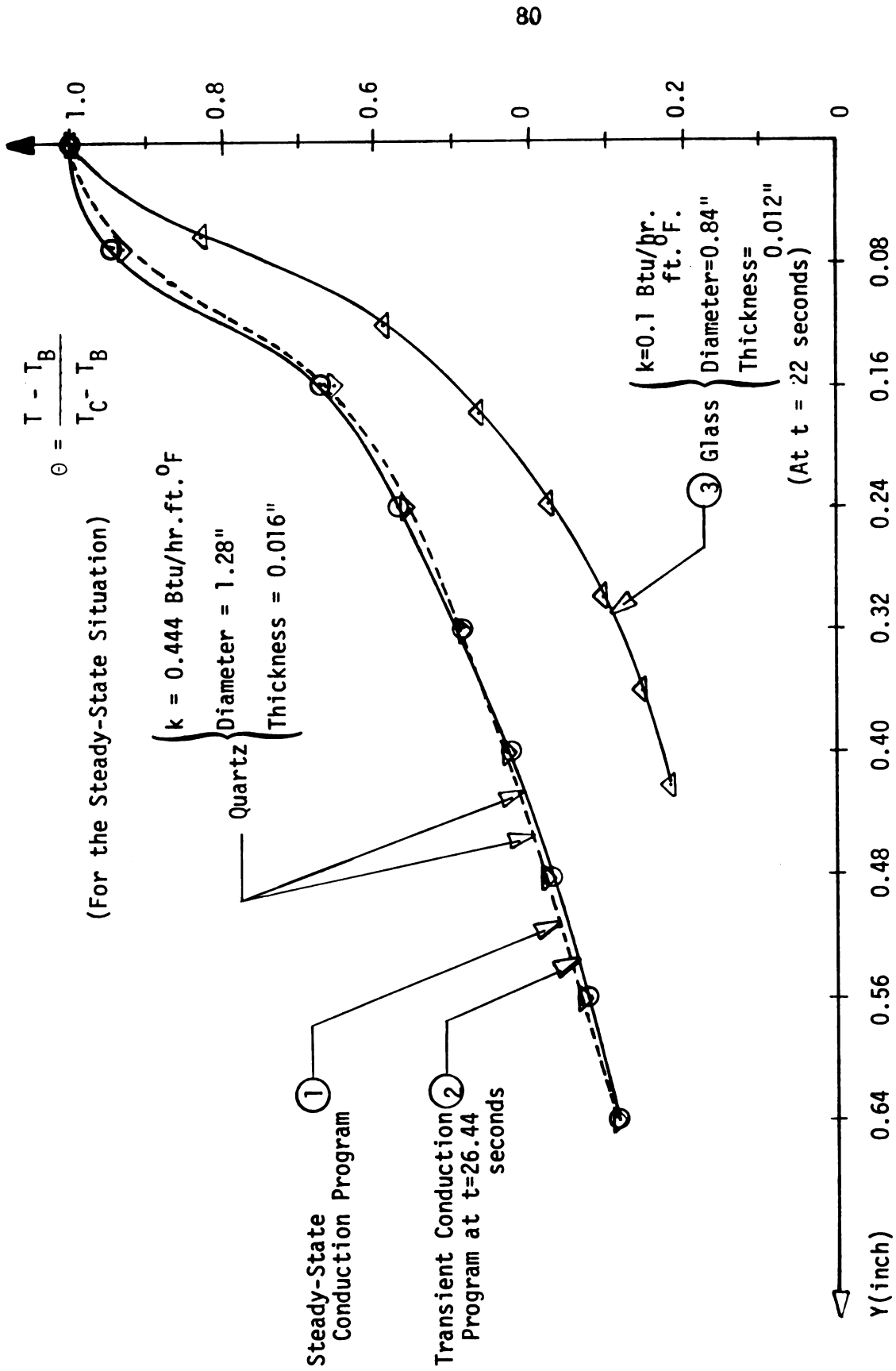


Figure 7.7 Comparison of Non-dimensional Temperature Distribution on the Top Surface of the Cryomicroscope Conduction Stage.

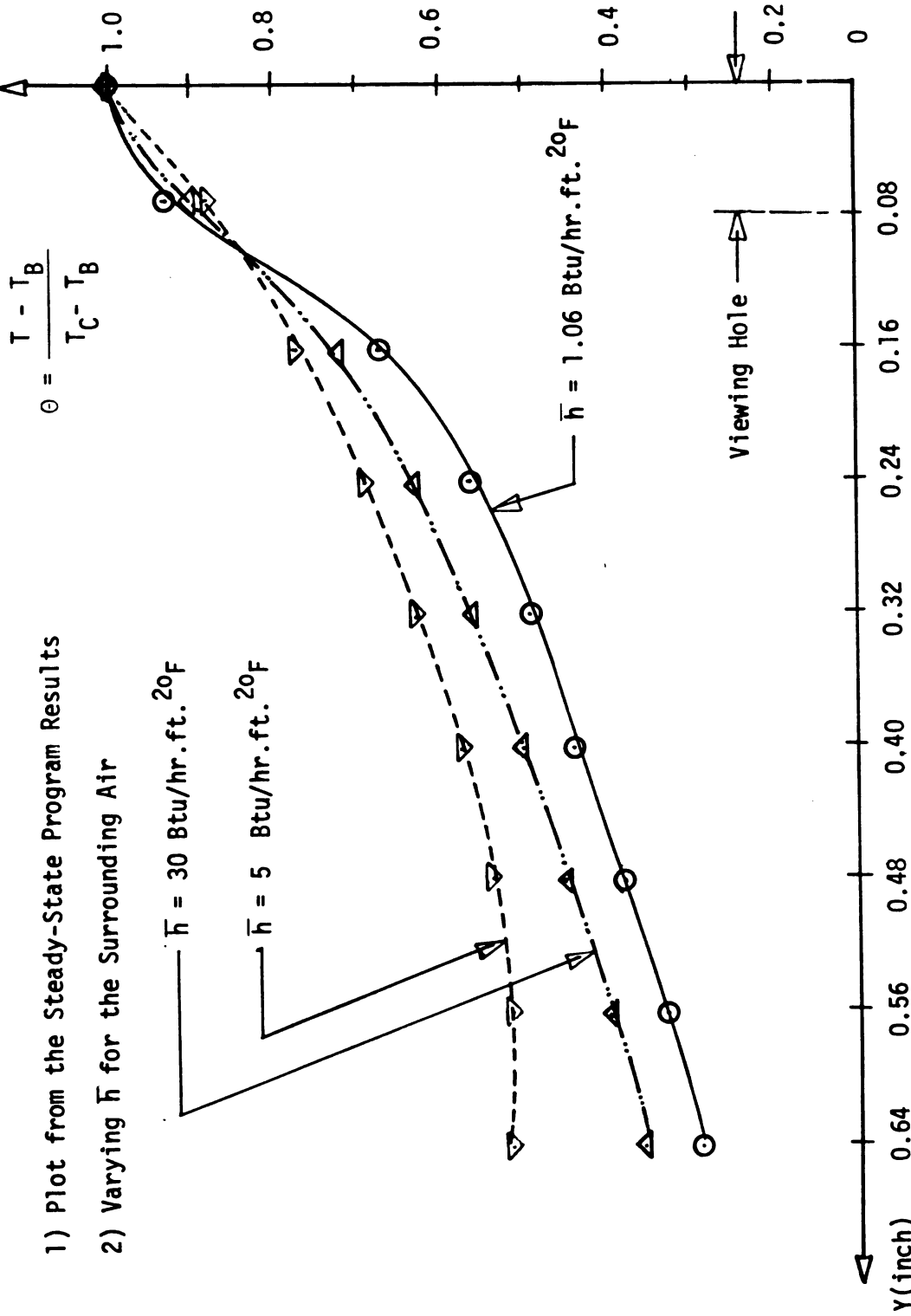


Figure 7.8 Comparison of Non-dimensional Temperature Distribution on the Top Surface of the Cryomicroscope Conduction Stage.

In summary the optimal Cryomicroscope Conduction Stage based on the alternatives considered above could not be specified exactly because if we want a uniform temperature gradient for the Cryomicroscope Conduction Stage, it will yield a slow transient response. It depends on a choice between the desirable characteristics of uniform temperature and rapid response. But in terms of its effectiveness, the width of heater dissipation (heater dissipation area) plays a major role in the Cryomicroscope Conduction Stage performance.

7.2 Suggestions for Future Work

Future work should be aimed at using these programs to study the following:

- a) Simulation using actual refrigerant conditions used in Cryomicroscopy.
- b) Substitute alternate backing materials for copper (i.e. sapphire, aluminum alloys, etc.)
- c) Study the effect of non-rectangular heater dissipation area.
- d) Study the effect of non-uniform energy dissipation.
- e) Study the effect of viewing hole size.

The program would also be a useful reference for developing a similar study of an existing Cryomicroscope Convection Stage.

This analysis will be useful when coupled with thermal stress analyses and feedback control analyses.

Owing to time constraints and also because the materials presented here satisfy the purpose of this research, we were not able to

modify and develop the Cryomicroscope Conduction Stage more than what has been done. We do hope that this thesis could be useful for future work that will lead to the modification and development of a specific and practical model for the Cryomicroscope Conduction Stage.

APPENDIX A

Nodal Equations for Two-Dimensional Steady-State Conduction

Interior Node Equation for the Composite Materials (Equation 3-5)

From Figure 3.3(a) and the application of the conservation of energy principle

$$\begin{aligned}
 & k_1 \frac{\Delta X}{2} \frac{(T_{i+1,j} - T_{i,j})}{\Delta Y} + k_2 \frac{\Delta X}{2} \frac{(T_{i+1,j} - T_{i,j})}{\Delta X} \\
 & + k_1 \Delta Y \frac{(T_{i,j-1} - T_{i,j})}{\Delta X} + k_1 \frac{\Delta X}{2} \frac{(T_{i-1,j} - T_{i,j})}{\Delta Y} \\
 & + k_2 \frac{\Delta X}{2} \frac{(T_{i-1,j} - T_{i,j})}{\Delta Y} + k_2 \Delta Y \frac{(T_{i,j+1} - T_{i,j})}{\Delta X} \\
 & + Q \Delta X \Delta Y = 0
 \end{aligned}$$

For $\Delta Y = m\Delta X$ and let $k_3 = k_1 + k_2$

$$\begin{aligned}
 & \frac{k_3}{2m} (T_{i+1,j} - T_{i,j}) + mk_1 (T_{i,j-1} - T_{i,j}) + \frac{k_3}{2m} (T_{i-1,j} - T_{i,j}) \\
 & + mk_2 (T_{i,j+1} - T_{i,j}) + mQ(\Delta X)^2 = 0
 \end{aligned}$$

Then we can get Equation (3-5)

$$\theta_{i,j} = \frac{\theta_{i+1,j} + \theta_{i-1,j} + 2m^2(k_1\theta_{i,j-1} + k_2\theta_{i,j+1})/k_3 + m^2(\overline{\Delta X})^2 N_2/k_3}{(2m^2+2)}$$

The Sides Node Equations with the
Boundary Condition

Consider the surface node as shown in Figure 3.4. Energy is conducted across three surfaces of the element, and convection occurs across the exposed surface.

$$k\Delta Y \frac{(T_{i,j-1} - T_{i,j})}{\Delta X} + k \frac{\Delta X}{2} \frac{(T_{i-1,j} - T_{i,j})}{\Delta Y} + \bar{h}_R \Delta Y (T_{\infty,R} - T_{i,j})$$

$$+ k \frac{\Delta X}{2} (T_{i+1,j} - T_{i,j}) + Q \frac{\Delta X}{2} \Delta Y = 0.$$

For $\Delta Y = m\Delta X$

$$T_{i,j} = \frac{T_{i-1,j} + T_{i+1,j} + 2m^2 T_{i,j-1} + 2m^2 \frac{\bar{h}_R \Delta X}{k} T_{\infty,R} + m^2 Q (\Delta X)^2 / k}{(2m^2 + 2 + 2m^2 \bar{h}_R \Delta X / k)}$$

Then the node equation for convection at the right vertical surface (Equation 3-6)

$$\Theta_{i,j} = \frac{\Theta_{i+1} + 2m^2 \Theta_{i,j-1} + \Theta_{i-1,j} + 2m^2 \overline{\Delta X} Bi_R \Theta_R + m^2 (\overline{\Delta X})^2 N1}{(2m^2 + 2 + 2m^2 \overline{\Delta X} Bi_R)}$$

In the same manner, we can get the Equation (3-7) for the left vertical surface.

The Top and End Node Equation
with the boundary condition

Consider the left end corner node as shown in Figure 3.6. We can see that conduction occurs across the two interior surfaces and convection occurs across the left side and the lower exposed surface.

The conservation of energy principle is applied to the end corner node, the result is

$$k \frac{\Delta X}{2} \frac{(T_{i-1,j} - T_{i,j})}{\Delta Y} + k \frac{\Delta Y}{2} \frac{(T_{i,j+1} - T_{i,j})}{\Delta X} + \bar{h}_E \frac{\Delta X}{2} (T_{\infty,E} - T_{i,j})$$

$$+ \bar{h}_L \frac{\Delta Y}{2} (T_{\infty,L} - T_{i,j}) + Q \left(\frac{\Delta X}{2}\right) \left(\frac{\Delta Y}{2}\right) = 0.$$

Again $\Delta Y = m\Delta X$, $\bar{\Delta X} = \Delta X/\ell$ and solving for $T_{i,j}$

$$T_{i,j} = \frac{T_{i-1,j} + m^2 T_{i,j+1} + m \frac{\bar{h}_E \ell}{k} \bar{\Delta X} T_{\infty,E} + m^2 \frac{\bar{h}_L \ell}{k} \bar{\Delta X} T_{\infty,R} + \frac{m^2}{2} \frac{Q \ell^2}{k} (\bar{\Delta X})^2}{\left(m \frac{\bar{h}_E \ell}{k} \bar{\Delta X} + m^2 \frac{\bar{h}_L \ell}{k} \bar{\Delta X} + m^2 + 1\right)}$$

$$\Theta_{i,j} = \frac{\Theta_{i-1,j} + m^2 \Theta_{i,j+1} + m \text{Bi}_E \bar{\Delta X} \Theta_E + m^2 \text{Bi}_L \bar{\Delta X} \Theta_L + \frac{m^2}{2} (\bar{\Delta X})^2 \text{N1}}{(m^2 + 1 + m \text{Bi}_E \bar{\Delta X} + m^2 \text{Bi}_L \bar{\Delta X})}$$

(The above equation is Equation 3-11).

In the same manner, we can get Equation (3-8) (3-9), (3-10), (3-12) and (3-13).

The Node Equations for the Convection at an Interior Corner Node with Composite Materials

From Figure 3.7 for the left and interior corner node, we can write

$$k_1 \frac{\Delta Y}{2} \frac{(T_{i,j-1} - T_{i,j})}{\Delta X} + (k_1 + k_2) \frac{\Delta X}{2} \frac{(T_{i-1,j} - T_{i,j})}{\Delta Y}$$

$$+ k_2 \Delta Y \frac{(T_{i,j+1} - T_{i,j})}{\Delta X} + k_2 \frac{\Delta X}{2} \frac{(T_{i+1,j} - T_{i,j})}{\Delta Y}$$

$$+ \bar{h}_L \left(\frac{\Delta X + \Delta Y}{2}\right) (T_{\infty,L} - T_{i,j}) + Q \left(\frac{3}{4}\right) \Delta X \Delta Y = 0$$

For $\Delta Y = m\Delta X$, $k_1 = k_2 + k_3$ and solving for $T_{i,j}$

$$\begin{aligned}
& T_{i,j} (m^2 k_1 / k_3 + 1 + 2m^2 k_2 / k_3 + k_2 / k_3 + (m^2 + m) \bar{h}_L \Delta X / k_3) \\
& = m^2 k_1 T_{i,j-1} / k_3 + T_{i-1,j} + 2m^2 k_2 T_{i,j+1} / k_3 + k_2 T_{i+1,j} / k_3 \\
& + (m^2 + m) \bar{h}_L \Delta X T_{\infty,L} / k_3 + 3m^2 Q (\Delta X)^2 / 2k_3
\end{aligned}$$

In non-dimensional form we can get Equation (3-15)

$$\theta_{i,j} = \frac{2m^2 k_5 \theta_{i,j+1} + k_5 \theta_{i+1,j} + (m^2 + m) Bi \Delta X \theta_{\infty} + m^2 k_4 \theta_{i,j-1} + \theta_{i-1,j} + \frac{3}{2} m^2 (\Delta X)^2 N'}{((2m^2 + 1)k_5 + m^2 k_4 + (m^2 + m) Bi \Delta X + 1)}$$

The Equation (3-14) can be obtained in the same manner as Equation (3-15).

APPENDIX B

Nodal Equations for Two-Dimensional Transient Conduction

Interior Node Equation for the Composite Materials

From Figures 3.4 and the general energy equation

$$\frac{\partial}{\partial X} \left(k \frac{\partial T}{\partial X} \right) + \frac{\partial}{\partial Y} \left(k \frac{\partial T}{\partial Y} \right) + Q = \rho C_p \frac{\partial T}{\partial t}$$

We can write

$$\begin{aligned} & \frac{1}{(\Delta X)^2} \left[k_1 (T_{i,j-1}^n - T_{i,j}^n) - k_2 (T_{i,j}^n - T_{i,j+1}^n) \right] + \frac{1}{(\Delta Y)^2} \\ & \left[\frac{(k_1+k_2)}{2} (T_{i-1,j}^n - T_{i,j}^n) - \frac{(k_1+k_2)}{2} (T_{i,j}^n - T_{i+1,j}^n) \right] + Q \\ & = \left(\frac{\rho_1 C_{p1} + \rho_2 C_{p2}}{2} \right) \frac{(T_{i,j}^{n+1} - T_{i,j}^n)}{\Delta t} \end{aligned}$$

In the same manner as we used for Equation (3-18), $\Delta Y = m\Delta X$ and $k_3 = k_1 + k_2$. The non-dimensional equation becomes

$$\begin{aligned} & 2m^2 \left[\frac{k_1}{k_3} (\theta_{i,j-1}^n - \theta_{i,j}^n) - \frac{k_2}{k_3} (\theta_{i,j}^n - \theta_{i,j+1}^n) \right] + \theta_{i-1,j}^n - 2\theta_{i,j}^n \\ & + \theta_{i+1,j}^n + 2m^2 N_2 (\Delta X)^2 = \frac{m^2}{F_1} (\theta_{i,j}^n - \theta_{i,j}^n) \end{aligned}$$

Then Equation (3-19) can be obtained.

$$\begin{aligned}\theta_{i,j}^{n+1} = & 2F1 \frac{k1}{k3} (\theta_{i,j-1}^n - \theta_{i,j}^n) - 2F1 \frac{k2}{k3} (\theta_{i,j}^n - \theta_{i,j+1}^n) + \theta_{i,j}^n \\ & + \frac{F1}{m^2} (\theta_{i-1,j}^n - 2\theta_{i,j}^n + \theta_{i+1,j}^n) + 2F1N2(\overline{\Delta X})^2\end{aligned}$$

The Sides Node Equations with the
Boundary Condition

When convective occurs at the boundary the energy conducted to the surface is equal to the energy leaving the surface by convection.

Using a forward difference approximation for $\partial T/\partial X$ and $\partial T/\partial Y$ at the left surface. This method yields

$$\begin{aligned}k\Delta Y \frac{(T_{i,j+1}^n - T_{i,j}^n)}{\Delta X} + k \frac{\Delta X}{2} \frac{(T_{i+1,j}^n - T_{i,j}^n)}{\Delta Y} + k \frac{\Delta X}{2} \frac{(T_{i-1,j}^n - T_{i,j}^n)}{\Delta Y} \\ + Q \left(\frac{\Delta X}{2}\right) \Delta Y = \bar{h}_L \Delta Y (T_{i,j}^n - T_{\infty,L}^n)\end{aligned}$$

To write a central finite difference approximation for a convective boundary condition at the left surface ($j = 1$), it is necessary to use a fictitious node outside the solid at $j-1$. Likewise, at the right surface ($j = N$) a fictitious node at $j+1$ is used.

$$\begin{aligned}k\Delta Y \frac{(T_{i,j+1}^n - T_{i,j-1}^n)}{2\Delta X} + k \frac{\Delta X}{2} \frac{(T_{i+1,j}^n - T_{i,j}^n)}{\Delta Y} + k \frac{\Delta X}{2} \frac{(T_{i-1,j}^n - T_{i,j}^n)}{\Delta Y} \\ + Q \frac{\Delta X}{2} \Delta Y = \bar{h}_L \Delta Y (T_{i,j}^n - T_{\infty,L}^n)\end{aligned}$$

For $\Delta Y = m\Delta X$, non-dimensionalized and solving for $\theta_{i,j-1}^n$

$$\begin{aligned}\theta_{i,j-1}^n = \frac{1}{m^2} \left[m^2 \theta_{i,j+1}^n + \theta_{i+1,j}^n + \theta_{i-1,j}^n - 2\theta_{i,j}^n + m^2 N1 (\overline{\Delta X})^2 \right. \\ \left. - 2m^2 Bi_L \overline{\Delta X} (\theta_{i,j}^n - \theta_L^n) \right]\end{aligned}$$

Substituting this equation into Equation (3-18) to eliminate $\theta_{i,j-1}^n$, then we can get Equation (3-20). Equation (3-21) for the right vertical surface can be solved in the same manner.

The Top and End Node Equations with the Boundary Condition

Consider the left end corner node as shown in Figure (3-6).

At time n , we can write

$$\begin{aligned} k \frac{\Delta Y}{2} \frac{(T_{i,j+1}^n - T_{i,j}^n)}{\Delta X} + k \frac{\Delta X}{2} \frac{(T_{i-1,j}^n - T_{i,j}^n)}{\Delta Y} + q \frac{\Delta X}{2} \frac{\Delta Y}{2} \\ = \bar{h}_L \frac{\Delta Y}{2} (T_{i,j}^n - T_{\infty,L}^n) + \bar{h}_E \frac{\Delta X}{2} (T_{i,j}^n - T_{\infty,E}^n) \end{aligned}$$

Consider $\Delta Y = m\Delta X$, $T_{\infty,E} = T_{\infty,L}$, $\bar{h}_E = \bar{h}_L$, $T_{\infty,T} = T_{\infty,R}$ and \bar{h}_T and \bar{h}_R .

Write in non-dimensional form.

$$m^2(\theta_{i,j+1}^n - \theta_{i,j-1}^n) + \theta_{i-1,j}^n - \theta_{i+1,j}^n + m^2 N1 (\overline{\Delta X})^2 = 2m(m+1)$$

$$\overline{\Delta X} Bi_E (\theta_{i,j}^n - \theta_T^n)$$

$$\theta_{i+1,j}^n = m^2(\theta_{i,j+1}^n - \theta_{i,j-1}^n) + \theta_{i-1,j}^n + m^2 N1 (\overline{\Delta X})^2 - 2m(m+1)$$

$$\overline{\Delta X} Bi_E (\theta_{i,j}^n - \theta_T^n)$$

Substituting $\theta_{i+1,j}^n$ in Equation (3-17), we obtain Equation (3-22).

In the same manner, we can get Equations (3-23), (3-24), (3-25), (3-26) and (3-27).

APPENDIX C

The Assumptions of the Cryomicroscope Conduction Stage

By running the steady-state program with the quartz and the glass properties, in the same boundary conditions, there was not much in the temperature difference between the quartz and the glass. Then we assumed that the temperatures in the glass are the same as the temperatures in the quartz and so neglected the glass by adding the thickness of the quartz from 0.014 in. to 0.016 in.

Possible errors in the predicted temperature distribution resulting from the omission of the tape and silver epoxy were approximated by examining the respective thermal resistances in the X and Y directions (see Figure 4.2).

In X-direction

Quartz	$R = 0.056$	$\text{hr-}^{\circ}\text{F/Btu}$
Tape	$R = 0.1$	$\text{hr-}^{\circ}\text{F/Btu}$
Silver Epoxy	$R = 3.7 \times 10^{-5}$	$\text{hr-}^{\circ}\text{F/Btu}$
Copper	$R = 7.5 \times 10^{-4}$	$\text{hr-}^{\circ}\text{F/Btu}$
Air	$R = 24$	$\text{hr-}^{\circ}\text{F/Btu}$

In Y-direction

Quartz	$R = 10$	$\text{hr-}^{\circ}\text{F/Btu}$
Tape	$R = 22,000$	$\text{hr-}^{\circ}\text{F/Btu}$
Silver Epoxy	$R = 0.52$	$\text{hr-}^{\circ}\text{F/Btu}$
Copper	$R = 0.8$	$\text{hr-}^{\circ}\text{F/Btu}$
Refrigerant	$R = 0.55$	$\text{hr-}^{\circ}\text{F/Btu}$

From these resistance values the following conclusions were made:

a) The dominant in X-direction resistance is the natural convection on the top and bottom surfaces of the Cryomicroscope Conduction Stage. Hence omission of the tape and silver epoxy will have an insignificant effect on the overall temperature profile in the X-direction. Also the tape and silver epoxy are placed away from the centerline. Thus, the changes in the temperature distribution would tend to be localized away from the centerline temperature of primary interest.

b) The least resistance path in the Y-direction would be through the copper plate. A comparison of a representative path resistance through the copper lone ($R = 0.8$) is not altered significantly by including the resistance of the tape. The effect of omitting the tape is therefore considered negligible, especially at the centerline temperature which is removed from the local effects close to the tape.

Note that the absence or presence of the tape will have a negligible effect for the transient results because the thermal capacitance of the tape is extremely small due to its tiny volume.

APPENDIX D

The Convective Heat Transfer Coefficient for the Refrigerant and Surrounding Air

Convective Heat Transfer Coefficient for the Refrigerant

In this experiment using $\Delta\rho = 20$ psig = 2880 psig. Assume the fully-developed turbulent flow occurs in the refrigerant tube.

$$\text{From } f = \frac{\Delta\rho}{F(\ell/D_H)(\rho V^2/2)} = \frac{0.046}{(\rho V D_H/\mu)^{0.2}} \quad (\text{Ref. 16})$$

$$\text{Then } V = \left[\frac{(\Delta\rho)(\mu/\rho D_H)^{0.2}}{0.184(\ell/D_H)(\rho/2)} \right]^{1/1.8} \quad (1)$$

where $D_H = 0.207$ in. = 0.0173 ft.

$\ell = 0.47$ ft.

The properties of air at 20 psig

$$\mu = 1.08 \times 10^{-5} \text{ lb/ft. sec.}$$

$$\rho = 0.075 \text{ lb/ft.}^3$$

$$\text{Pr} = 0.7$$

$$k = 0.016 \text{ Btu/hr.ft.}^\circ\text{F}$$

Substituting the above properties into Equation (1), we get

$$V = 126 \text{ ft./sec.}$$

To check the Reynolds number

$$\text{Re}_{D_H} = \rho V D_H/\mu = 15,100$$

This value of Re_{D_H} shows the turbulent flow and valid for the

assumption.

For the turbulent flow in tube or duct

$0.5 < Pr < 1.0$ (Gas)

(Ref. 7)

$$\bar{N}u_{D_H} = 0.022 Pr^{0.6} Re_{D_H}^{0.8}$$

$$= 39.15$$

$$\bar{h} = \bar{N}u_{D_H} k/D_H$$

$$\bar{h}_{ref.} = 36.85 \text{ Btu/hr.ft.}^{20F}$$

(air at 20 psig.)

Convective Heat Transfer Coefficient
for the Surrounding Air

For free convection from horizontal surfaces to air at atmospheric pressure,

Assume for laminar case

$$h = 1.32 \left(\frac{\Delta T}{\ell}\right)^{0.25} \quad (\text{Ref. 16})$$

In our case, $\ell = 1.28 \text{ in.} = 0.036 \text{ m.}$

Assume the average of the temperature difference $\Delta T = T_W - T_\infty \approx 8.5^\circ\text{C.}$

Then

$$h_{\chi=\ell} = 1.32 \left(\frac{8.5}{0.036}\right)^{0.25} = 5.01 \text{ W/m}^{20C}$$

For the constant heat rate, $\bar{h} = \frac{5}{4} h_{\chi=\ell}$ (Ref. 16)

$$\bar{h} = 6.26 \text{ W/m}^{20C}$$

$$\bar{h} = 1.06 \text{ Btu/hr.ft.}^{20F}$$

The Approximation of the Average Value
of \bar{h} Between \bar{h}_{air} and \bar{h}_{ref}

$$\text{For } \bar{h}_{\text{air}} = 1.06 \text{ Btu/hr.ft.}^{20}\text{F}$$

$$\bar{h}_{\text{ref}} = 36.85 \text{ Btu/hr.ft.}^{20}\text{F}$$

On the basis of the area contacted for the Cryomicroscope

Conduction Stage

Area in contact with air/Area in contact with refrigerant $\approx 3:1$

$$\begin{aligned} \text{The average } \bar{h} &= \frac{3(\bar{h}_{\text{air}}) + (\bar{h}_{\text{ref}})}{4} \\ &= 9.93 \text{ Btu/hr.ft.}^{20}\text{F} \end{aligned}$$

REFERENCES

1. J. J. McGrath, The Dynamics of Freezing and Thawing Mammalian Cells: The Hilla Cell, M.S.M.E. Thesis, MIT., pp. 48-64, 1974.
2. J. A. Adams, and D. F. Rogers, Computer-Aided Heat Transfer Analysis, McGraw-Hill, Inc., 1973.
3. M. N. Ozisik, Boundary Value Problems of Heat Conduction, International Textbook, Scranton, 1966.
4. G. D. Smith, Numerical Solution of Partial Differential Equations, Oxford, London, 1965.
5. G. E. Myers, Analytical Methods in Conduction Heat Transfer, McGraw Hill, Inc., 1971.
6. H. Z. Barakat, and J. A. Clark, On the Solution of the Diffusion Equations by Numerical Network, J. Heat Transfer, Vol. 88, ser C, pp. 421-427, 1966.
7. W. M. Kays, Convective Heat and Mass Transfer, McGraw-Hill, Inc., 1966.
8. G. E. Cooperatate Research and Development, Heat Transfer Data Book, 1975.
9. H. A. Luther, B. Cannahan, and J. O. Wikes, Applied Numerical Methods, Wiley, New York, 1969.
10. Y. S. Touloukian, Thermophysical Properties, Plenum Press, New York, 1967.
11. J. Crank and P. Nicolson, A Practical Method for Numerical Solutions of Partial Differential Equation of the Heat Conduction Type, Proc. Cambridge Phil. Soc., Vol. 43, pp. 50-67, 1967.
12. H. S. Carslaw and J. G. Jaeger, Conduction of Heat in Solids, Claredon Press, Oxford, 1959.
13. G. M. Dusenberre, Heat Transfer Calculations by the Finite Differences, International Textbook, Scranton, Pa., 1961.
14. M. L. James, G. M. Smith and J. C. Wolford, Analog and Digital Computer Methods in Engineering Analysis, International Textbook, Scranton, Pa., 1965.

15. R. D. Richtmeyer, *Difference Methods for Initial Value Problems*, Interscience, New York, 1967.
16. J. P. Holman, *Heat Transfer*, McGraw-Hill, Inc., 1976.
17. W. M. Rohsenow and H. Y. Choi, *Heat, Mass and Momentum Transfer*, McGraw Hill, Inc., 1968.

MICHIGAN STATE UNIV. LIBRARIES



31293104658632